

Test Handbook

TOUGH2-GRS
Version 2

TOUGH2-MP-GRS
Version 0



Gesellschaft für Anlagen-
und Reaktorsicherheit
(GRS) gGmbH

Test Handbook

TOUGH2-GRS
Version 2

TOUGH2-MP-GRS
Version 0

Martin Navarro
Jens Eckel
Heidemarie Fischer
Stephan Hotzel
Ingo Kock

September 2018

Remark:

This study has been funded by the German Federal Ministry for the Environment, Nature Conservation, Building and Nuclear Safety (BMU) under the support codes UM13A03400 and 4715E03230.

The work was conducted by the Gesellschaft für Anlagen- und Reaktorsicherheit (GRS) gGmbH.

The authors are responsible for the content of the report.

GRS - 402
ISBN 978-3-944161-83-9

Keywords:

Test, TOUGH2, TOUGH2-GRS, TOUGH2-MP, TOUGH2-MP-GRS, Verification

Kurzfassung

Der vorliegende Bericht dokumentiert Verifikationstest für die Codes TOUGH2-GRS, Version 2, und TOUGH2-MP-GRS, Version 0. Die Codetests wurden mit dem Code SITA, einem Werkzeug zur Durchführung automatischer Codetests, durchgeführt.

Abstract

The present report documents verifications tests for the codes TOUGH2-GRS, version 2, and TOUGH2-MP-GRS, version 0. Code tests have been conducted using the code SITA, a tool for automated code testing.

Content

1	Introduction	1
2	Isothermal Gas Flow	3
2.1	Analytical solution for steady state	3
2.2	Flux in steady state	5
2.3	A note on gas (phase) dynamic viscosities	6
2.4	Main results and conclusion	8
3	COMP Module.....	9
3.1	Reference Test Case <i>comp-R0</i>	12
3.2	Test Case <i>comp-1: $f\phi$</i>	14
3.3	Test Case <i>comp-3: ft</i>	15
3.4	Test Case <i>comp-5: fT</i>	17
3.5	Test Case <i>comp-5a: fT and $f\phi$</i>	19
3.6	Test Case <i>comp-6: fP</i>	21
3.7	Test Case <i>comp-7: fP</i>	23
3.8	Test Case <i>comp-12a: fP and fT</i>	26
4	Compressibility Test.....	29
5	CORFL Module	31
6	CORRO Module	35
6.1	Reference test case	35
6.2	Test cases derived from the reference case	38
7	DEGRA Module.....	47
8	FISS Module.....	49
8.1	Fissure permeability as a linear function of the excess pressure.....	49
8.2	Pressure-dependent porosity with porosity-dependent permeability.....	50
8.3	Positive rate limit for porosity change	51

8.4	Exponential decrease of the porosity change rate	52
8.5	Linear softening without time-dependency	53
8.6	Linear softening with minimum softening rate	55
9	PRLIM Module	57
10	RELA Module	59
10.1	Porosity–permeability relation	59
10.2	Leverett scaling of capillary pressure	60
10.3	Temperature-dependent capillary pressure	60
11	RN Module	63
11.1	Time Stepping Control	63
11.2	SAMR1	64
11.2.1	Model description	65
11.2.2	Analytical solution	65
11.2.3	Main results	67
11.2.4	No radioactive decay	67
11.2.5	Radioactive decay	68
11.2.6	Coarse time discretization	69
11.3	RN Anion Exclusion	71
11.3.1	Advective Transport	71
11.3.2	Diffusive Transport	72
	References	75
	List of Figures	79
	List of Tables	83

1 Introduction

GRS uses the family of TOUGH2 codes /PRU 99/ to simulate flow and transport processes in deep geological repository systems. GRS has added several features to the TOUGH2 code, which resulted in the code TOUGH2-GRS /NAV 18/. The new code parts of TOUGH2-GRS have also been ported to the code TOUGH2-MP /ZHA 08/ and the resulting code has been called TOUGH2-MP-GRS /NAV 18/.

For performance analysis calculations of deep geological repositories (DGR) it is of great concern whether the simulation codes work correctly. To demonstrate correctness and reliability to the extent possible a quality assurance programme has been set up for TOUGH2-GRS /HOT 16/, which also applies to TOUGH2-MP-GRS. This programme includes the definition of a software quality model made up of ten quality characteristics, the identification of quality requirements, and the implemented measures and tools to fulfil these requirements, including verification and – where possible – validation.

The codes TOUGH2-GRS and TOUGH2-MP-GRS are still under development so that there is a need for frequent code verification in the development process. For automated testing of TOUGH2 based codes GRS has developed the code SITA, which is a “*a simulation and code testing assistant for TOUGH2*” /SEH 16/. The development of SITA is part of the GRS software development project for the quality assurance of codes /GRS 13/. With SITA, simulation results can be compared to analytical solutions and with results of other codes or code versions.

This report defines SITA test cases for the quality assurance of TOUGH2-GRS and TOUGH2-MP-GRS. The documented tests have been performed with version 2 of TOUGH2-GRS and version 0 of TOUGH2-MP-GRS, both compiled with the Fortran compiler *gfortran*. In principle, all tests should be repeated for the specific code version, EOS module, compiler, compiler flags, and (platform dependent) libraries that are in use.

All test cases have been developed in the projects UM13A03400 and 4715E03230 of the Federal Ministry for the Environment, Nature Conservation and Nuclear Safety (BMU):

Test cases developed in project UM13A03400 (authors in brackets):

- Isothermal gas flow (*Stephan Hotzel*)

- Test of module COMP (*Heidemarie Fischer*)
- Compressibility test (*Martin Navarro*)
- Test of module CORFL (*Stephan Hotzel*)
- Test of module CORRO (*Martin Navarro*)
- Test of module DEGRA (*Martin Navarro*)
- Test of module PRLIM (*Martin Navarro*)
- Test of module RN: benchmark SAMR1 (*Jens Eckel*)

Test cases developed in project 4715E03230 (authors in brackets):

- Test of module FISS (*Martin Navarro*)
- Test of module RELA (*Martin Navarro*)
- Test of module RN: anion exclusion (*Martin Navarro*)
- Test of module RN: time stepping control (*Martin Navarro*)

The present report is a compilation of test case documentations written by different authors, and since we have not strived for conformity, depth and style of test case descriptions may vary.

The present report is not a stand-alone report but one that is supplementary to the user manual of TOUGH2-GRS and TOUGH2-MP-GRS /NAV 18/. For a full description of mathematical models, symbols and input parameters please refer to the user manual.

2 Isothermal Gas Flow

We consider isothermal air flow through a 1-dimensional column (no gravity) with fixed pressure (Dirichlet) boundary conditions. An analytical solution exists for the steady state condition. This test case is described in /KOL 12/ and we use, as far as practical, parameters similar to theirs (see their Table 8.2) to design our test setup in the following way:

We use a 100-element horizontal column, made of 1 m by 1 m by 1 m cubes. Boundary elements on both ends have a very large volume and a very small distance to the interface with the column. We run TOUGH2-GRS and TOUGH2-MP-GRS in single-phase gas mode (air mass fraction = 1, brine mass fraction = 0). Gas phase (air) viscosity is calculated TOUGH2-internally as usual. The (constant) temperature is chosen such that gas phase viscosity is 17.6 $\mu\text{Pa s}$. The boundary conditions of the model are set to $p_1 \equiv p(x_1) = p(x=0 \text{ m}) = 3 \text{ MPa}$, $p_2 \equiv p(x_2) = p(x=100 \text{ m}) = 101.325 \text{ kPa}$. The initial condition is $p(x) = p_2$ for $0 \text{ m} < x < 100 \text{ m}$. Porosity is $\phi = 0.35$, permeability is $k = 2.7 \cdot 10^{-11} \text{ m}^2$. Seven full printouts are generated as follows: The very first printout is generated at the beginning of the simulation (initial condition, at $t = 0 \text{ s}$).¹ Subsequent printouts are generated at times $t = 10^n \text{ s}$, with $n=0, 1, 2, 3, 4, 5$.

This SITA test case can be run with the EOS7 and EOS7R modules. However, the actual code test runs presented here (in the figures) are on the EOS7 module (of the TOUGH2-GRS and TOUGH2-MP-GRS codes) only.

2.1 Analytical solution for steady state

The x-component of the flux density is

$$F = -\frac{k}{\eta} \rho \frac{dp}{dx} . \quad (2.1)$$

Using the ideal gas law to substitute

$$\rho = \frac{M}{RT} p \quad (2.2)$$

¹ This is a feature of the codes TOUGH2-GRS and TOUGH2-MP-GRS.

and employing the inverse chain rule we get

$$F = -\frac{k M}{\eta RT} \frac{1}{2} \frac{dp^2}{dx} \quad (2.3)$$

or

$$\frac{dp^2}{dx} = \frac{-2F\eta RT}{kM} \quad (2.4)$$

Since all variables on the right hand side are either natural constants (R : Universal gas constant), constants (M : Molar mass of the gas) or assumed constant in the test domain (T : Temperature of the gas, assumed isothermal; η : Viscosity of the gas, assumed to be independent of pressure; F : Flux density, constant in 1-dimensional steady state), we can integrate both sides of the equation easily from x_1 to x to yield $p^2(x) - p^2(x_1)$, or from x_1 to x_2 to yield $p^2(x_2) - p^2(x_1)$. Rearranging both equations we get

$$\frac{p^2(x) - p^2(x_1)}{x - x_1} = \frac{-2F\eta RT}{kM} = \frac{p^2(x_2) - p^2(x_1)}{x_2 - x_1} \quad (2.5)$$

This way we have found under steady state conditions the pressure p at any position x in the column:

$$p(x) = \sqrt{p_1^2 + (p_2^2 - p_1^2) \frac{x - x_1}{x_2 - x_1}} \quad (2.6)$$

This is all we need to plot the steady state analytical solution.

The first three analyses in the SITA test case “Isothermal Gas Flow” are bound to demonstrate that the numerical simulation coincides, in steady state, with the analytical solution. In the first analysis (see Fig. 2.1), we plot the gas pressure profile at the last printout and the steady state analytical solution (2.6), which should match perfectly.

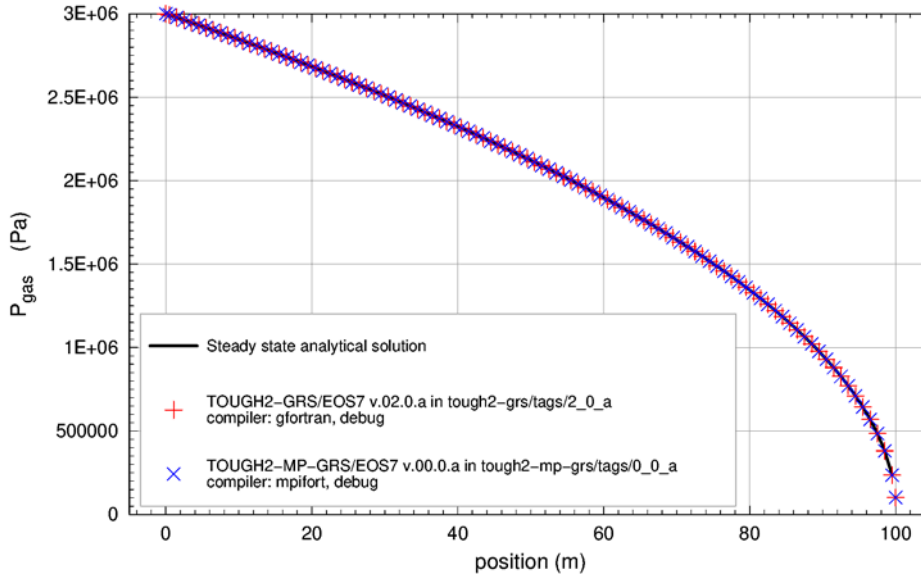


Fig. 2.1 Isothermal gas flow, steady state pressure profile

SITA analysis no. 1 on the executables as indicated in the figure legend. The numerical gas pressure profiles and the analytical solution match perfectly.

2.2 Flux in steady state

In steady state condition, the total flux, $Q = A \cdot F$ through the column can be calculated easily by inserting the first derivative of the analytical solution for $p(x)$, (2.6), and the ideal gas law for ρ , (2.2), into the equation for F , (2.1):

$$Q = \frac{AkM}{2L\eta RT} (p_1^2 - p_2^2) \quad (2.7)$$

With ϕ , k , η , L , A , p_1 , p_2 , as given above and $T = (5.54+273.15)$ K, $R = 8.31456$ J/(K*mol), $M(\text{Air}) = 0.02896$ kg/mol we calculate $Q = 0.861799$ kg/s. In order to check the accuracy of the numerical simulation, we need this value to the highest possible precision. Therefore, we adopt for η the precise value used by TOUGH2-GRS and TOUGH2-MP-GRS ($0.17599998479179784582\text{E}-04$; all other parameter values used to calculate Q are already the very TOUGH2-values used). With this we calculate a total air flux of $Q_{\text{check}} = 0.861,798,717,543,56$ kg/s.

The sixth analysis in this SITA test case checks – by printing the scalar value of the gas flux, “FLO(GAS)” – that the numerical simulation, after reaching steady state, produces the same flux as calculated with the analytical solution (2.7). If the relative deviation of the two numbers FLO(GAS) and Q_{check} is small, this deviation provides a good 1-number

indicator for the difference between the two pressure profiles, with which this SITA test case started (see first analysis above), since it is extremely unlikely that two differing pressure profiles would lead to the same flux density by accident.

Running this SITA test case with TOUGH2-GRS and TOUGH2-MP-GRS (EOS7), the result of the sixth analysis is equality between Q and $|FLO(GAS)|$ up to the 6-significant-digits output format provided by the codes (and thus SITA). Higher accuracy comparison outside SITA (source code intervention for higher accuracy printouts and analysis of the flux column in the COFT file required) yields the following results:

- Numerical steady state, i. e. unchanging flux terms (up to full numerical precision), at position x_1 is reached at $t = 0.9 \times 10^4$ s, at position x_2 is reached at $t = 1.3 \times 10^4$ s.
- The calculated steady state flux at x_1 is $Q_{x1} = 0.861,798,739,076,65$ kg/s. At x_2 it is $Q_{x2} = 0.861,798,739,076,64$ kg/s. Thus, Q_{x1} and Q_{x2} are identical almost up to the precision of 64-bit, double-precision, floating-point arithmetic.
- As the analytical steady state solution yields $Q_{check} = 0.861,798,717,543,56$ kg/s, Q_{x2} and Q_{check} are identical up to a relative deviation of $\sim 10^{-8}$. It is interesting to note that this is just the precision of 32-bit, single-precision, floating-point arithmetic.

2.3 A note on gas (phase) dynamic viscosities

According to the TOUGH2 Manual /PRU 99/ (p. 35, p. 56) TOUGH2 calculates the gas phase (air-vapor mixture) viscosity “from a formulation given by /HIR 64/. In the source code (files eos7_grs.f and eos7r_grs, SUBROUTINE VISCO) it says

```
“THIS ROUTINE COMPUTES THE VISCOSITY OF VAPOR-AIR MIXTURES. IT
USES A MODIFIED VERSION OF A FORMULATION BASED ON KINETIC GAS
THEORY, AS GIVEN BY J.O. HIRSCHFELDER, C.F. CURTISS, AND R.B.
BIRD, MOLECULAR THEORY OF GASES AND LIQUIDS, JOHN WILEY & SONS,
1954, PP. 528-530. THE MODIFICATION MADE TO THE HIRSCHFELDER ET
AL. EXPRESSIONS IS THAT FOR VAPOR VISCOSITY ACCURATE (EMPIRICAL)
VALUES ARE USED, RATHER THAN THE FIRST ORDER EXPRESSION OF KINETIC
THEORY. THE FORMULATION MATCHES EXPERIMENTAL DATA ON VISCOSITIES
```

OF VAPOR-AIR MIXTURES IN THE TEMPERATURE RANGE FROM 100 TO 150 DEG. C, FOR ALL COMPOSITIONS, TO BETTER THAN 4%.”

The calculus in the source code (subroutine VISCO, calling subroutine VISS and function COVIS) looks complex in detail. However, in general it can be said that the vapour-air-mixture viscosity calculated by these routines depends on temperature and pressure (subroutine VISS calculates steam viscosity as function of temperature and density, but the density was calculated as function of temperature and pressure before by subroutine SUPST). Also, it can be said that in the special case that air mass fraction = 1 (i. e. single-phase gas mode and all other components' mass fractions = 0), the gas phase viscosity, i. e. the air viscosity, is calculated independent of pressure as

$$\eta = 2.6693 * (28.96 * \text{tem})^{0.5} / (3.617^2 * (1.188 - \text{tem} * 0.051/97.0)) , \quad (2.8)$$

where $\eta = \eta / (\mu\text{Pa s})$ is the numerical value of the viscosity in unit $\mu\text{Pa s}$ and $\text{tem} = T / (\text{K})$ is the numerical value of the Temperature in unit K. This formula seems to be an implementation of the so called “Chapman-Enskog equation” for dilute gases (/HIR 64/ cited by <http://en.wikipedia.org/wiki/Viscosity>), which is independent of pressure.

In general, TOUGH2 accepts temperatures in the range $1^\circ\text{C} < T < 500^\circ\text{C}$.

According to the kinetic theory of gases, gas viscosities are independent of pressure and increase with temperature (<http://en.wikipedia.org/wiki/Viscosity> [14-JAN-2015]). However, real gases viscosities increase with pressure. The figures in <http://de.wikipedia.org/wiki/Viskosität> and in <http://en.wikipedia.org/wiki/Viscosity> suggest the following:

- For air, N_2 and H_2 : Viscosity increases (at $T=290\text{ K}$, $p=0.1\text{ MPa}$) with increasing temperature or pressure by approx. $0.2\text{ \%}/\text{K}$ or $1.7\text{ \%}/\text{MPa}$, respectively.
- Therefore, air viscosity should increase by about 5 \% in this test setup between x_2 (5°C , 0.1 MPa) and x_1 (5°C , 3 MPa)
- For N_2 : The temperature dependence vanishes and eventually changes sign at higher pressures (i. e., at $\sim 20\text{ MPa}|275\text{ K}$ or $30\text{ MPa}|300\text{ K}$ or $40\text{ MPa}|350\text{ K}$), e. g. at 30 MPa , η increases with T up to a temperature of 300 K , and decreases with further increasing T .

- For N₂: The pressures dependence increases somewhat at higher pressures and considerably at lower temperatures (i. e., at ~10 MPa|300 K or 7 MPa|250 K or 4 MPa|200 K).

Thus, we can deduce that the TOUGH2 statement that the TOUGH2 “formulation matches experimental data on viscosities of vapor-air mixtures in the temperature range from 100 to 150 °C, for all compositions, to better than 4 %” may hold for the dilute gas (=low pressure) regime of the Chapman-Enskog equation only, i. e. for pressures well below 3 MPa.

Note that generally (for temperatures above 0 °C and pressures below 20 MPa), the (dynamic) viscosity of gases increases with temperature. While the viscosity of liquids decreases with temperature.

In Tab. 2.1, we compare air viscosities calculated by TOUGH2, using Eqn. (2.8), with literature values.

2.4 Main results and conclusion

A number of results and insights have been mentioned already in the previous sections and some general conclusions will be mentioned here. These were obtained by running and analysing this SITA test case with TOUGH2-GRS version 2 and TOUGH2-MP-GRS version 0 (EOS7) in September 2018. The main result is that TOUGH2 is able to reproduce the analytical steady state solution with very high accuracy.

These results should apply in principle (i. e. without excluding any peculiar software bug in any of the earlier TOUGH2 versions or revision numbers) to standard TOUGH2 and all versions of TOUGH2-GRS, since the modules mainly affected by this test case have not undergone any development in TOUGH2-GRS yet. However, future development of these very code sections may well be possible. In fact, a module to optionally replace the non-condensable gas component “air” by a different component (e. g. H₂) is under development. Such a module may well (optionally) replace the calculus of the gas phase viscosity as a function of pressure, temperature, saturation etc. For pressure dependent viscosities, this SITA test case needed to be further developed or an alternative test case needed to be designed.

Tab. 2.1 Some literature/Wikipedia values of gas viscosities

Gas	@ <i>T</i>	@ <i>p</i>	η (TOUGH2)	η (Reference)	Reference
Air	15 °C	n.s.	17.98 $\mu\text{Pa s}$	18.0 $\mu\text{Pa s}$	http://de.wikibooks.org/wiki/Tabellen-sammlung_Chemie/_Dynamische_Viskosität_gasförmiger_Stoffe [14-JAN-2015]",
	18.0 °C	n.a.	18.10 $\mu\text{Pa s}$	18.27 $\mu\text{Pa s}$	http://en.wikipedia.org/wiki/Viscosity [14-JAN-2015] referencing Smits, Alexander J. and Dussauge, Jean-Paul (2006) Turbulent shear layers in supersonic flow, Birkhäuser, ISBN 0-387-26140-0 p. 46
	273 K	100 kPa	17.37 $\mu\text{Pa s}$	17.4 $\mu\text{Pa s}$	http://en.wikipedia.org/wiki/Viscosity [14-JAN-2015] referencing Lide, D. R., ed. (2005). CRC Handbook of Chemistry and Physics (86th ed.). Boca Raton (FL): CRC Press. ISBN 0-8493-0486-5
	300 K	100 kPa	18.46 $\mu\text{Pa s}$	18.6 $\mu\text{Pa s}$	http://en.wikipedia.org/wiki/Viscosity [14-JAN-2015] referencing Lide, D. R., ed. (2005). CRC Handbook of Chemistry and Physics (86th ed.). Boca Raton (FL): CRC Press. ISBN 0-8493-0486-5
H ₂	15 °C	n.s.		8.6 $\mu\text{Pa s}$	http://de.wikibooks.org/wiki/Tabellen-sammlung_Chemie/_Dynamische_Viskosität_gasförmiger_Stoffe [14-JAN-2015]",
	20.7 °C	n.a.		8.76 $\mu\text{Pa s}$	http://en.wikipedia.org/wiki/Viscosity [14-JAN-2015] referencing Smits, Alexander J. and Dussauge, Jean-Paul (2006) Turbulent shear layers in supersonic flow, Birkhäuser, ISBN 0-387-26140-0 p. 46
	273 K	100 kPa		8.4 $\mu\text{Pa s}$	http://en.wikipedia.org/wiki/Viscosity [14-JAN-2015] referencing Lide, D. R., ed. (2005). CRC Handbook of Chemistry and Physics (86th ed.). Boca Raton (FL): CRC Press. ISBN 0-8493-0486-5
	300 K	100 kPa		9.0 $\mu\text{Pa s}$	http://en.wikipedia.org/wiki/Viscosity [14-JAN-2015] referencing Lide, D. R., ed. (2005). CRC Handbook of Chemistry and Physics (86th ed.). Boca Raton (FL): CRC Press. ISBN 0-8493-0486-5
CH ₄	300 K	100 kPa		11.2 $\mu\text{Pa s}$	http://en.wikipedia.org/wiki/Viscosity [14-JAN-2015] referencing Lide, D. R., ed. (2005). CRC Handbook of Chemistry and Physics (86th ed.). Boca Raton (FL): CRC Press. ISBN 0-8493-0486-5
CO ₂	300 K	100 kPa		15.0 $\mu\text{Pa s}$	http://en.wikipedia.org/wiki/Viscosity [14-JAN-2015] referencing Lide, D. R., ed. (2005). CRC Handbook of Chemistry and Physics (86th ed.). Boca Raton (FL): CRC Press. ISBN 0-8493-0486-5

3 COMP Module

The COMP Module implements the combined process of converging of mining cavities in rock salt and the resulting compaction of crushed salt backfill /NAV 18/. The permeability of the backfill is calculated using a porosity-permeability relationship /NAV 16/. These processes can be described by an empirical model which is discussed in /NAV 13/. To fully understand the test cases described here, the reader should be familiar with the user manual for TOUGH2-GRS and TOUGH2-MP-GRS /NAV 18/.

The empirical model of convergence and compaction is part of the code MARNIE (**M**odell zur **A**usbreitung von **R**adio**N**ukliden **I**m **E**ndlagerbergwerk) /MAR 02/. The correctness of the MARNIE-results have been shown by several substantial test- and benchmark-calculations /KOC 13/. Since the mathematical models for calculating the rate of convergence and permeability are identical in MARNIE, TOUGH2-GRS and TOUGH2-MP-GRS, all specified test cases have also been simulated with MARNIE. The aim of the following test cases is to demonstrate the correct implementation of the COMP module in TOUGH2.

The rate of convergence described in /NAV 13/ depends on various factors. The correctness of the implementation is checked by comparing the results of simulations (test cases) from MARNIE and TOUGH2. In these test cases each of the factors are tested separately and partly combined. An overview of the documented test cases is given in Tab. 3.1.

The input parameter `RE1` for the tolerance of the convergence criterion (see /PRU 99/) has a strong influence on the quality of the simulation results. To reach a very good agreement between TOUGH2-GRS and MARNIE results, it is necessary to reduce `RE1` by one or two orders of magnitude (default value: 10^{-5}).

Tab. 3.1 List of test cases for the COMP module

Test case name	tested factor	S_{liq}	K_{ref} [a^{-1}]	P [Pa]	T [$^{\circ}C$]	ϕ_r	left boundary condition	right boundary condition
comp-R0	-	0	$1 \cdot 10^{-2}$	$1 \cdot 10^5$	25	$1 \cdot 10^{-4}$	$1 \cdot 10^5$ Pa	$1 \cdot 10^5$ Pa
comp-1	f_{ϕ}	0	$1 \cdot 10^{-2}$	$1 \cdot 10^5$	25	0.3	$1 \cdot 10^5$ Pa	$1 \cdot 10^5$ Pa
comp-3	f_t	0	$1 \cdot 10^{-6}$	$1 \cdot 10^5$	25	$1 \cdot 10^{-4}$	$1 \cdot 10^5$ Pa	$1 \cdot 10^5$ Pa
comp-5	f_T	0	$1 \cdot 10^{-2}$	$1 \cdot 10^5$	calc.	$1 \cdot 10^{-4}$	$1 \cdot 10^5$ Pa	$1 \cdot 10^5$ Pa
comp-5a	$f_T + f_{\phi}$	0	$1 \cdot 10^{-2}$	$1 \cdot 10^5$	calc.	0.3	$1 \cdot 10^5$ Pa	$1 \cdot 10^5$ Pa
comp-6	f_P	1	$1 \cdot 10^{-2}$	calc.	25	$1 \cdot 10^{-4}$	no flow	no flow
comp-7	f_P	1	$1 \cdot 10^{-2}$	calc.	25	$1 \cdot 10^{-4}$	no flow	$1 \cdot 10^5$ Pa
comp-12a	$f_P + f_T$	1	$1 \cdot 10^{-2}$	calc.	calc.*	$1 \cdot 10^{-4}$	no flow	$1 \cdot 10^5$ Pa

3.1 Reference Test Case *comp-R0*

The goal of the reference case is to verify if – in absence of other factors – the rate of convergence remains constant. This test case considers a single element bounded by boundary elements on the left-hand and right-hand side. We assume that the central element is filled with crushed salt with an initial porosity of 50 %. The initial fluid pressure is set to $p_{atm} = 10^5$ Pa and the reference temperature is $T_G(z_{ref}) = 25$ $^{\circ}C$. The liquid saturation is $S_{liq} = 0$, which means that the pore space is fully saturated with gas. To avoid an increase of the gas pressure during convergence, the gas permeability of the backfill is set to a constant value of 10^{-6} m². The boundary elements are open boundaries with a pressure of 10^5 Pa on both sides.

The temperature of the fluid (gas) $T(z, t)$ is equal to the reference temperature. Furthermore, we assume that the crushed salt offers no mechanical resistance to convergence, which means that the current (calculated) porosity ϕ has to be equal to or larger than the reference porosity ϕ_r at all times. We therefore set $\phi_r = 1 \cdot 10^{-4}$, which is lower than the porosity limit (minimum porosity) $\phi_{min} = 1 \cdot 10^{-3}$.

The reference convergence rate is set to $K_{ref} = 0,01$ a⁻¹ ($3.1688 \cdot 10^{-10}$ s⁻¹), which in this case is equal to the initial convergence rate K_0 . The factor f_{loc} , which can be used to describe a depth dependency of K_{ref} , is set to 1. The most important parameters for the reference

case can be found in Tab. 3.1. The tolerance parameters RE1 and RE2 are set to 10^{-7} and 1, respectively.

Results

The results of the reference case are shown in Fig. 3.1 and Fig. 3.2. The convergence rate remains constant (see Fig. 3.1) until the porosity limit ϕ_{\min} of 10^{-3} is reached after $2.2 \cdot 10^9$ s \approx 70 a (see Fig. 3.2). The figures show that the convergence rates and the resulting evolution of the porosity, calculated by TOUGH2-GRS, TOUGH2-MP-GRS and MARNIE match very well.

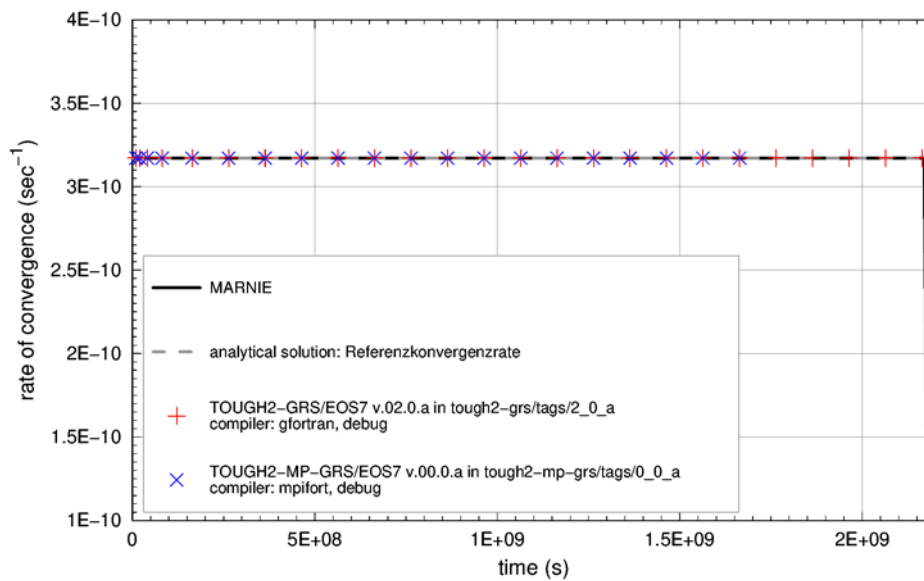


Fig. 3.1 COMP reference case: Evolution of the convergence rate

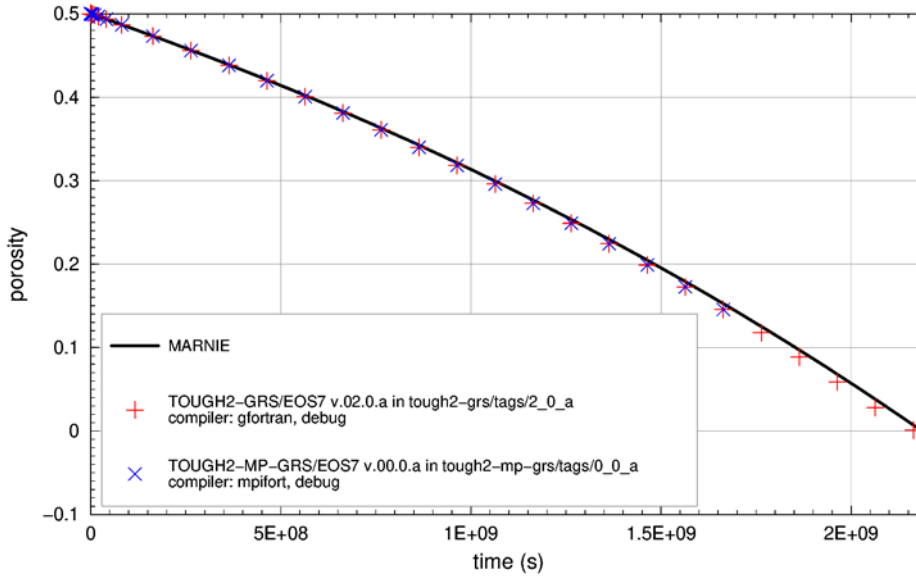


Fig. 3.2 COMP Reference case: Evolution of porosity

3.2 Test Case *comp-1*: f_ϕ

The factor f_ϕ in the empirical convergence model /NAV 18/, /NAV 13/, /NAV 16/ describes the resistance of the backfill against the convergence of the cavity.

Various parameters are used to calculate f_ϕ . The following parameters are not varied in the test cases. We set

- $m_\phi = m_p = 4$,
- $h_1 = -2, g_1 = -1$.

Parameter g_2 is set to 100, which corresponds to dry backfill since the central element is saturated with gas.

All other parameters are the same as in the reference test case except for a reference porosity ϕ_r of 0.3. The reference porosity is the porosity at which the support of the backfill commences. The most important parameters can be found in Tab. 3.1.

Results

The simulation results are shown in Fig. 3.3 and Fig. 3.4. The simulation starts with a constant reference convergence rate (see Fig. 3.3) and the porosity decreases from 0.5

to 0.3 (see Fig. 3.4). Backfill support starts at about 10^9 s $\approx 1.2 \cdot 10^{10}$ s (38 a). After that, the rate of convergence decreases (see Fig. 3.3) until the porosity limit ϕ_{\min} of 10^{-3} is reached (see Fig. 3.4) at about $2.85 \cdot 10^{10}$ s (900 a). Fig. 3.3 and Fig. 3.4 show that the results of TOUGH2-GRS, TOUGH2-MP-GRS and MARNIE match very well.

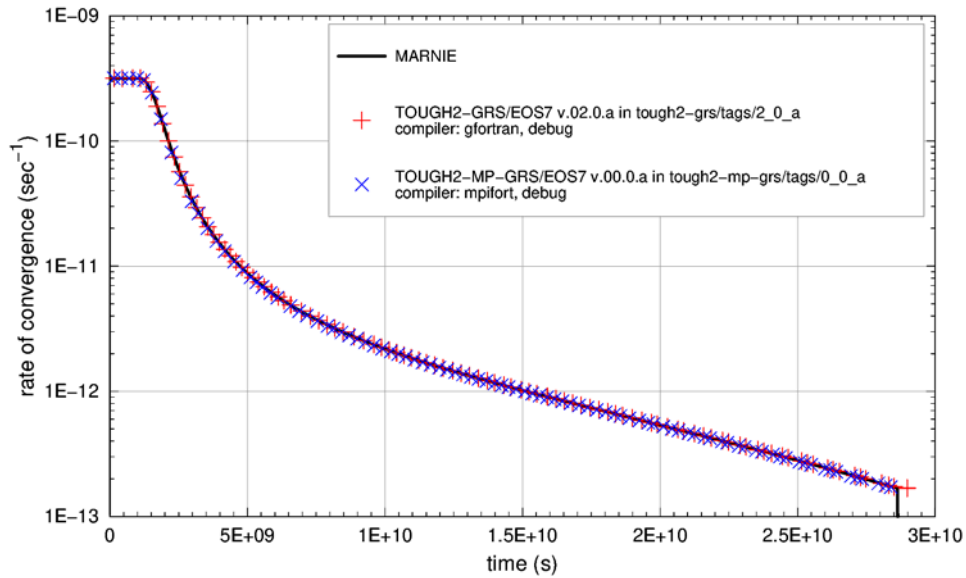


Fig. 3.3 COMP test case *comp-1*: Evolution of the convergence rate

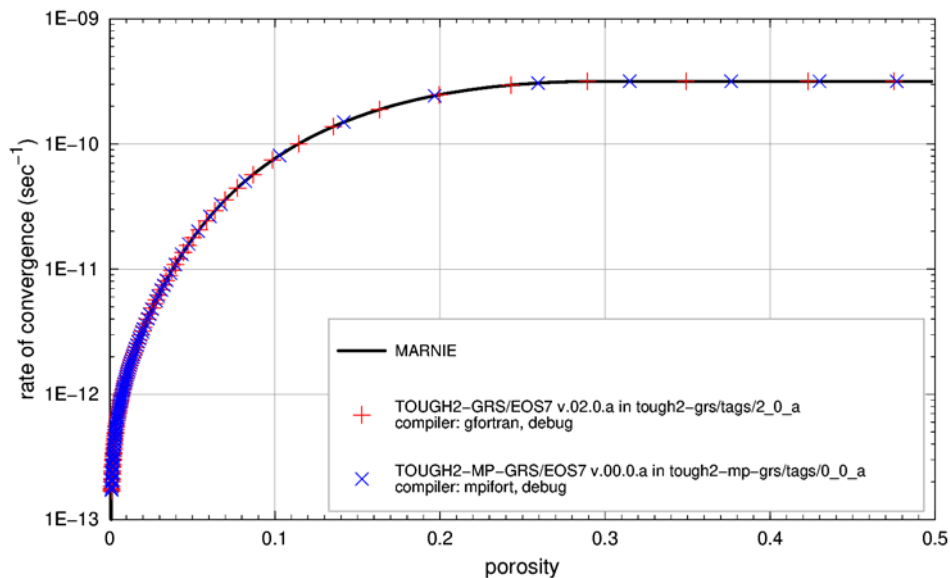


Fig. 3.4 COMP test case *comp-1*: Convergence rate versus porosity

3.3 Test Case *comp-3*: f_t

The factor f_t in the empirical convergence model /NAV 18/, /NAV 13/, /NAV 16/ describes the time dependency of convergence. The parameters can be determined or

calibrated by mechanical calculations. The following three parameters have a major influence on f_t :

- The initial convergence rate $K_0(z_{\text{ref}})$ at reference depth. This parameter is set to $3.1688 \cdot 10^{-10} \text{ s}^{-1}$ ($0,01 \text{ a}^{-1}$).
- The reference convergence rate K_{ref} for this test case. This parameter is set to $K_{\text{ref}} = 3.1710 \cdot 10^{-14} \text{ s}^{-1}$ (0.000001 a^{-1}).
- The fitting parameter λ_s , which is determined by mechanical calculations. In this test case we set $\lambda_s = 0.025$.

All other parameters remain the same as in the reference test case. The most important parameters for the test case can be found in Tab. 3.1.

Results

Fig. 3.5 and Fig. 3.6 show that the results of TOUGH2-GRS, TOUGH2-MP-GRS and MARNIE match well. The convergence rate decreases until the porosity limit ϕ_{min} of 10^{-3} is reached (see Fig. 3.6).

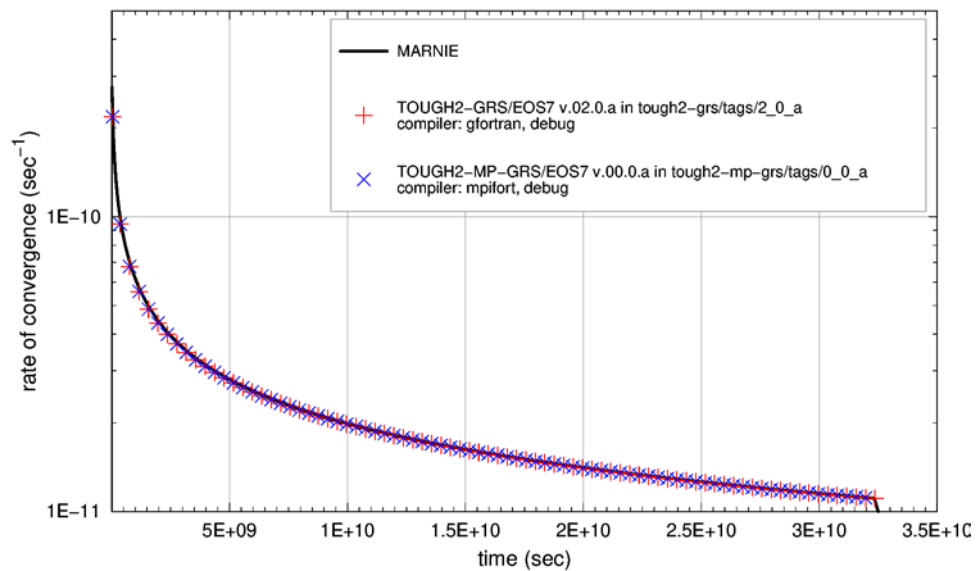


Fig. 3.5 COMP test case *comp-3*: Evolution of the convergence rate

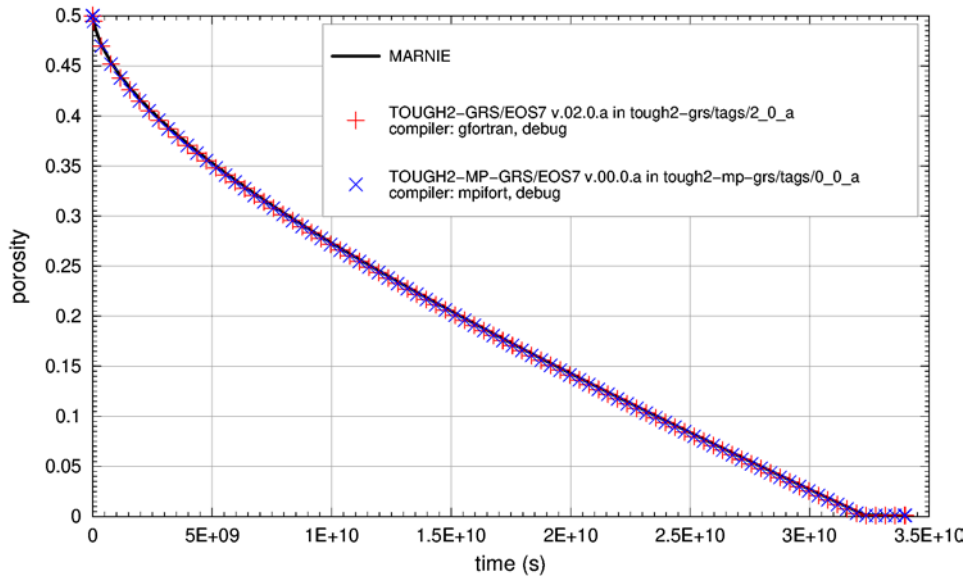


Fig. 3.6 COMP test case *comp-3*: Evolution of porosity

3.4 Test Case *comp-5*: f_T

The factor f_T in the empirical convergence model /NAV 18/, /NAV 13/, /NAV 16/ describes the temperature dependency of convergence. The model for f_T is based on the BGRb law for salt creep /BRÄ 11/ and requires various parameters. The parameters R , Q_1 , Q_2 , and a (see /NAV 18/, /NAV 13/, /NAV 16/) are held constant:

- $R = 8.31456 \text{ J/mol/K}$,
- $a = 0.029$,
- $Q_1 = 5.404 \cdot 10^4 \text{ J/mol}$,
- $Q_2 = 1.0810^5 \text{ J/mol}$.

We consider the temperature dependency of the convergence process by varying the temperature by a variable heat source with an initial capacity of 0.12 J/s until $5 \cdot 10^8 \text{ s}$. Afterwards the heat source successively reduced and finally switched off after $5.15 \cdot 10^8 \text{ s}$. The temperatures calculated by TOUGH2-GRS were transferred to MARNIE. All other parameters are the same as in the reference test case. The most important parameters for this test case can be found in Tab. 3.1.

Results

The results are shown in Fig. 3.7, Fig. 3.8 and Fig. 3.9. The calculated rate of convergence is identical for MARNIE and both TOUGH2 based codes (see Fig. 3.7). The same can be said for the evolution of porosity with time (see Fig. 3.8) except for the first time-steps (see Fig. 3.9). In general, however, the results of TOUGH2-GRS, TOUGH2-MP-GRS and MARNIE match very well.

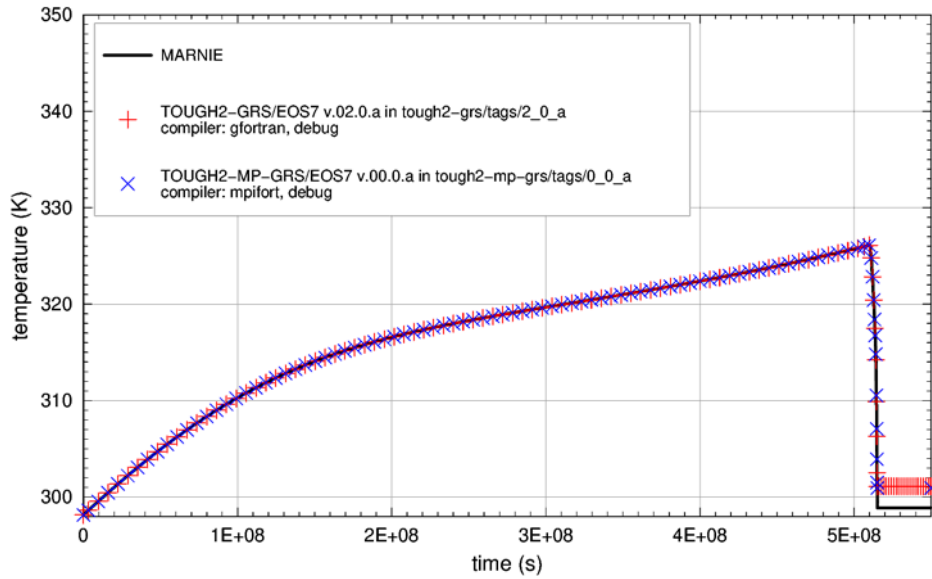


Fig. 3.7 COMP test case *comp-5*: Evolution of temperature

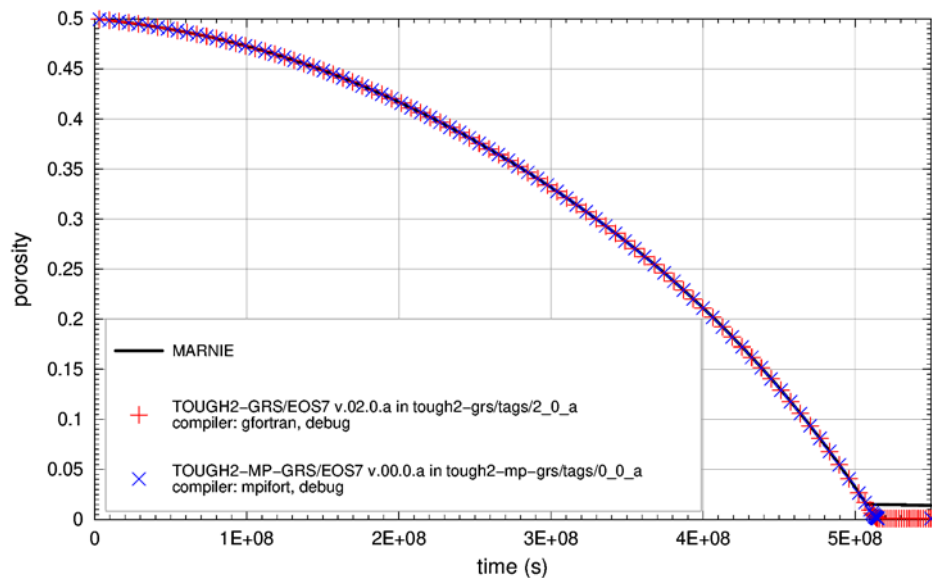


Fig. 3.8 COMP test case *comp-5*: Evolution of porosity

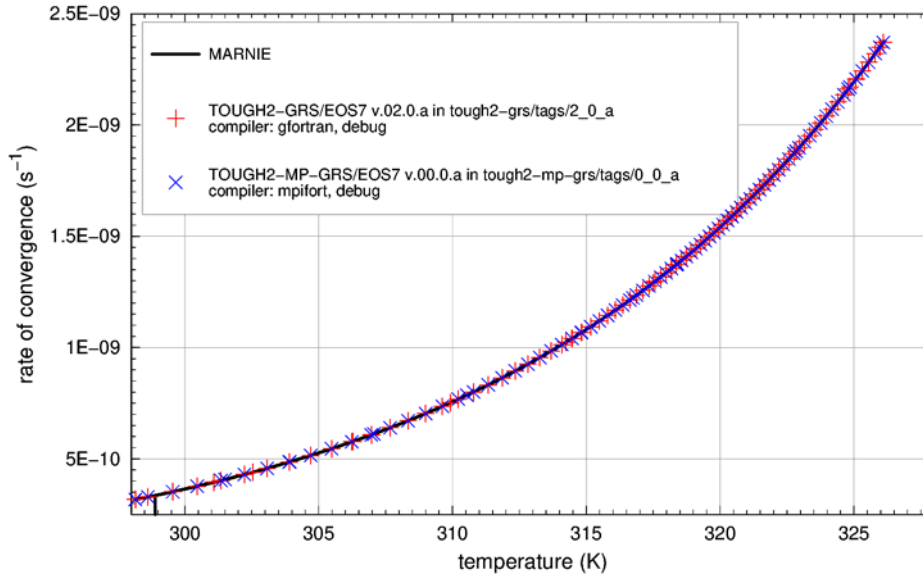


Fig. 3.9 COMP test case *comp-5*: Convergence rate versus temperature

3.5 Test Case *comp-5a*: f_T and f_ϕ

We consider the temperature dependency of the convergence process in combination with the supporting effect of the compacted backfill. The input parameters for f_ϕ and f_T are the same as for test cases *comp-1* and *comp-5*, respectively (chap. 3.2 and 3.4). However, the heat source has an initial capacity of 0.1 J/s until $5 \cdot 10^8$ s here and a following successive reduction until it is switched off after $9 \cdot 10^8$ s. The most important parameters can be found in Tab. 3.1. The parameter RE1 is set to 10^{-6} .

Results

The results are shown in Fig. 3.10, Fig. 3.11 and Fig. 3.12. The evolution of temperature (see Fig. 3.10), the relation between temperature and convergence rate (Fig. 3.11) and the development of porosity with time (Fig. 3.12) show good correspondence.

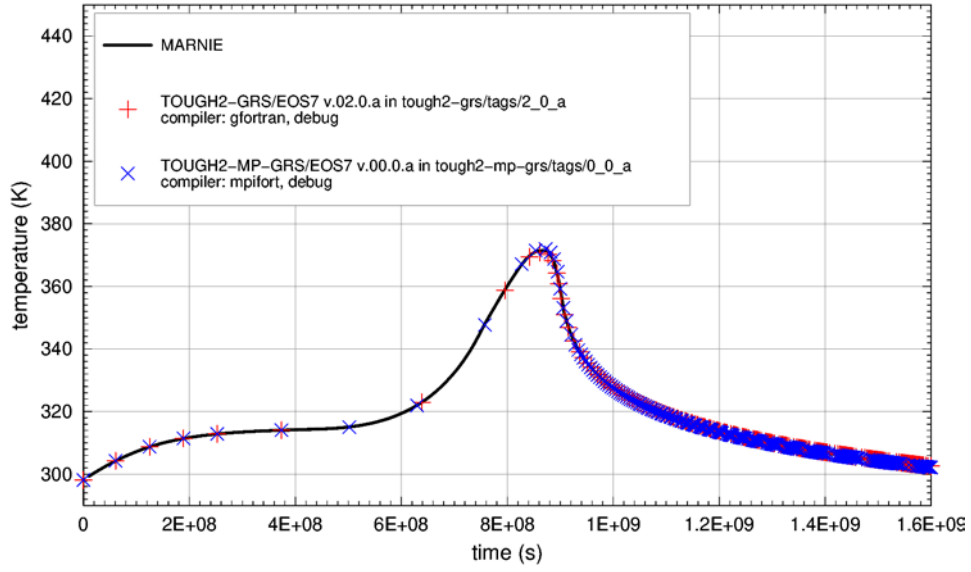


Fig. 3.10 COMP test case *comp-5a*: Evolution of temperature

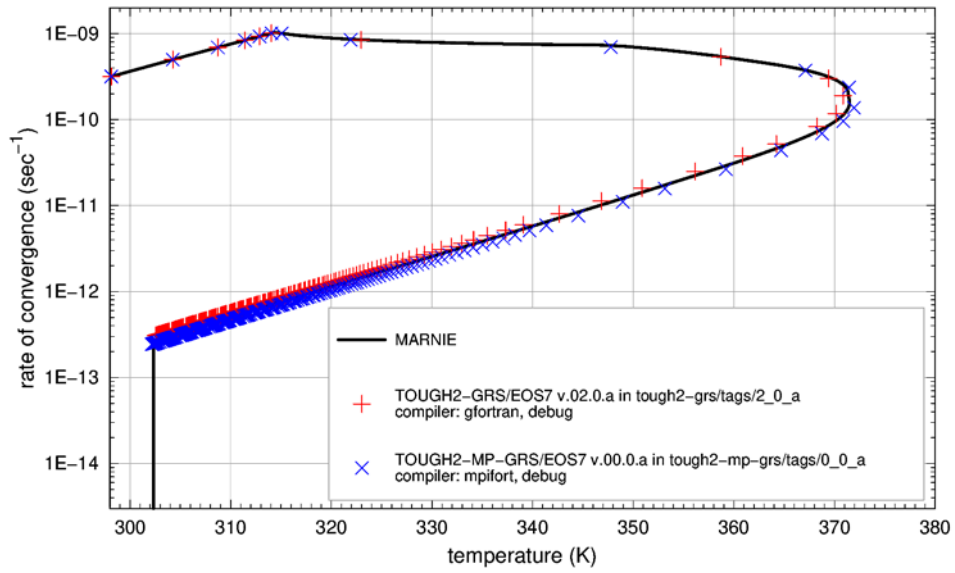


Fig. 3.11 COMP test case *comp-5a*: Convergence rate versus temperature

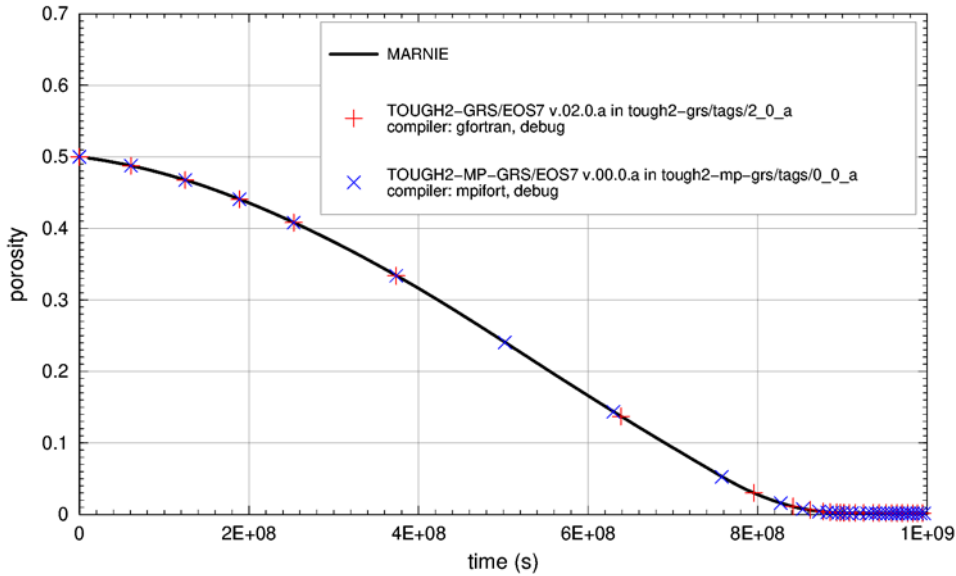


Fig. 3.12 COMP test case *comp-5a*: Evolution of porosity

3.6 Test Case *comp-6*: f_p

We consider the dependency of the rate of convergence on fluid pressure by assuming a fast increase of the liquid pressure due to closed boundaries. In this test case, we use a horizontal column composed of two active elements.

The two central elements are completely saturated with liquid (air mass fraction = 0, brine mass fraction = 1) with an initial pressure of 10^5 Pa. Permeability is calculated using a power-law relation to porosity /NAV 16/. The reference density of the liquid is set to 1185 kg/m^3 , which is valid for a temperature of $25 \text{ }^\circ\text{C}$ and a pressure of 10^5 Pa. The boundary elements on both sides are no-flow boundary conditions. All other parameters are the same as in the reference test case. The most important parameters of this test case can be found in Tab. 3.1. The parameter REL is set to 10^{-7} .

Results

The results are shown in Fig. 3.13, Fig. 3.14 and Fig. 3.15. In Fig. 3.13 we observe a rapid decrease of the convergence rate in the central elements. Consequently, porosity (see Fig. 3.14) and permeability decrease (see Fig. 3.15) only slightly. The evolution of the convergence rate, pressure, and porosity as well as the permeability-porosity relation show very good agreement between MARNIE, TOUGH2-GRS, and TOUGH2-MP-GRS.

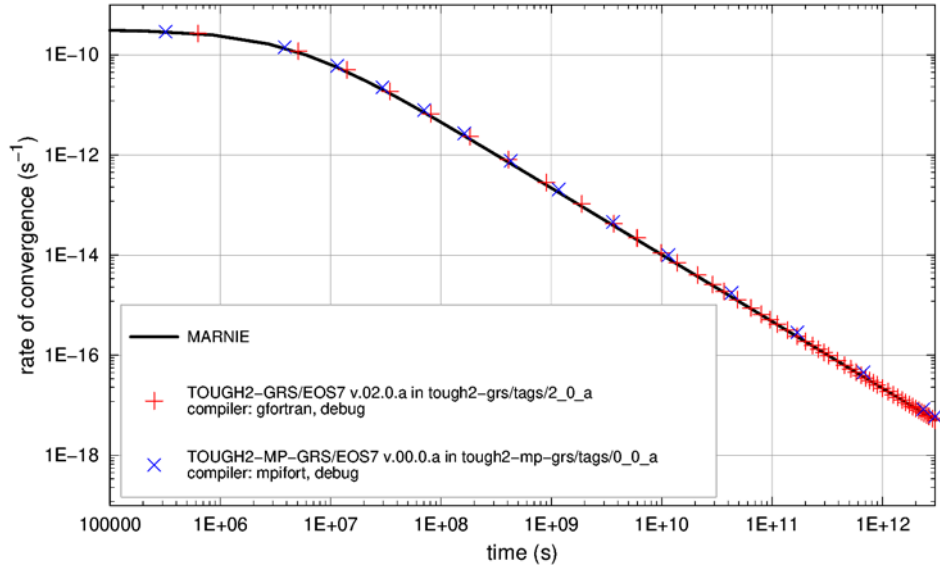


Fig. 3.13 COMP test case *comp-6*: Evolution of convergence rate

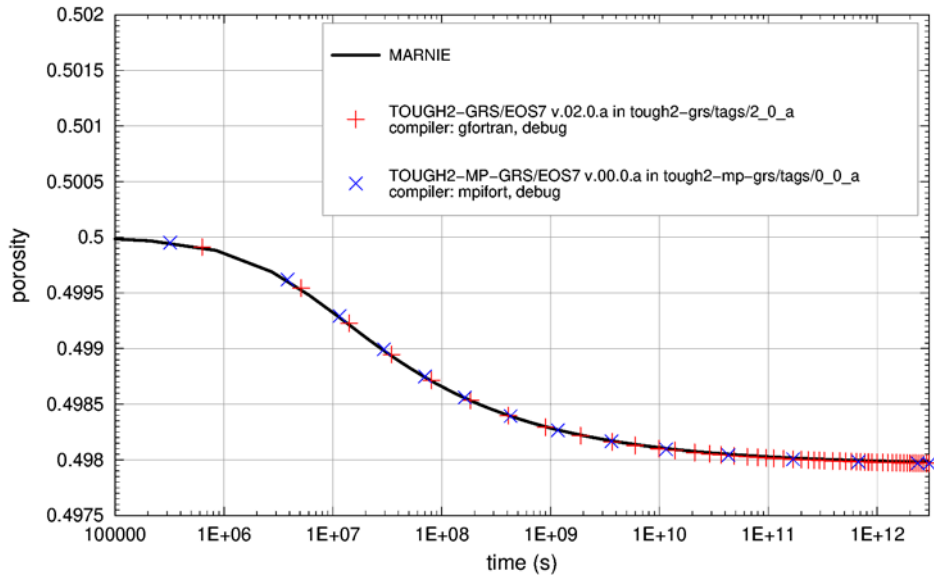


Fig. 3.14 COMP test case *comp-6*: Evolution of porosity

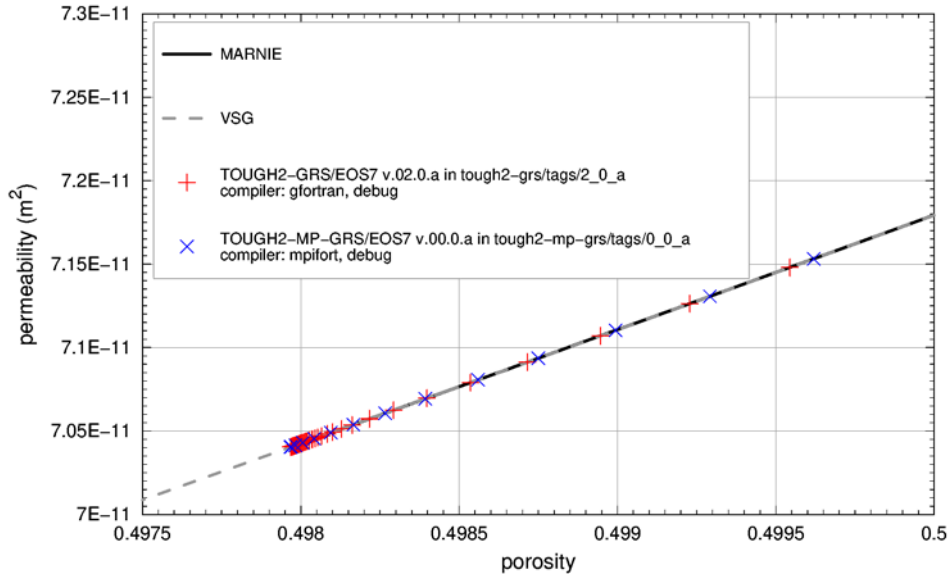


Fig. 3.15 COMP test case *comp-6*: Permeability versus porosity

3.7 Test Case *comp-7*: f_p

Here, we consider the pressure dependency of the convergence process by assuming a moderate increase of the liquid pressure. We use a 1–element horizontal column. The boundary at the left side of the column is closed but the boundary at the right side is open with a pressure boundary of $1 \cdot 10^5$ Pa. The porosity limit (minimum porosity) ϕ_{\min} is set to 10^{-4} . All other parameters remain the same as in the reference test case. The most important parameters of this test case can be found in Tab. 3.1. The parameter `RE1` is set to 10^{-7} .

Results

The results are shown in Fig. 3.16, Fig. 3.17, Fig. 3.18, Fig. 3.19 and Fig. 3.20. Compared to case *comp-6*, a slower decrease of convergence rate and a slower increase of pressure can be observed (see Fig. 3.16 and Fig. 3.17). The relation between convergence rate and liquid pressure is shown in Fig. 3.18. Since liquid flow is possible through the right hand side boundary, permeability and porosity can decrease to much lower values compared to case *comp-6* (see Fig. 3.19 and Fig. 3.20). The results calculated by TOUGH2-GRS, TOUGH2-MP-GRS, and MARNIE match very well.

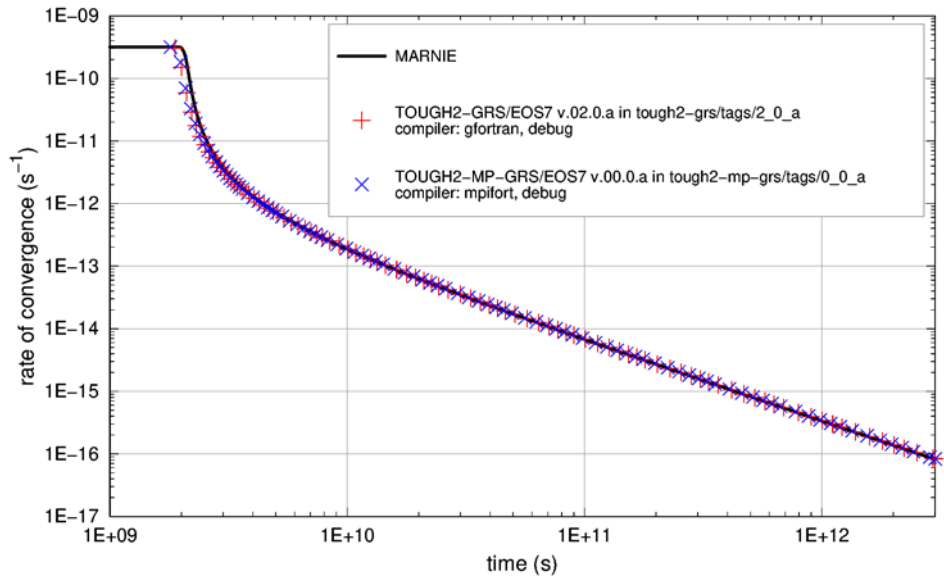


Fig. 3.16 COMP test case *comp-7*: Evolution of convergence rate

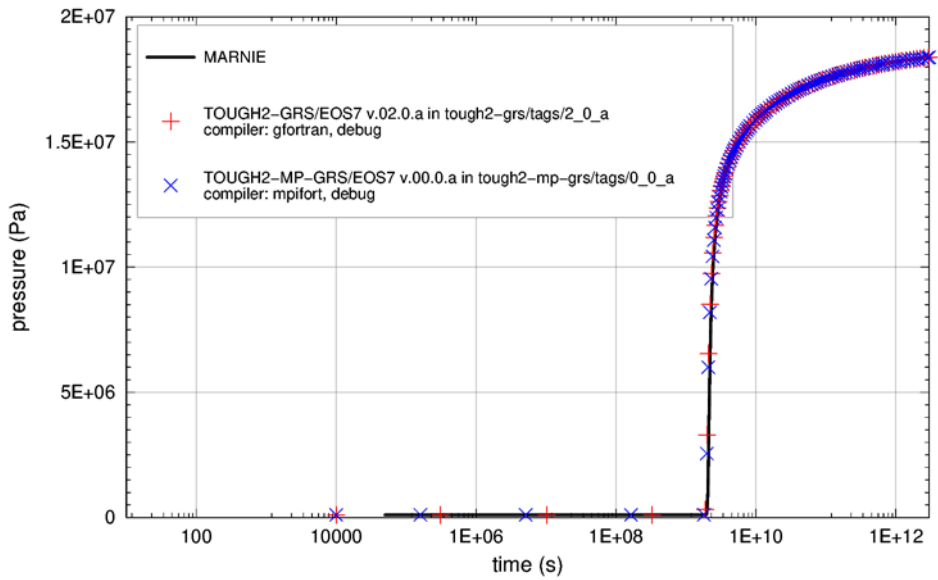


Fig. 3.17 COMP test case *comp-7*: Evolution of liquid pressure

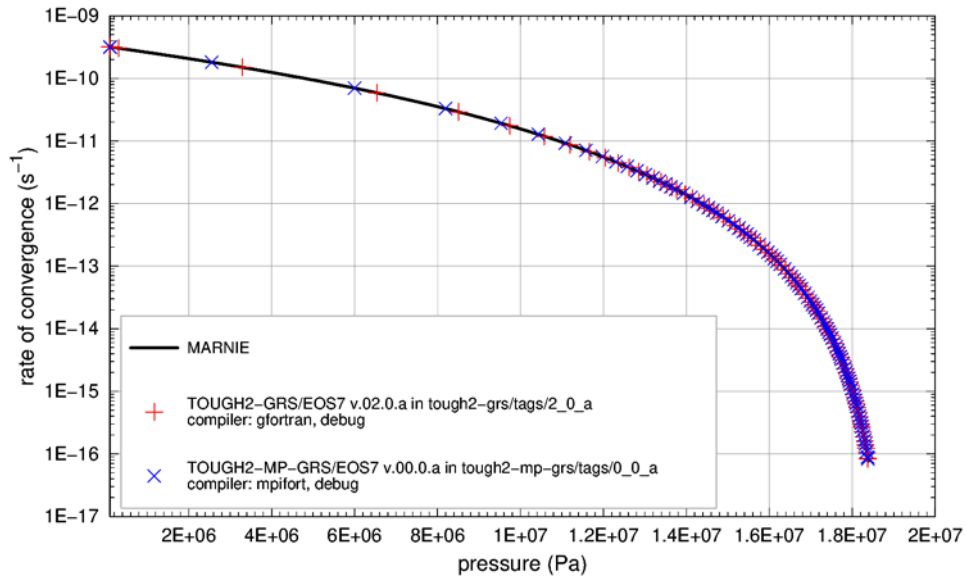


Fig. 3.18 COMP test case *comp-7*: Convergence rate versus pressure

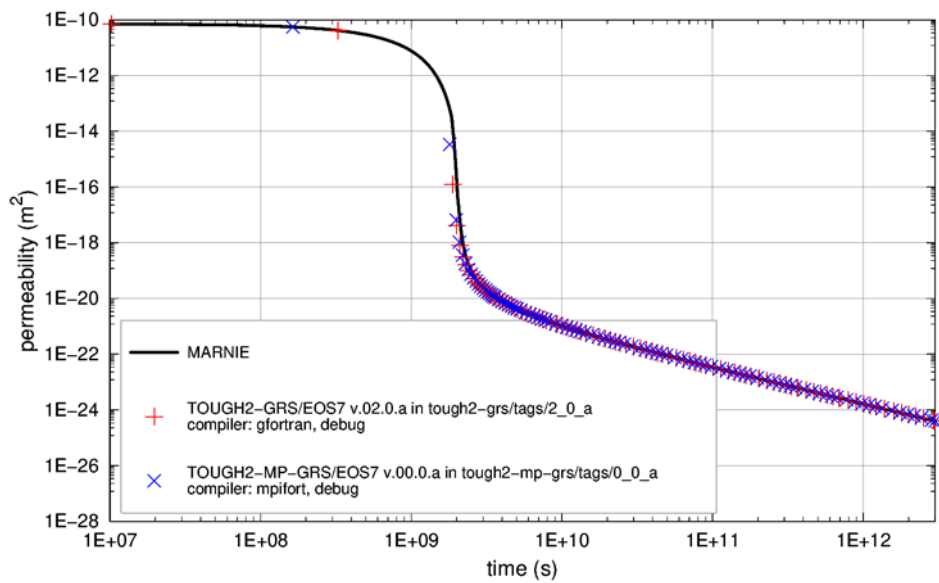


Fig. 3.19 COMP test case *comp-7*: Evolution of permeability

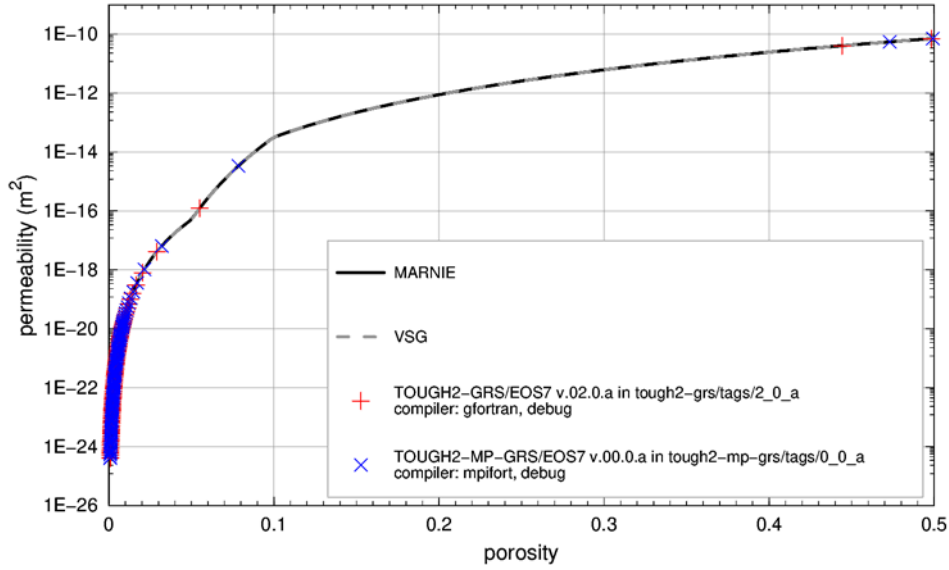


Fig. 3.20 COMP test case *comp-7*: Permeability versus porosity

3.8 Test Case *comp-12a*: f_P and f_T

We consider the pressure and temperature dependency of the convergence process without compacting backfill. The reference porosity ϕ_r is set to 10^{-4} to account for the missing effect of a supporting backfill. The temperature evolution is calculated by considering a heat source with an initial capacity of 17 J/s and a linear decrease until it is switched off after $1.6 \cdot 10^8$ s \approx 50 a.

The model assumptions and the input parameters are identical to those of test case *comp-6* except for the porosity limit ϕ_{\min} of 10^{-3} and the parameters of factor f_T . The constant input parameters for the calculation of factor f_T can be taken from chapter 3.4. The temperature evolution is calculated by considering a heat source with an initial capacity of 17 J/s and a subsequent successive reduction until it is switched off after $1.6 \cdot 10^8$ s \approx 50 a. The parameter `REL` is set to 10^{-7} .

The simulation time is set to 10^{12} s \approx 31800 a. At this time, porosity has decreased to $1.15 \cdot 10^{-3}$ (porosity limit $\phi_{\min} = 10^{-3}$) and pressure has increased to $1.825 \cdot 10^7$ Pa (lithostatic pressure $p_G(z) = 1.88 \cdot 10^7$ Pa). That means that the process of convergence is almost completed.

Results

Fig. 3.22, Fig. 3.23 and Fig. 3.23 show that the calculated results of TOUGH2-GRS, TOUGH2-MP-GRS and MARNIE match very well.

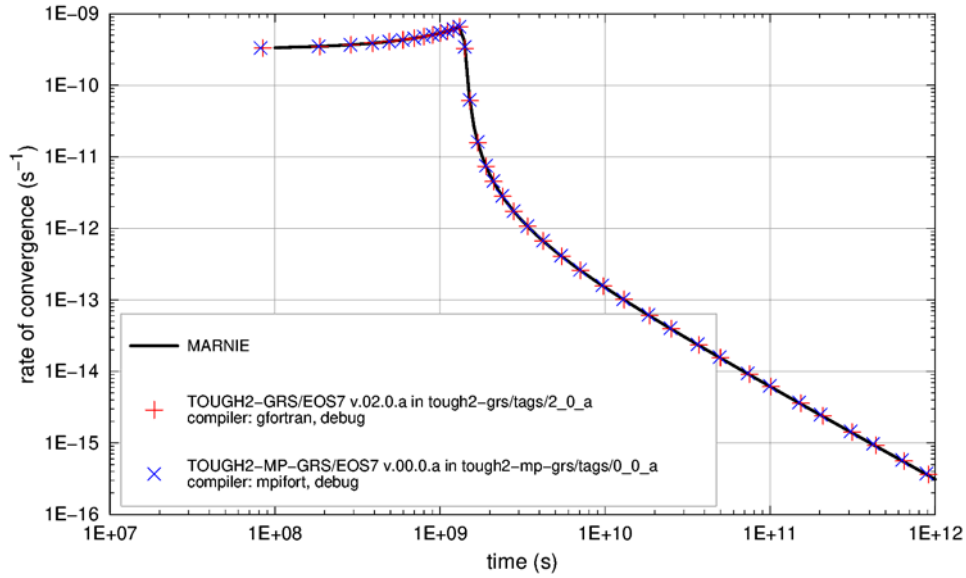


Fig. 3.21 COMP test case *comp-12a*: Evolution of convergence rate

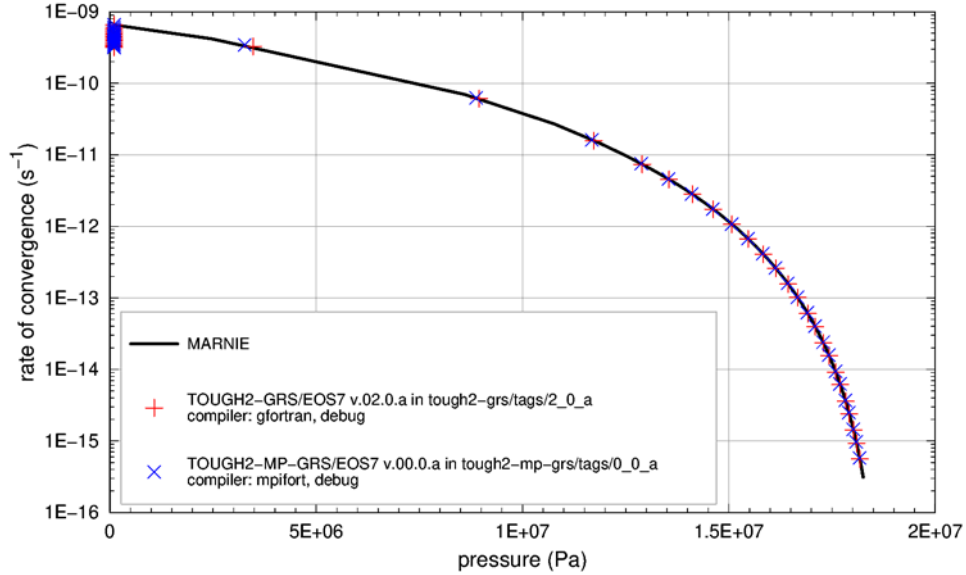


Fig. 3.22 COMP test case *comp-12a*: Convergence rate versus pressure

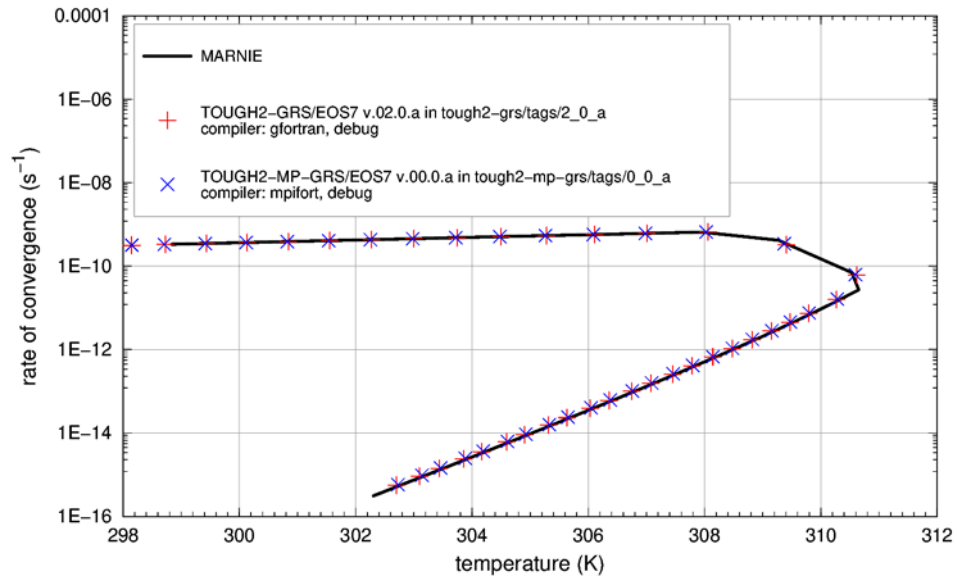


Fig. 3.23 COMP test case *comp-12a*: Convergence rate versus temperature

4 Compressibility Test

This test case has been designed to detect a coding error that has been observed during a code review of TOUGH2/EOS9nt (V2.0, April 2003). The error causes mass conservation errors if porosity is changed due to matrix compression. The test case generates strong porosity changes in order to visualize the effects of a possible coding error.

The model grid is made up of two interconnected elements which are aligned laterally, each with a volume of 1 m³. Both elements are fully saturated with an initial porosity of 0.01 and an initial pressure of 2·10⁵ Pa. Each element holds a water source with constant generation rate of 9·10⁻⁵ kg/sec. Compressibility is set to high value of 0.1 Pa⁻¹ to keep pressure changes small (consequently, water density remains near to constant). Water temperature is set to 4 °C to bring the water density close to 1000 kg/m³ (this does not work for EOS9, which uses a reference temperature). Due to the constant water generation rate porosity should rise linearly from 0.01 at time zero to 0.1 at 1·10⁶ seconds. Fig. 4.1 shows the correct slope of the porosity-time curve. Fig. 4.2 plots the evolution of the porosity error (calculated porosity divided by expected porosity). Values near to 1 show the correct implementation.

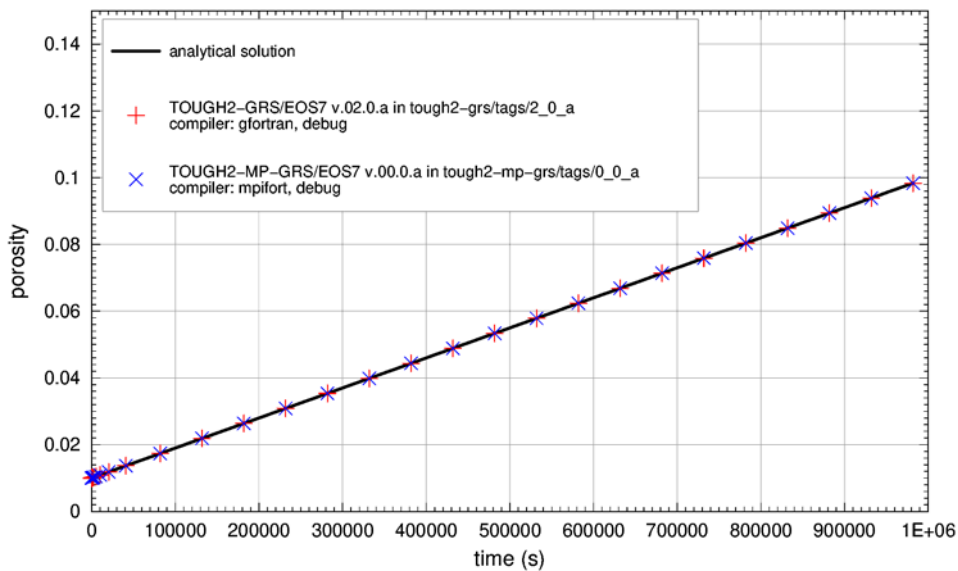


Fig. 4.1 Compressibility test: porosity evolution

Lines should match. Simulated data and analytical solution match sufficiently well.

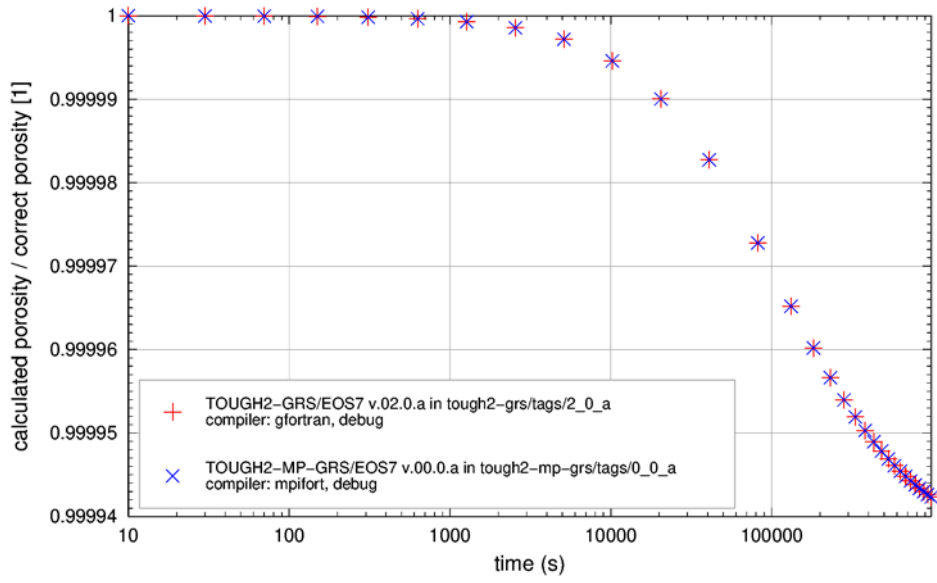


Fig. 4.2 Compressibility test: Evolution of the porosity error

5 CORFL Module

The CORFL module implements the mechanism of seal corrosion described in report /BFS 09/, chapter 7.7, pp. 154 – 166.

This test case describes the corrosion of a horizontal seal under fully saturated conditions calculated by the CORFL module. The seal is composed of 10 elements with a total length $\Delta X = 26$ m and a cross section area $A = 1$ m². There are inactive elements on both ends of the horizontal column defining fixed pressure boundary conditions, which introduce a pressure difference $\Delta P = 1$ MPa between the up and downstream side. The interface distance of these elements is set to a very small value. A constant pressure gradient is prescribed as initial condition using an INCON file. All elements are fully saturated during the entire simulation. The initial brine mass fraction of the seal is 0.98, which is defined (by the CORFL module: $x_{b2} = 0.98$) as non-corrosive water. Corrosive water is injected into the seal from the upstream boundary condition. Liquid with $X_B = X_{B1}$ (here $x_{b1} = 0.97$) is defined as corrosive water for which the parameter κ_L (“Korrosionskapazität” or “Umlösekapazität” /BFS 09/) was determined. The brine properties are set to those of pure water to avoid variable viscosities for the calculation of the effective permeability. The seal has a porosity of $\phi = 0.2$, and an initial permeability of $k_0 = 10^{-18}$ m².

This SITA test case can be run with the EOS7 and EOS7R modules. However, the actual code test runs presented here (in the figures) are on the EOS7 module (of the TOUGH2-GRS and TOUGH2-MP-GRS codes) only.

The analytical solution to this test is derived in report /BEC 09/, pp. 162 – 165. Assuming constant porosities, constant viscosities and no EDZ, the analytical solution (Eqn. 7.36) simplifies to

$$k_{\text{eff}}(n) = \frac{k_0}{1 - n \frac{\phi \kappa_L}{1 - \phi + \phi \kappa_L} (1 - 10^{-\varepsilon})} \quad \text{for } 0 < n < \frac{1}{\phi \kappa_L} - \frac{1}{\kappa_L} + 1, \quad (5.1)$$

where $n = n(t) = V_{\text{inj}}(t)/V_\phi$ is the number of percolations, defined as the volume of the corrosive liquid injected until time t into the (first element of the) saturated seal divided by the seal’s pore volume. κ_L (parameter “UK” in SITA) is defined as the (volumetric) amount of the solid phase that can be corroded by (a standard volumetric amount of) the

corrosive fluid. ε (parameter “Ek” in SITA) is the number of magnitudes of the local permeability increase by corrosion. $k_{\text{eff}} = -F\eta / \left(\rho \frac{\Delta p}{\Delta x} \right)$ is the effective permeability of the whole seal, defined by the actual flux density and the actual pressure gradient. For $n = 0$, the seal has an effective permeability identical to the initial permeability. The seal is fully corroded with an effective permeability of $k_0 10^\varepsilon$ when $n \geq 1/(\phi\kappa_L) - 1/\kappa_L + 1$.

The first three analyses in the SITA test case “Effective Permeability of a Seal” are bound to demonstrate that the evolution of the effective seal permeability in dependence of the number of percolations coincides in the numerical simulation and in the analytical solution (5.1). In the first analysis (see Fig. 5.1), we plot the effective permeability relative increase over the number of percolations, according to the simulation with

$$k_{\text{eff}}(t) = \frac{Q(t)\eta\Delta X}{A\rho\Delta P}, \quad (5.2)$$

where the total flux, $Q(t) = A * F(t)$, at all timestep times, is available in the SITA parameters “FLO(LIQ.)” (OUTFILE) and “Fliq” (COFT file). The number of percolations must be calculated at all timestep times according to

$$n(t) = \frac{V_{\text{inj}}(t)}{V_\phi} = \frac{\int_0^t \frac{Q(t)}{\rho} dt}{A\Delta X\phi}. \quad (5.3)$$

In practice, the integral is calculated as $\rho V_{\text{inj}}(t_k) = Q(t_1)(t_1 - t_0) + 0.5 \sum_{i=2}^k (Q(t_i) + Q(t_{i-1}))(t_i - t_{i-1})$, where $k = 1, 2, 3, \dots$ is the time step number (parameter “KCYC” in TOUGH2) and $V_{\text{inj}}(t_0) = 0$.

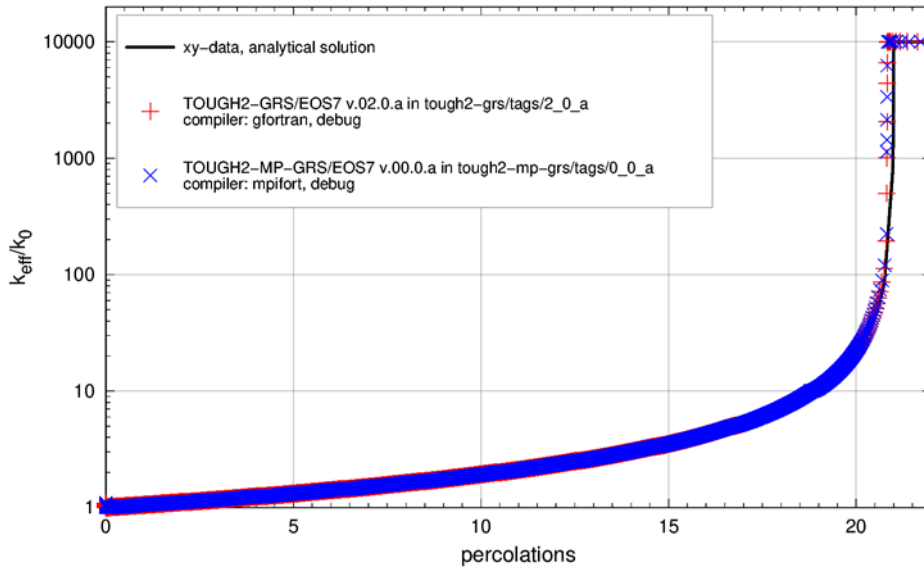


Fig. 5.1 CORFL test: Evolution of the effective seal permeability

There is a good agreement between the numerical and the analytical solution.

Module CORFL changes the brine mass fraction because of the corrosion process. The module aims at implementing this as an isobaric process, which means that the pressure in the seal should remain the same. Fig. 5.2 shows that the CORFL module works correctly with regard to this aspect.

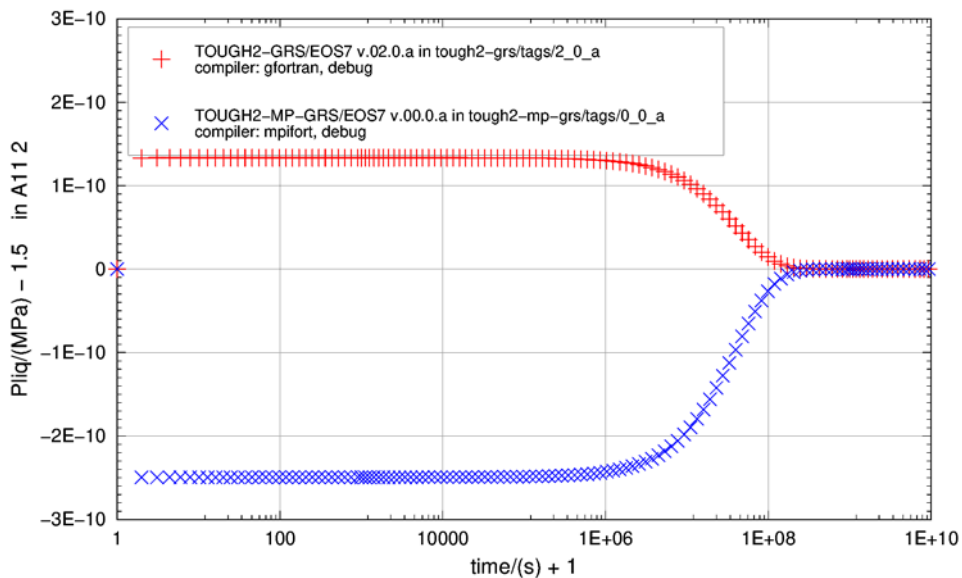


Fig. 5.2 CORFL test: Pressure evolution inside the seal

Pressure changes should be negligible.

6 CORRO Module

The CORRO module implements the processes of gas production and water consumption due to metal corrosion. Several test cases have been derived from a reference test case to test the different functions and options of the module.

6.1 Reference test case

The reference case uses all three water sources (canister water, water component and brine component) to generate gas. A gas source is placed in a closed system, which is composed of two interconnected elements (element volume: 2 m³, porosity: 0.5). Gas sources are distributed homogeneously in the domain so that both elements have the same gas production. Consequently, no flow should take place between both elements.

Both elements have an initial liquid saturation of 0.01 and an initial brine mass fraction of 0.9. It is assumed that the brine component has a consumable water fraction of $\text{CORRO_waterMassPerBrineMass} = 0.5$ (i. e. consumption of 1 kg of physical water would require the consumption of 2 kg brine). The initial mass of canister water is $\text{CORRO_canisterWaterMass} = 0.5$ kg. The initial gas pressure is 0.1 MPa.

The gas source, which is distributed homogeneously between the two elements, can produce $\text{CORRO_moleGas} = 50000$ mol of gas at maximum. The corrosion rate is $1 \cdot 10^{-8}$ mol/s. This value remains constant ($\text{CORRO_B} = 0$) throughout the simulation. We assume that one mole of water is consumed per mole of produced gas (by setting $\text{CORRO_moleWaterPerMoleGas} = 1$). The following CORRO options have been used.

- Consumption of canister and pore water
($\text{CORRO_consumeWater} = 1$ and $\text{CORRO_consumePoreWater} = 1$)
- Corrosion is independent of liquid saturation ($\text{CORRO_assumeWaterTable} = 0$)
- The rate function is an exponential function ($\text{CORRO_useFunction2} = 0$)
- Corrosion depends on the degree of corrosion ($\text{CORRO_dependsOnTime} = 0$)

Analytical functions are defined for the temporal evolution of gas pressure, liquid saturation, degree of corrosion, brine mass fraction, and canister water mass. All functions are based on piecewise linear functions for the consumed mass of canister water, water component, and brine component as well as for the produced amount of gas.

The liquid density is used to calculate liquid saturation from water and brine component masses. Liquid density is calculated using the corresponding function of the EOS7 module

$$\rho = \frac{1}{\frac{1 - X_b}{\rho_w} + \frac{X_b}{\rho_b}}$$

The density of pure water ρ_w and the density of the reference brine ρ_b are assumed to be approximately independent of pressure.

Figures Fig. 6.1 to Fig. 6.4 show the evolution of gas pressure, degree of corrosion, liquid saturation and brine mass fraction for the reference case.

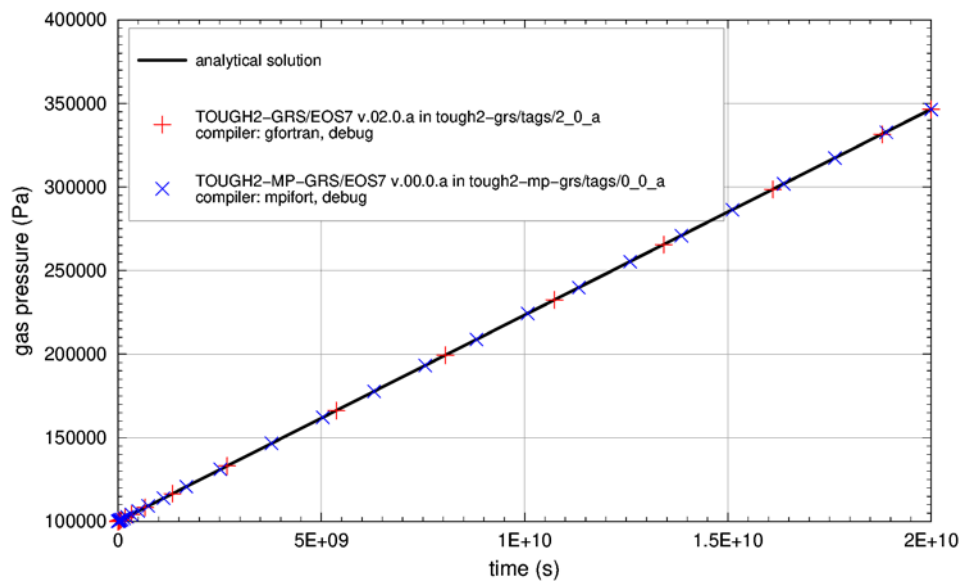


Fig. 6.1 Evolution of the gas pressure

The constant gas generation rate and the near to constant saturation lead to a linear pressure increase. The simulation and the analytical solution match very well.

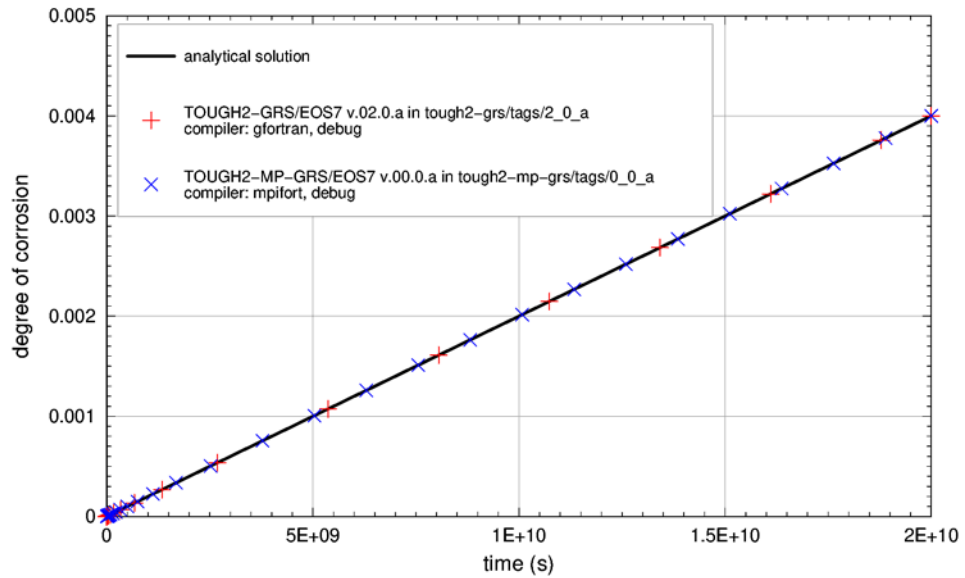


Fig. 6.2 Evolution of the degree of corrosion

The degree of corrosion increases linearly due to the constant generation rate. The simulation and the analytical solution match very well.

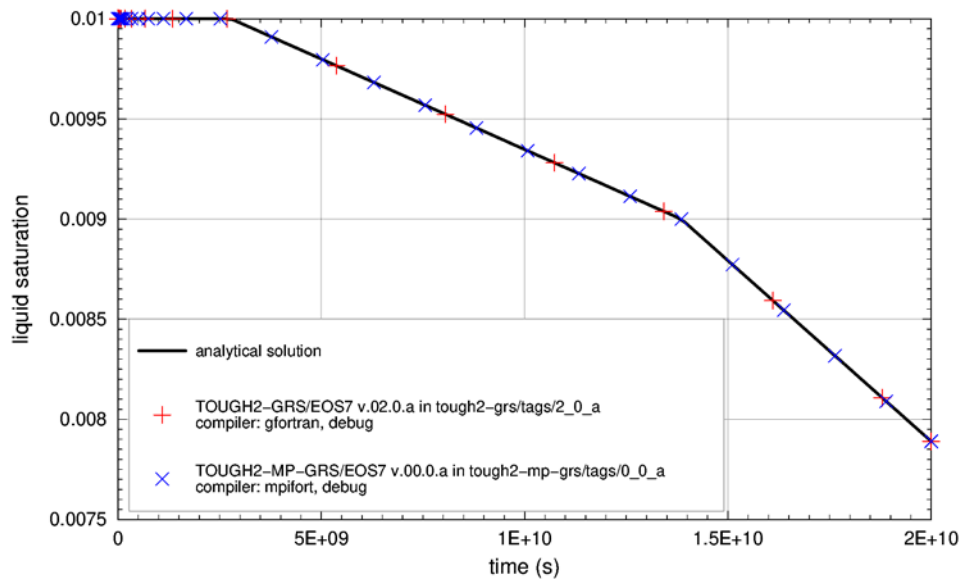


Fig. 6.3 Evolution of the liquid saturation

The curve should show three stages: In the first stage, canister water is consumed, which has no effect on liquid saturation. In the second phase, the water component is consumed. In the third stage, there is only brine consumption. The slope should steepen by a factor of 2 in the transition from stage two to three because the reference brine has a water mass fraction of 50 %. The simulation and the analytical solution match very well.

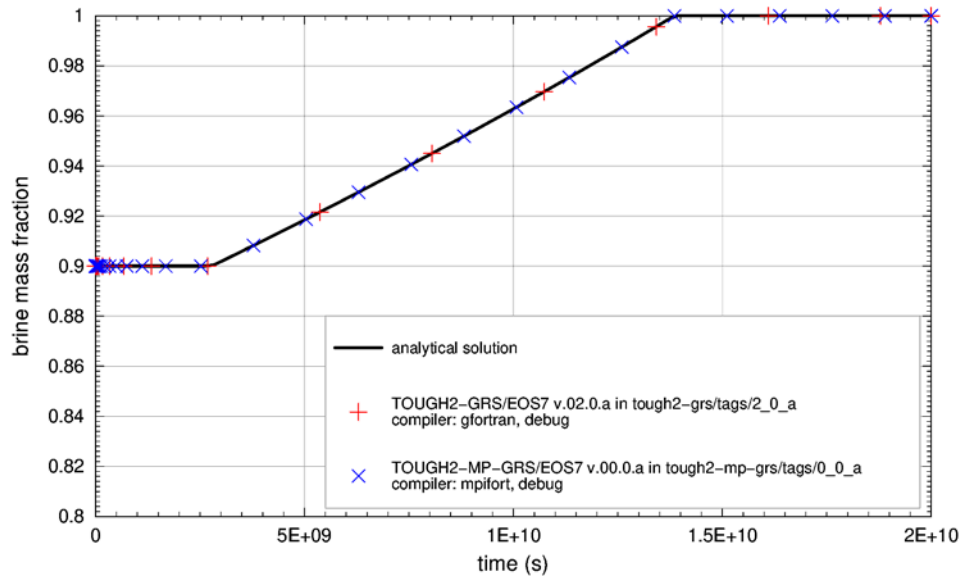


Fig. 6.4 Evolution of the brine mass fraction

The curve shows three stages: Brine mass fraction remains constant in the first stage because only canister water is consumed. In stage 2, the consumption of the water component raises the brine mass fraction. A value of 1 should be reached. Note that some versions of the CORRO module consume either the water or the brine component during a time step (never both), so that only brine is consumed if there is not enough water available. This may lead to the presence of residual water.

6.2 Test cases derived from the reference case

Several test cases have been derived from the reference case to test different functions of the CORRO module. Tab. 6.1 gives a complete list of these test cases. The corresponding figures are listed for every test case.

Tab. 6.1 Test cases for the CORRO module, which have been derived from test case number 1 (the reference test case)

Note that the sources are assigned to materials in the reference case, so that every element receives gas sources with halved corrosion rate, canister water, and total amount of gas.

No.	Test case file and intended system behaviour	Changed input parameters (Input parameters are explained in /NAV 16/. Arrows indicate value changes relative to reference case.)	Figures
2	corro-limitedgasamount.json Complete corrosion during simulation time.	CORRO_moleGas: 50000 mole → 50 mole	Fig. 6.5
3	corro-limitedsaturation.json Corrosion should stop as liquid saturation reaches 0.009. The water component should be consumed completely.	CORRO_Sliqempty: 0 → 0.009 Initial brine mass fraction: 0.9 → 0.95	Fig. 6.6, Fig. 6.7

No.	Test case file and intended system behaviour	Changed input parameters (Input parameters are explained in /NAV 16/. Arrows indicate value changes relative to reference case.)	Figures
5	corro-rundry.json Total consumption of liquid due to an increased corrosion rate.	CORRO_Aliquid: $1 \cdot 10^{-8} \rightarrow 1 \cdot 10^{-7}$	Fig. 6.8
6	corro-superposition.json Same as reference case.	The reference case assigns a single gas source to the entire domain. This gas source is split up into three sources. One is assigned to the domain, the two others to the two elements, in order to check the source assignment algorithm.	Fig. 6.9, Fig. 6.10
7	corro-noporewaterconsumption.json Only canister water is consumed.	CORRO_consumePoreWater: $1 \rightarrow 0$	Fig. 6.11
8	corro-onlycanisterwater.json Unsaturated system. Only canister water is consumed.	Initial gas saturation: $0.99 \rightarrow 1$ Initial brine mass fraction: $0.9 \rightarrow 0$ CORRO_B: $0 \rightarrow -1 \cdot 10^{-30}$ (uses different parts of the program as 0) CORRO_Aliquid: $1 \cdot 10^{-8} \rightarrow 1 \cdot 10^{-7}$	Fig. 6.12
9	corro-nowaterconsumption.json Gas production without water consumption.	CORRO_consumeWater: $1 \rightarrow 0$	Fig. 6.13, Fig. 6.14
10	corro-watertable.json Linear increase of saturation causing an increase of the corrosion rate.	Grid changed: A single element is placed between two fully saturated, inactive elements with gas pressures of 3 MPa and 1 MPa. Initially, the central element is unsaturated and has a gas pressure of 2 MPa. CORRO_assumeWaterTable: $0 \rightarrow 1$ CORRO_Avapour: $0 \rightarrow 1 \cdot 10^{-9}$ CORRO_canisterWaterMass: $0.5 \rightarrow 0$ Gas source is placed in one element, only.	Fig. 6.15
11	corro-dependsontime.json Corrosion rate is an exponential function of time.	CORRO_dependsOnTime: $0 \rightarrow 1$ CORRO_consumeWater: $0 \rightarrow 1$ CORRO_Aliquid = $1 \cdot 10^{-8} \rightarrow 2 \cdot 10^{-8}$ CORRO_B = $-1 \cdot 10^{-8}$	Fig. 6.16
12	corro-erroneouslocationtype.json Simulation should fail.	Input data contains unknown location type 'Z'.	(simulation has failed)
13	corro-powerlaw-notimedependency.json Corrosion rate is a power function of the degree of corrosion.	CORRO_useFunction2: $0 \rightarrow 1$ CORRO_consumePoreWater: $1 \rightarrow 0$ CORRO_moleGas: 50000 mol \rightarrow 5500 mol (Canister water sufficient for complete corrosion of gas source) CORRO_f2_a: $1 \cdot 10^{-4}$ CORRO_f2_n: -0.6 CORRO_f2_t0: $1 \cdot 10^6$ CORRO_f2_tref: $1 \cdot 10^6$	Fig. 6.17
14	corro-powerlaw-timedependency.json Corrosion rate is a power law function of the degree of time.	CORRO_useFunction2: $0 \rightarrow 1$ CORRO_dependsOnTime: $1 \rightarrow 0$ CORRO_moleGas: 50000 mol \rightarrow 5500 mol (Canister water sufficient for complete corrosion of gas source) CORRO_f2_a: $1 \cdot 10^{-4}$ CORRO_f2_n: -0.6 CORRO_f2_t0: $1 \cdot 10^6$ CORRO_f2_tref: $1 \cdot 10^6$	Fig. 6.18

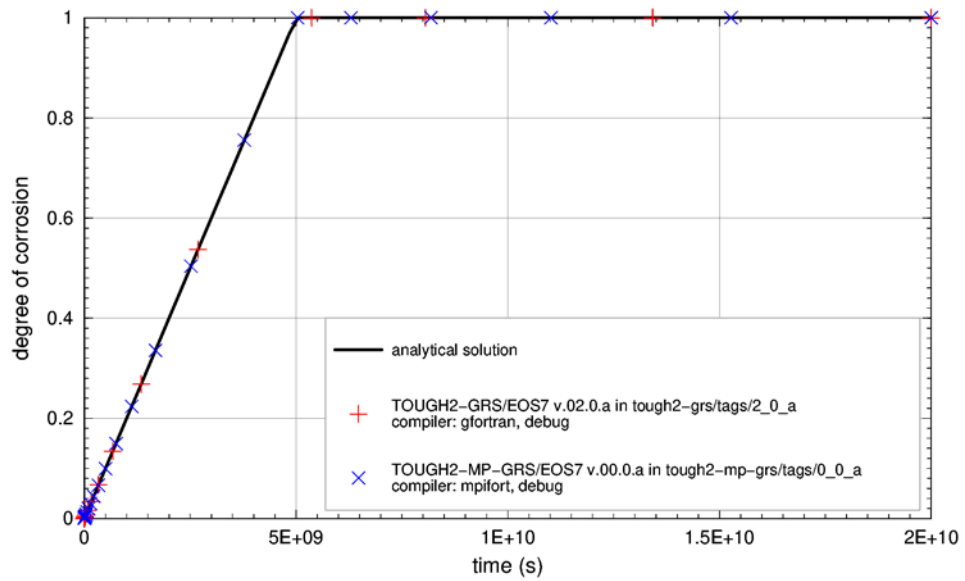


Fig. 6.5 CORRO test case 2: Degree of corrosion

Complete corrosion is achieved at $5 \cdot 10^9$ seconds due to the reduced amount of producible gas. The simulation matches the analytical solution very well.

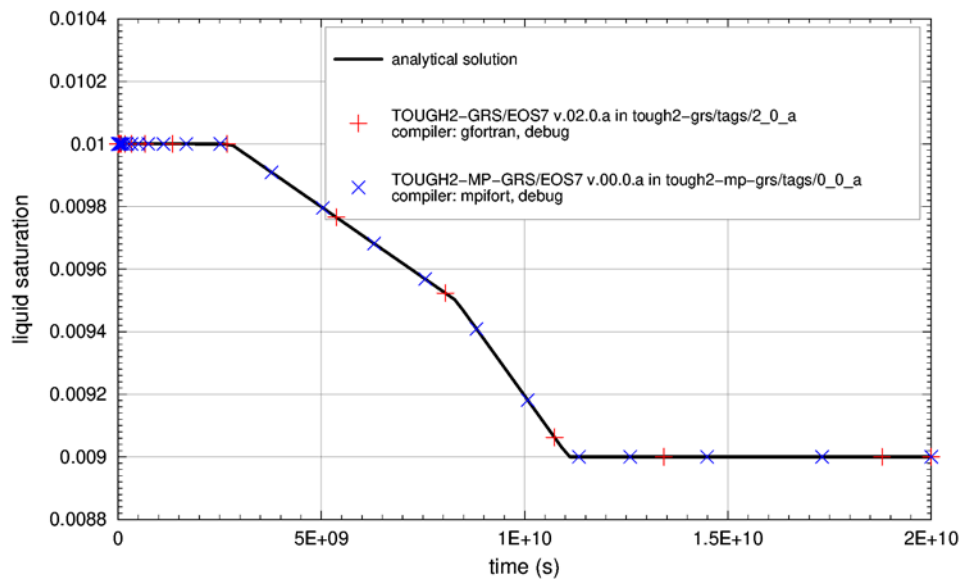


Fig. 6.6 CORRO test case 3: Liquid saturation

Corrosion should stop as soon as the liquid saturation reaches the limiting value of 0.009. The simulation matches the analytical solution very well.

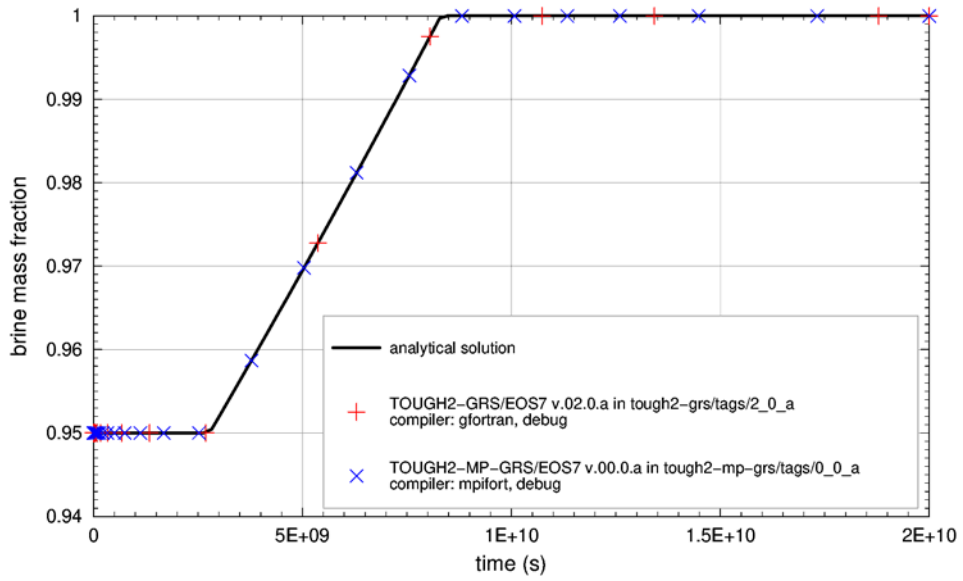


Fig. 6.7 CORRO test case 3: Brine mass fraction

The brine mass fraction should reach the value of 1 due to the reduced mass of the water component. The simulation matches the analytical solution very well.

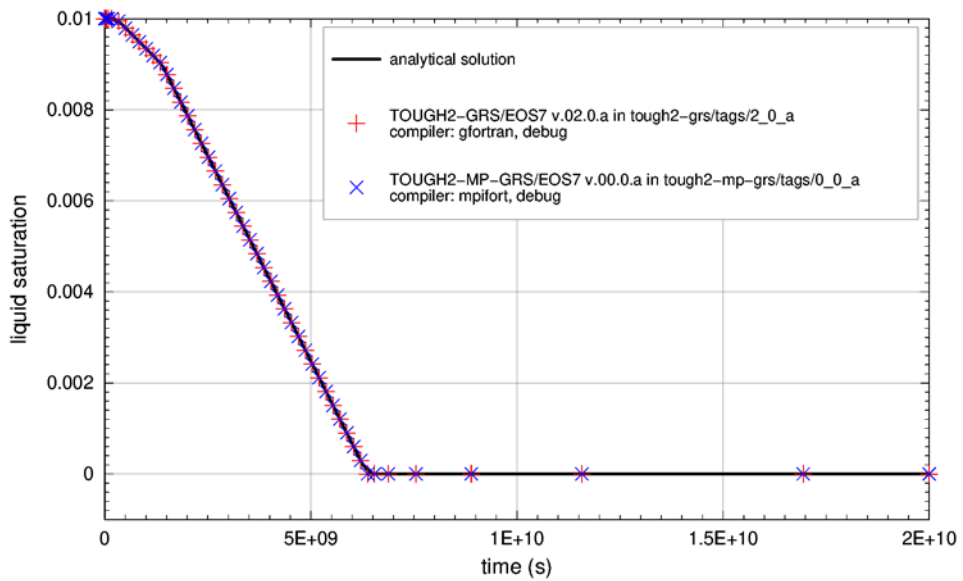


Fig. 6.8 CORRO test case 5: Liquid saturation

Total consumption of liquid (which causes problems with some EOS modules) due to an increased corrosion rate. The simulation does not fail at the transition to zero saturation. The simulation matches the analytical solution very well.

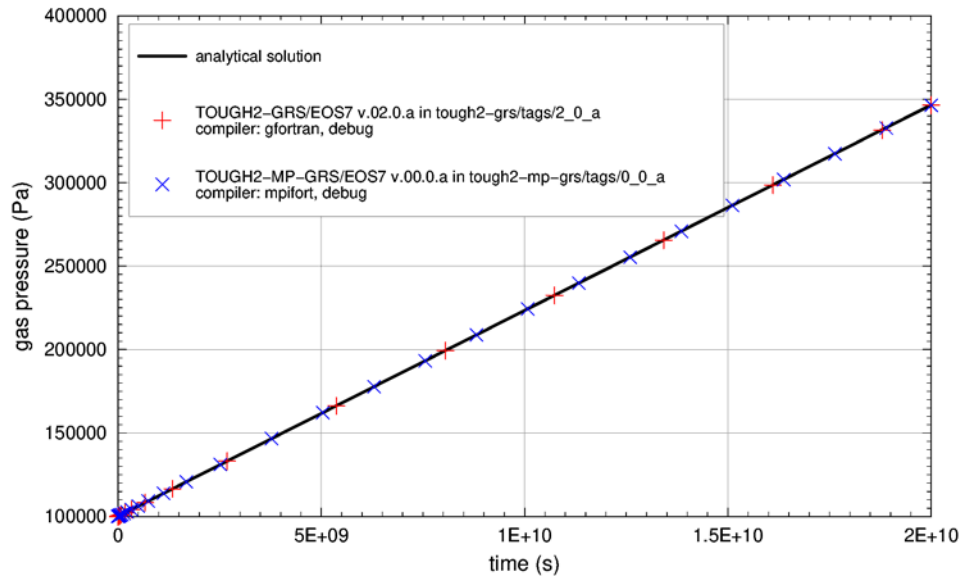


Fig. 6.9 CORRO test case 6: Gas pressure

Errors in the amount of produced gas should affect the gas pressure evolution. The simulation matches the analytical solution very well.

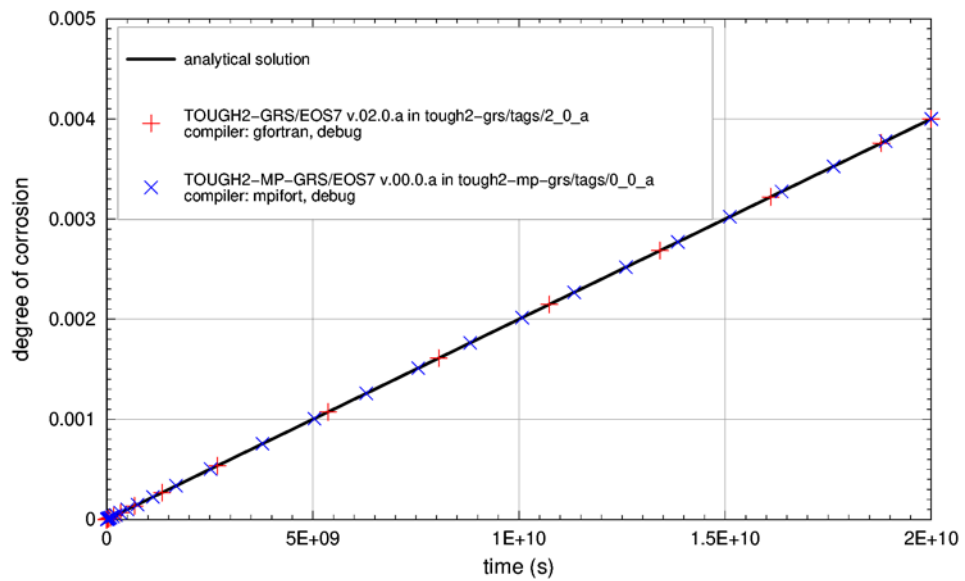


Fig. 6.10 CORRO test case 6: Mean degree of corrosion for all sources

The evolution of the degree of corrosion of should equal that of the reference case. The simulation matches the analytical solution very well.

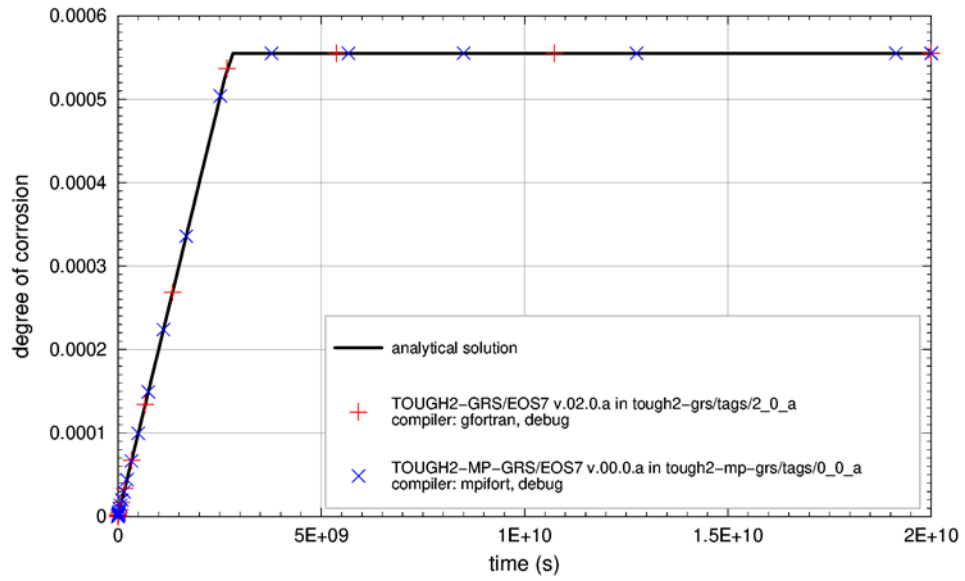


Fig. 6.11 CORRO test case 7: Degree of corrosion

Corrosion should stop as soon as the canister water has been consumed. The simulation matches the analytical solution very well.

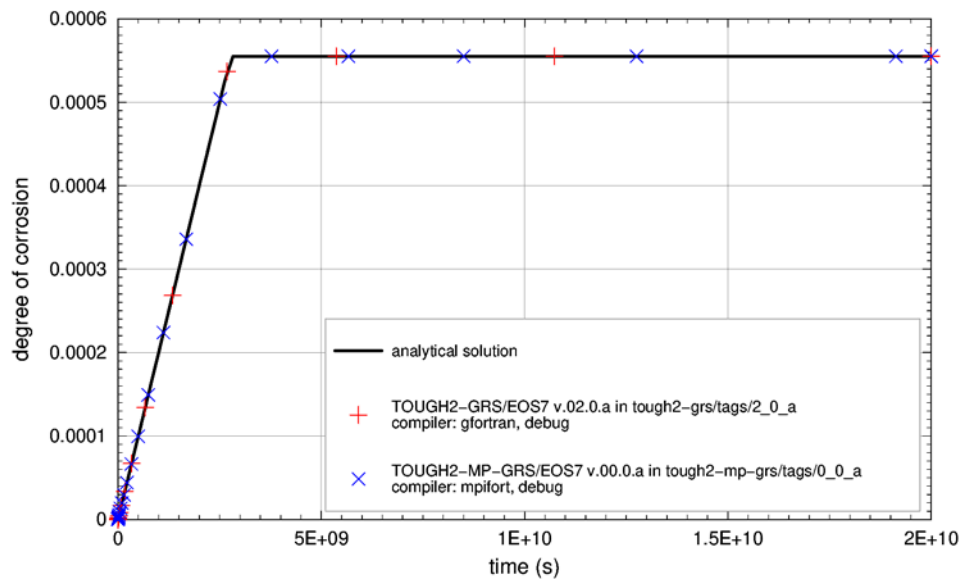


Fig. 6.12 CORRO test case 8: Degree of corrosion

The stability of the module under unsaturated conditions is tested. Corrosion stops as soon as the canister water is consumed. The simulation matches the analytical solution very well.

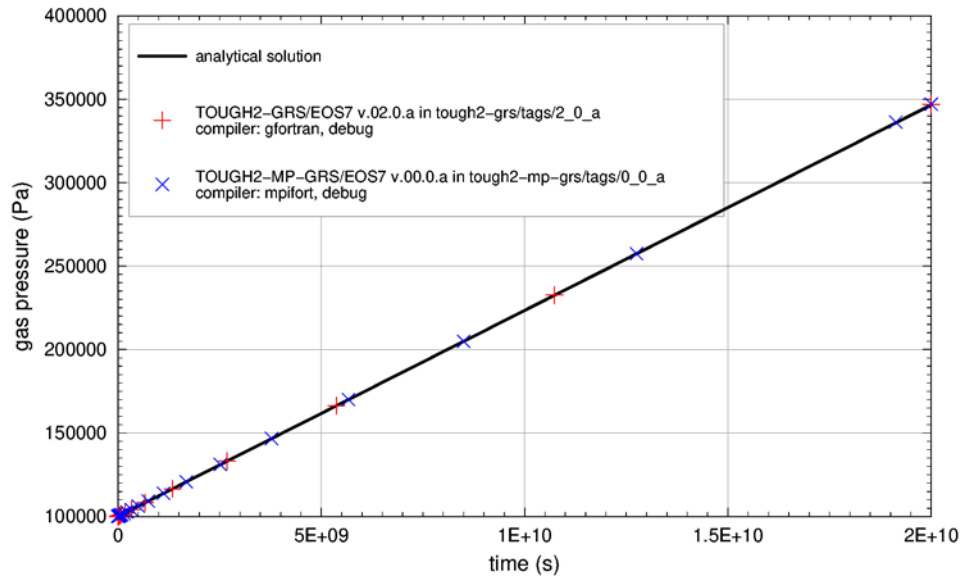


Fig. 6.13 CORRO test case 9: Gas pressure

No water should be consumed. This should not affect the evolution of the gas pressure. The simulation matches the analytical solution very well.

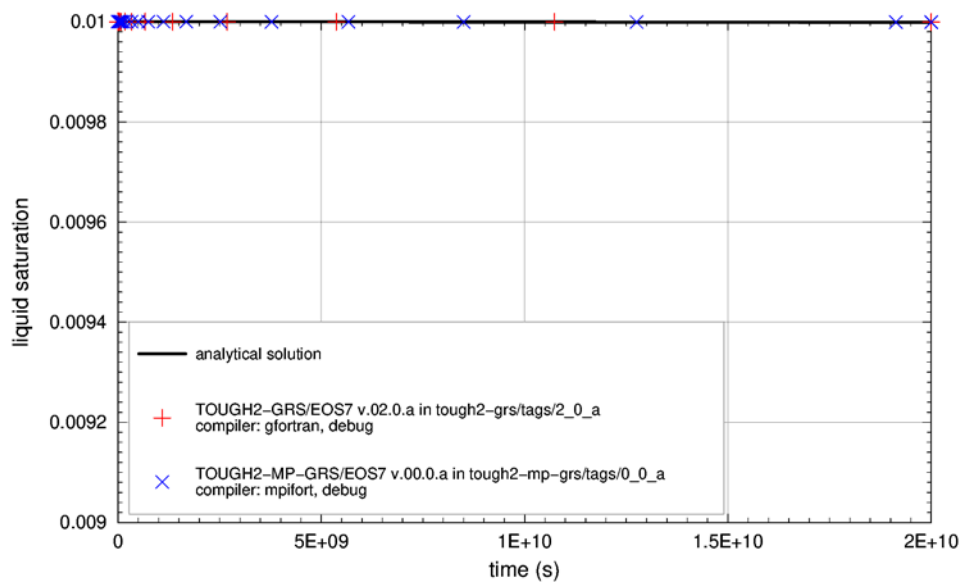


Fig. 6.14 CORRO test case 9: Liquid saturation

No pore water is consumed. The simulation matches the analytical solution very well.

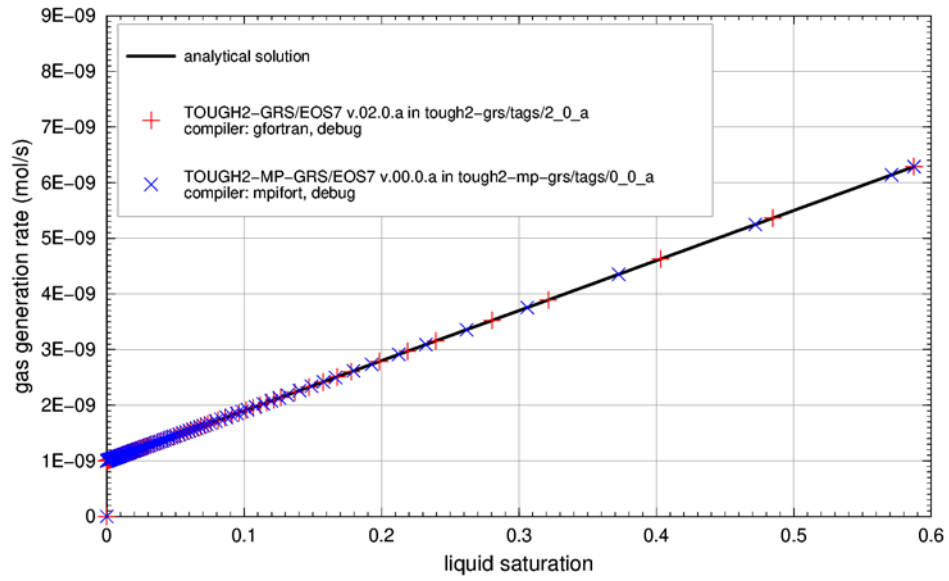


Fig. 6.15 CORRO test case 10: Gas generation rate

Liquid saturation rises and increases the gas generation rate. The simulation matches the analytical solution very well.

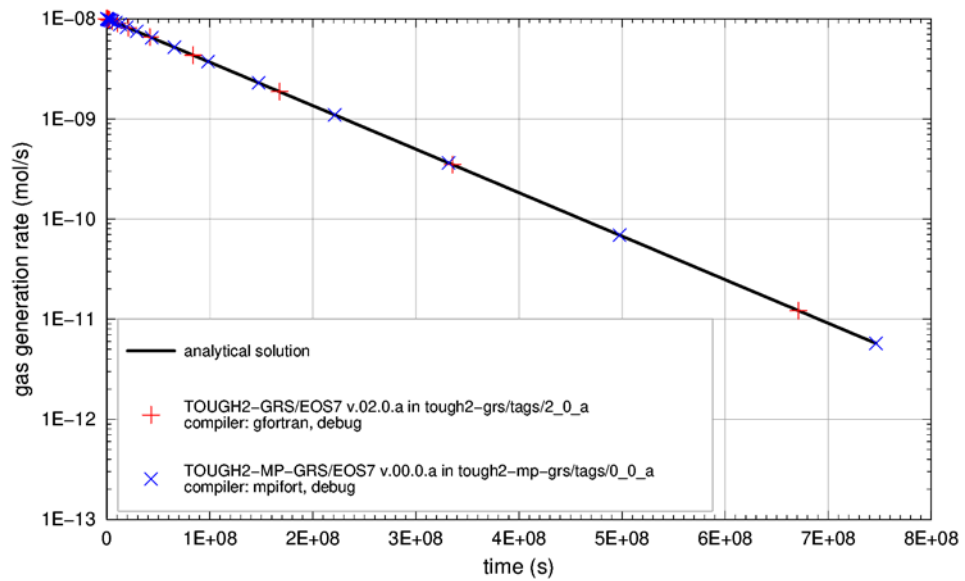


Fig. 6.16 CORRO test case 11: Gas generation rate

Gas generation rate is an exponential function of time. The simulation matches the analytical solution very well.

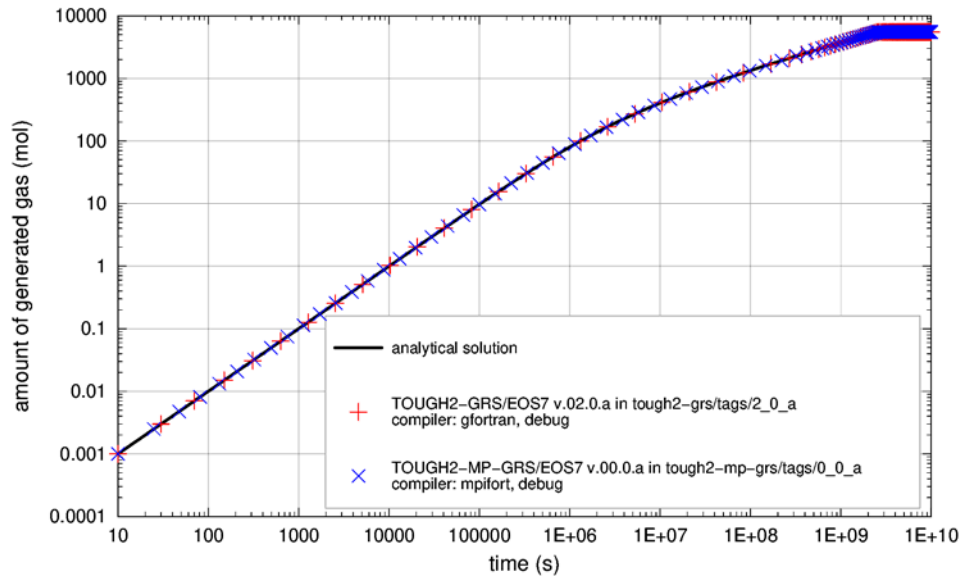


Fig. 6.17 CORRO test case 13: Amount of gas produced over time

Corrosion rate is a power function of the degree of corrosion. TOUGH2-GRS uses mean corrosion rates to match the evolution of the gas amount produced over time. The simulation matches the analytical solution very well.

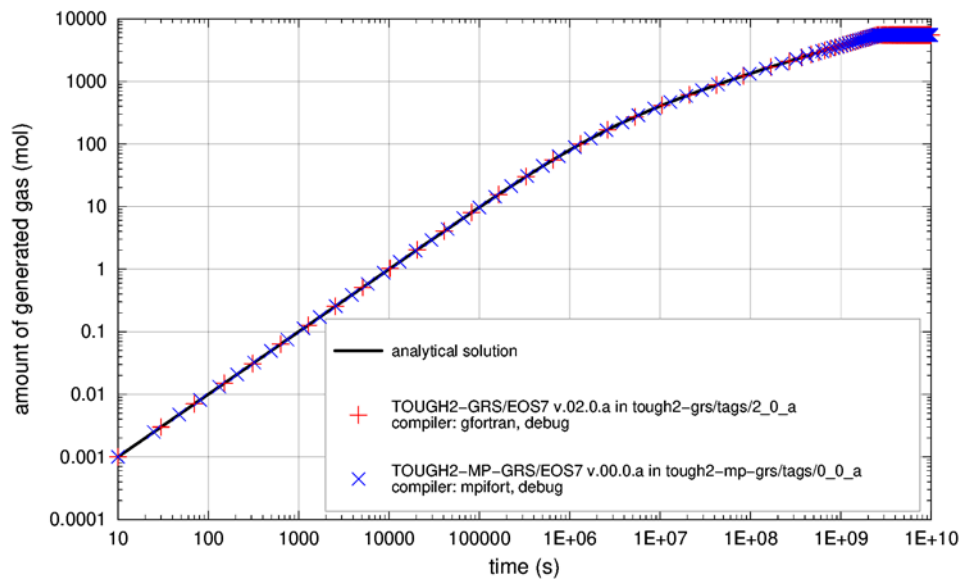


Fig. 6.18 CORRO test case 14: Amount of gas produced over time

Corrosion rate is a power function of time. TOUGH2-GRS uses mean corrosion rates to match the evolution of the gas amount produced over time. The simulation matches the analytical solution very well.

7 DEGRA Module

To test the DEGRA module we observe a simple system composed of a single percolated element, which changes its permeability with time. The initial permeability of the element is $1 \cdot 10^{-15} \text{ m}^2$. The DEGRA module increase the permeability linearly between $1 \cdot 10^{10} \text{ sec}$ and $2 \cdot 10^{10} \text{ sec}$ to a value of $1 \cdot 10^{-14} \text{ m}^2$. Since details of the flow system are not relevant here, they will not be described. Fig. 7.1 shows that the code matches the target function very well.

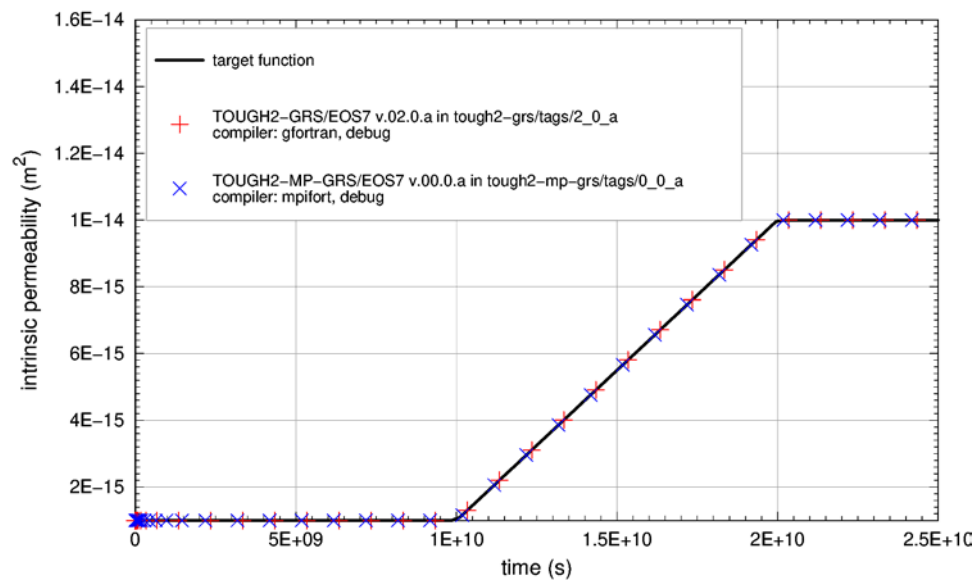


Fig. 7.1 DEGRA test: Evolution of the intrinsic permeability

8 FISS Module

We use a simple model to check the correctness of the implemented models of the FISS module for permeability, porosity, and threshold pressure change.

We consider a column of 4 elements, each element having a volume of 0.25 m³. Initially, all elements have a pressure of 0.1 MPa and are filled with gas. Gas sources with a constant rate of 1·10⁻⁷ kg/s are placed in elements 1 and 2. Element 3 is a seal with zero permeability. The gas pressure is expected to rise to the threshold pressure for micro fissuring. Element 4 is an inactive element with a gas pressure of 0.1 MPa and therefore introduces a fixed potential for the outflow of gas. Please note that gas can flow into the seal at pressures below the threshold pressure, because the fissure module only prevents gas from leaving the seal.

8.1 Fissure permeability as a linear function of the excess pressure

Test case `fiss-ifsoft0-ifpor0-ifper2-reference.json` introduces a threshold pressure of 0.2 MPa and links fissure permeability linearly to the excess pressure (pressure minus threshold pressure). The following parameters are used:

- No softening: `ifsoft=0`
- Zero fissure porosity: `ifpor=0`
- Fissure permeability is a linear function of the excess pressure: `ifper=2`, `fper(1)=0`, `fper(2)= 1·105`, `fper(3)=0`, `fper(4)=1·10-18`, `fper(5)=1`.
- Initial threshold pressure (`pthr0`): 2·10⁵ Pa

Fig. 8.1 shows the correctness of the implemented permeability–pressure relationship.

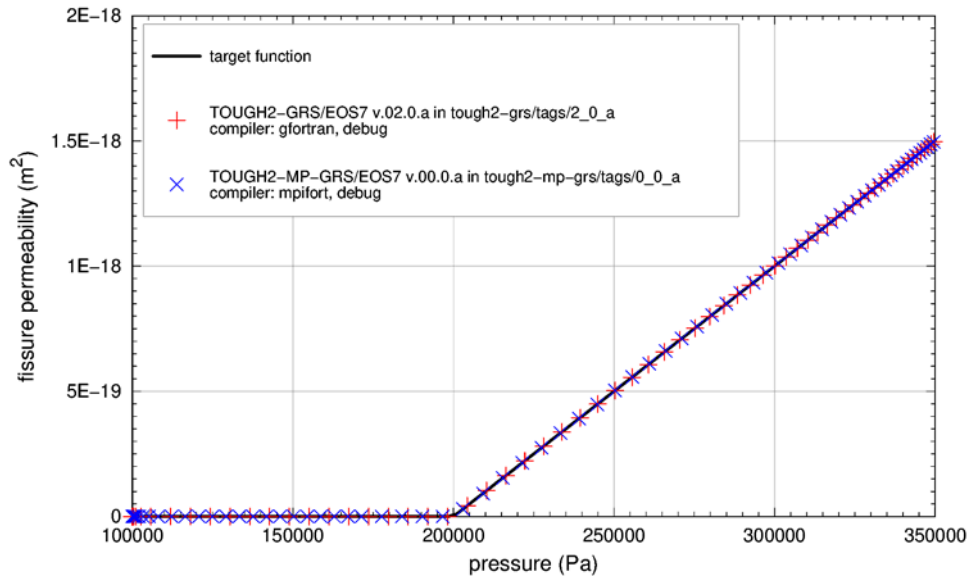


Fig. 8.1 FISS test: Relationship between fissure permeability and gas pressure

8.2 Pressure-dependent porosity with porosity-dependent permeability

Test case `fiss-ifsoft0-ifpor2-ifper1.json` introduces a threshold pressure of 0.2 MPa and links fissure permeability linearly to fissure porosity. Fissure porosity is a power-law function of the excess pressure. The following parameters are used:

- No softening: `ifsoft=0`
- Pressure-dependent fissure porosity following a power-law with upper cut-off: `ifpor=2`, `fpor(1)=1·105`, `fpor(2)=0.01`, `fpor(3)=1`, `fpor(4)=1`, `fpor(5)=0`.
- No time-dependency of porosity change: `fpor(5)=0`.
- Fissure permeability is a linear function of fissure porosity: `ifper=1`, `fper(1)=0`, `fper(2)= 0.01`, `fper(3)=0`, `fper(4)=1·10-18`, `fper(5)=1`.
- Initial threshold pressure (`pthr0`): $2 \cdot 10^5$ Pa.

Fig. 8.2 and Fig. 8.3 show the correctness of the implemented porosity–pressure and permeability–porosity relationships.

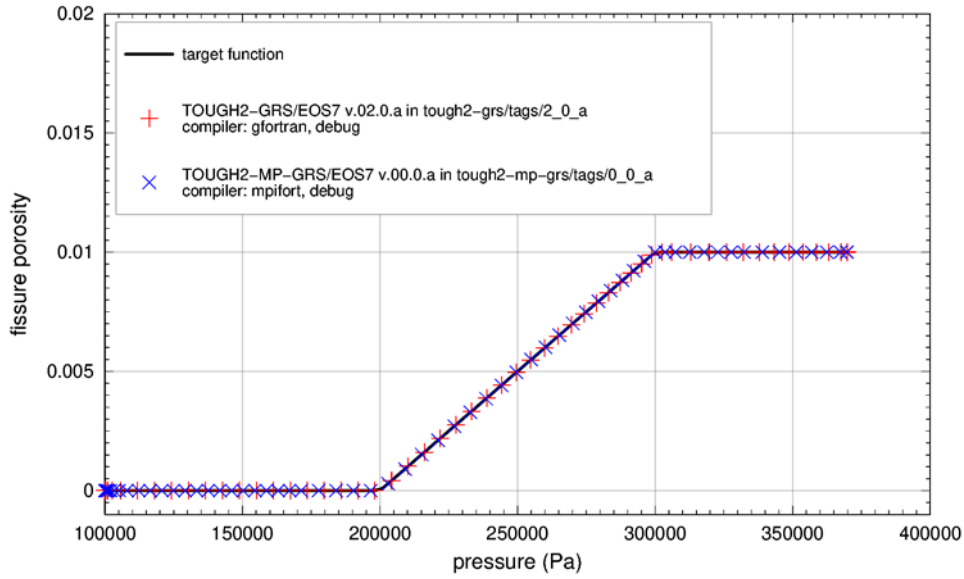


Fig. 8.2 FISS test: Relationship between fissure porosity and gas pressure

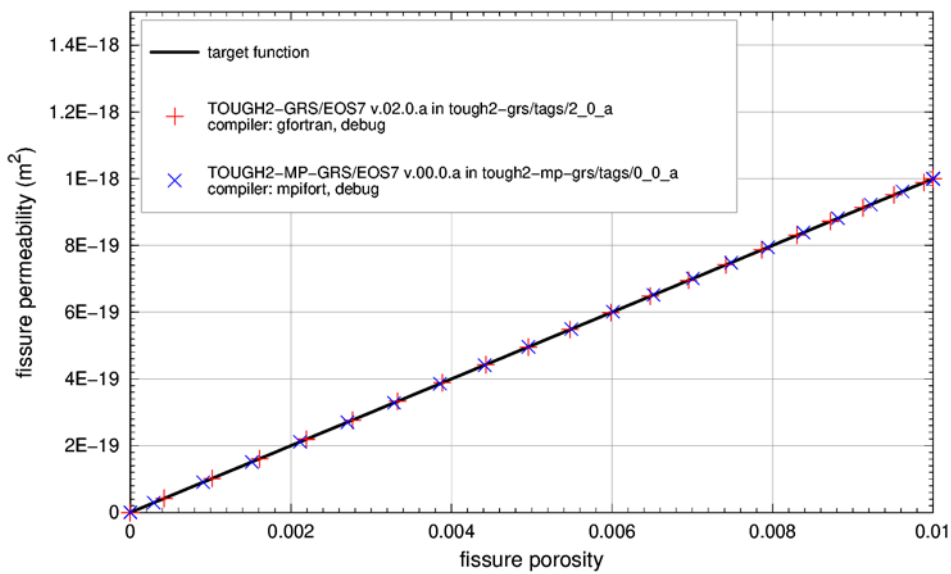


Fig. 8.3 FISS test: Relationship between fissure permeability and fissure porosity

8.3 Positive rate limit for porosity change

Test case `fiss-ifsoft0-ifpor1-ifper1.json` resembles the last test case except for the positive rate limit of porosity change. The following parameters are used:

- No softening (`ifsoft=0`)
- Fissure porosity tries to switch from 0 to 0.01 (`ifpor=1`). `fpor(1)=0.01`.

- Positive rate limit for porosity change: $fpor(5)=1$, $fpor(6)= 2 \cdot 10^{-9}$
- Fissure permeability is a linear function of fissure porosity: $ifper=1$, $fper(1)=0$, $fper(2)= 0.01$, $fper(3)=0$, $fper(4)= 1 \cdot 10^{-18}$, $fper(5)=1$.
- Initial threshold pressure ($pthr0$): $2 \cdot 10^5$ Pa.

Fig. 8.4 shows a constant porosity change rate, which is correct.

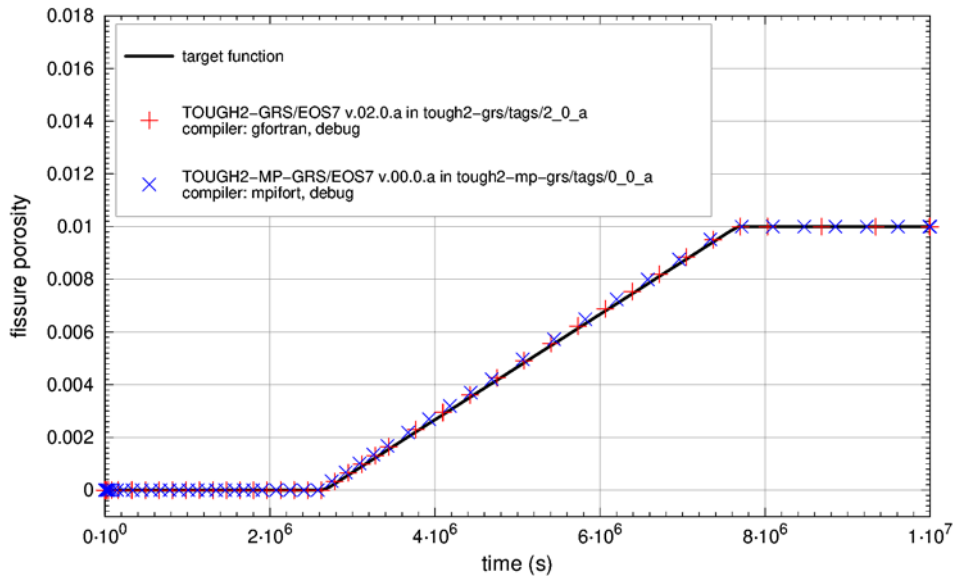


Fig. 8.4 FISS test: Evolution of fissure porosity for a constant rate of porosity change

8.4 Exponential decrease of the porosity change rate

Test case `fiss-ifsoft0-ifpor1-ifper1-b.json` resembles the last test case except for the exponential decrease of the porosity change. The following parameters are used:

- No softening ($ifsoft=0$)
- Fissure porosity tries to switch from 0 to 0.01 ($ifpor=1$). $fpor(1)=0.01$.
- Positive rate limit for porosity change: $fpor(5)=2$, $fpor(6)= 1 \cdot 10^6$
- Fissure permeability is a linear function of fissure porosity: $ifper=1$, $fper(1)=0$, $fper(2)= 0.01$, $fper(3)=0$, $fper(4)= 1 \cdot 10^{-18}$, $fper(5)=1$.

- Initial threshold pressure (pthr0): $2 \cdot 10^5$ Pa.

Fig. 8.5 shows the correct implementation of this porosity change model.

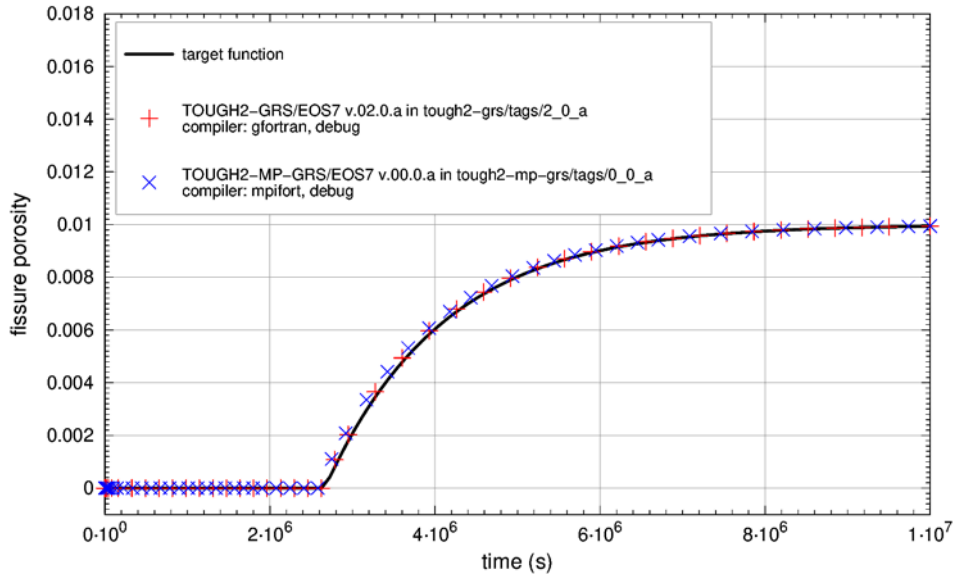


Fig. 8.5 FISS test: Evolution of fissure porosity with time for an exponential decrease of the porosity change rate

8.5 Linear softening without time-dependency

Test case `fiss-ifsoft1-ifpor2-ifper2.json` introduces a linear softening process that depends on the excess pressure. The following parameters are used:

- Linear softening without time-dependency: `ifsoft=1`, `fsoft(1)= $1 \cdot 10^5$` , `fsoft(2)= $1 \cdot 10^5$` , `fsoft(3)=0`.
- Fissure porosity depends linearly on the excess pressure: `ifpor=2`, `fpor(1)= $1 \cdot 10^5$` , `fpor(2)=0.01`, `fpor(3)=1`, `fpor(4)=1`
- Fissure permeability depends linearly on the excess pressure (`ifper=2`)
- Fissure permeability is a linear function of fissure porosity: `ifper=2`, `fper(1)=0`, `fper(2)= $1 \cdot 10^5$` , `fper(3)=0`, `fper(4)= $1 \cdot 10^{-18}$` , `fper(5)=1`.
- Initial threshold pressure (pthr0): $2 \cdot 10^5$ Pa.

Fig. 8.6 to Fig. 8.8 show that the simulated evolution of fissure porosity, fissure permeability and threshold pressure are correct.

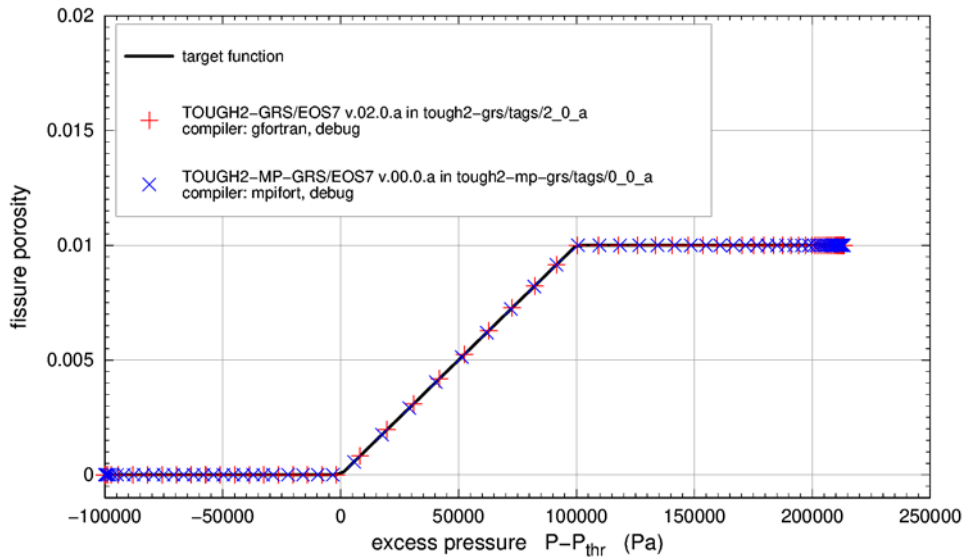


Fig. 8.6 FISS test: Relationship between fissure porosity and excess pressure

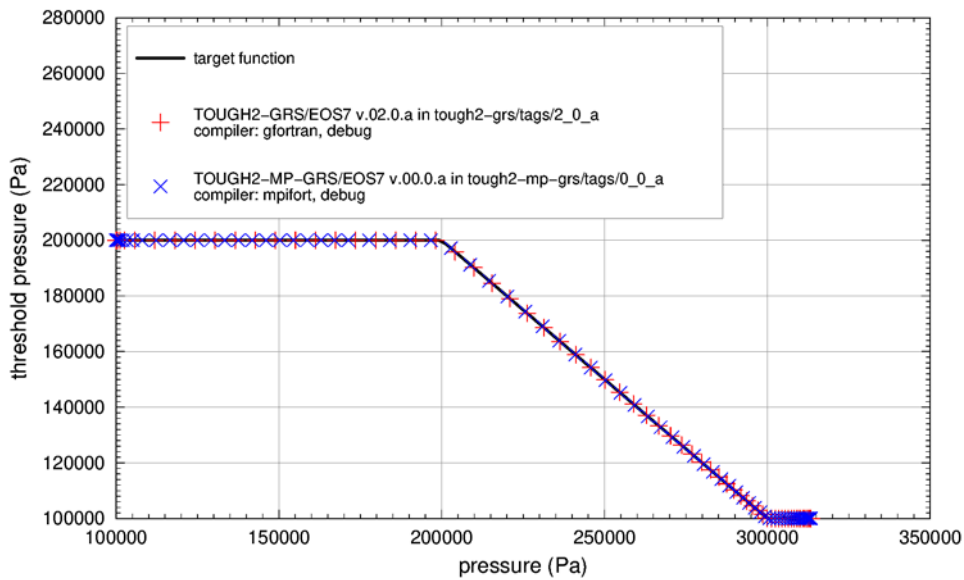


Fig. 8.7 FISS test: Relationship between the threshold pressure and gas pressure

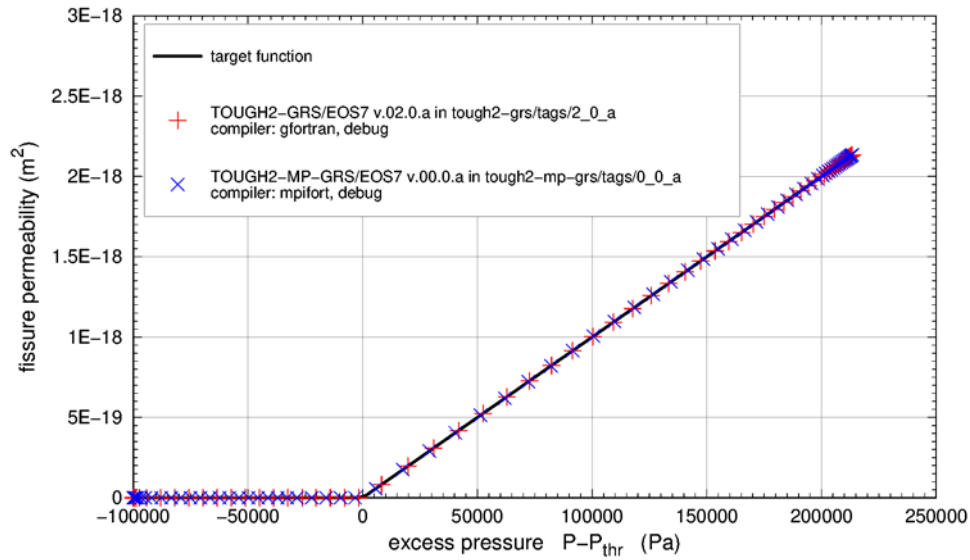


Fig. 8.8 FISS test: Relationship between fissure permeability and excess pressure

8.6 Linear softening with minimum softening rate

Test case `fiss-ifsoft1-ifpor2-ifper2-b.json` introduces a linear softening process with a minimum softening rate (expressed as threshold pressure change per time). The following parameters are used:

- Linear softening with minimum rate of 100000 Pa per $1 \cdot 10^{57}$ sec: `ifsoft=1`, `fsoft(1)= 1 \cdot 10^5`, `fsoft(2)=1 \cdot 10^5`, `fsoft(3)=1`, `fsoft(4)=0.01`
- Fissure porosity depends linearly on the excess pressure: `ifpor=2`, `fpor(1)= 1 \cdot 10^5`, `fpor(2)=0.01`, `fpor(3)=1`, `fpor(4)=1`
- Fissure permeability is a linear function of fissure porosity: `ifper=2`, `fper(1)=0`, `fper(2)= 1 \cdot 10^5`, `fper(3)=0`, `fper(4)= 1 \cdot 10^{-18}`, `fper(5)=1`.
- Initial threshold pressure (`pthr0`): $2 \cdot 10^5$ Pa.

Fig. 8.9 shows how the threshold pressure decreases linearly with time.

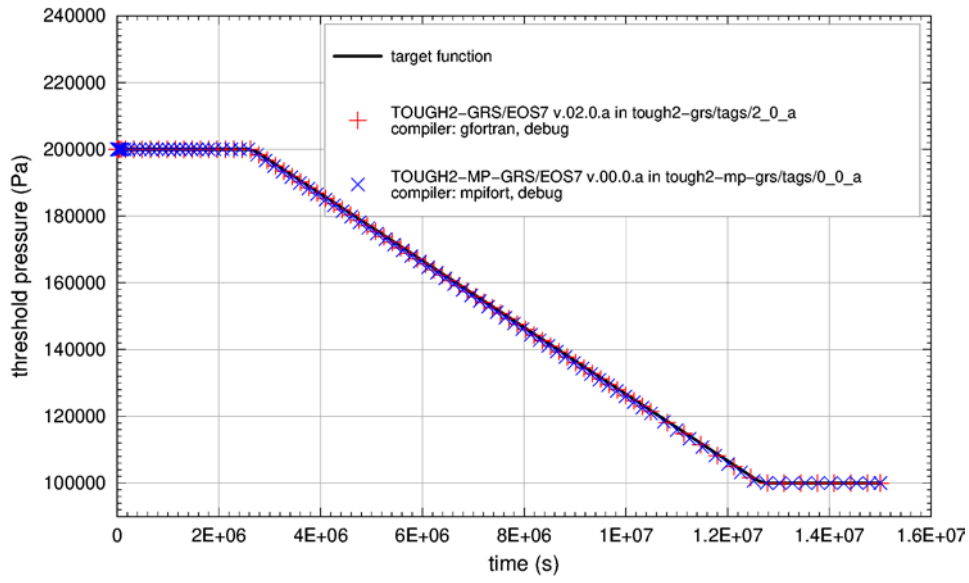


Fig. 8.9 FISS test: Evolution of the threshold pressure with time

9 PRLIM Module

We consider a simple model consisting of four elements, each with a volume of 0.25 m³. There only is air in the system. In each element there is a source generating air at a constant rate of $2.5 \cdot 10^{-8}$ kg/sec. Consequently, pressure rises to the limiting pressure of 200,000 Pa defined by the PRLIM module.

We compare the simulated pressures (Fig. 9.1) and the volume of gas removed from the system by the PRLIM module (Fig. 9.2) with analytical solutions. The simulation results match the analytical solutions well.

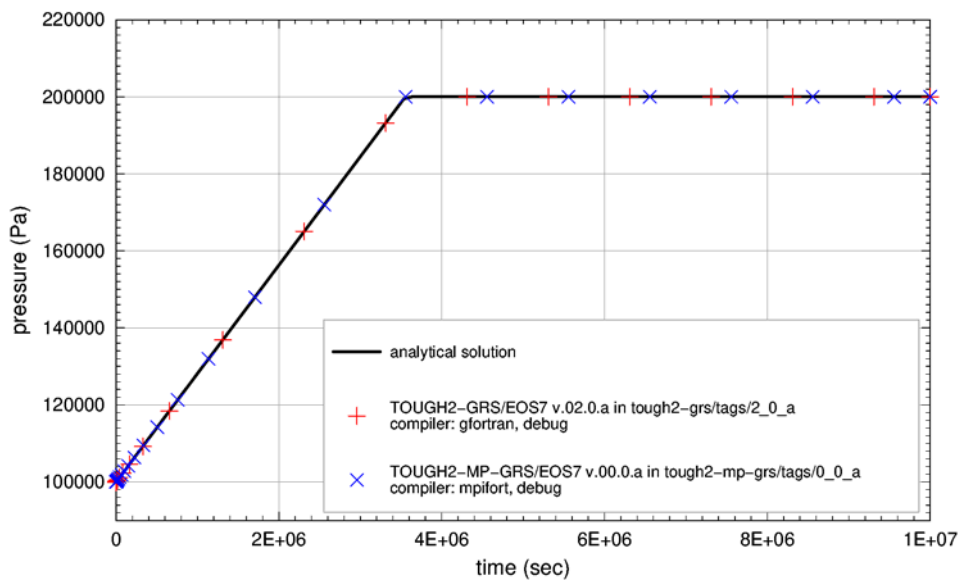


Fig. 9.1 PRLIM test: Pressure limitation

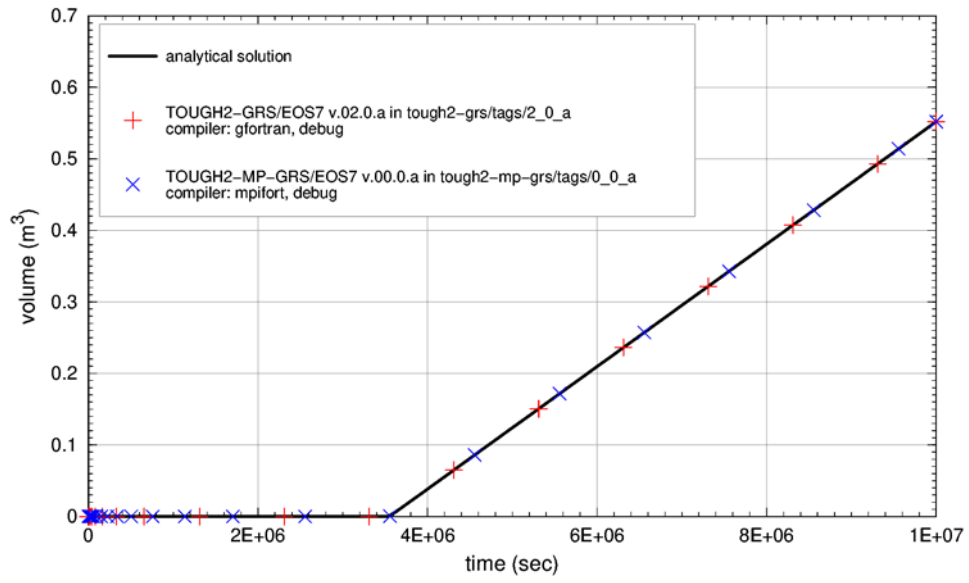


Fig. 9.2 PRLIM test: Gas volume removed from the system

10 RELA Module

10.1 Porosity-permeability relation

In order to verify the porosity-permeability relation of the RELA module we consider a single compressible element that increases its porosity due to a pressure increase. This element is initially filled with gas at a pressure of 1 MPa. It is connected to an inactive element, which is saturated and at a pressure of 10 MPa. Liquid flow from the inactive to the active element is possible. The active element has a compressibility of $2 \cdot 10^{-4} \text{ Pa}^{-1}$.

Using the RELA module we introduce a porosity-permeability relationship with input parameters $\text{COMP_PERA} = 1 \cdot 10^{-13}$ and $\text{COMP_PERA} = 2$. Fig. 10.1 shows that the simulated permeability-porosity relation matches the target function very well.

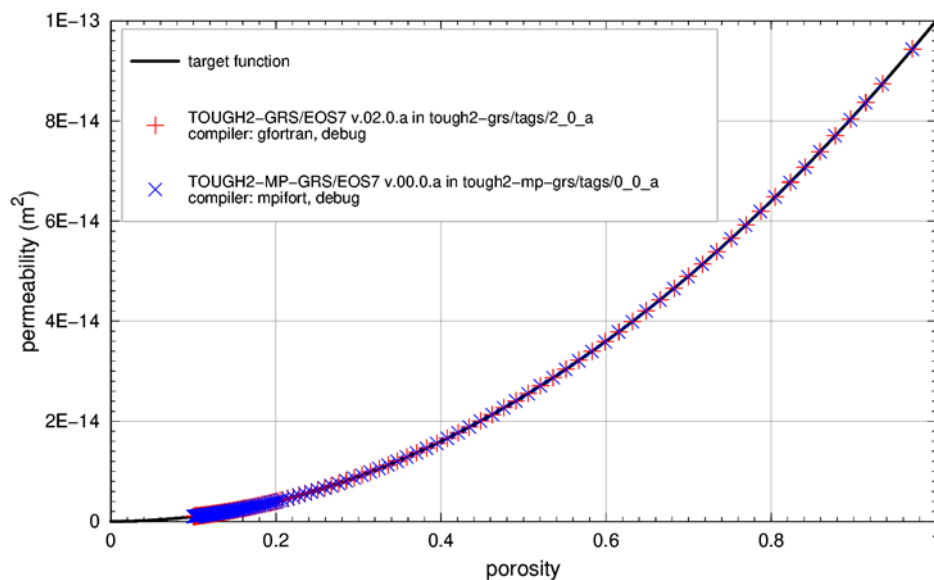


Fig. 10.1 RELA test: Porosity-permeability relation

10.2 Leverett scaling of capillary pressure

The same model is used to test the Leverett scaling of capillary pressures. The input parameters for the RELA module are $LEVPERREF = 1 \cdot 10^{-14}$, $LEVPHIREF = 0.1$, and $LEVEXP = 0.5$. Fig. 10.2 shows that the simulation results match the target function very well.

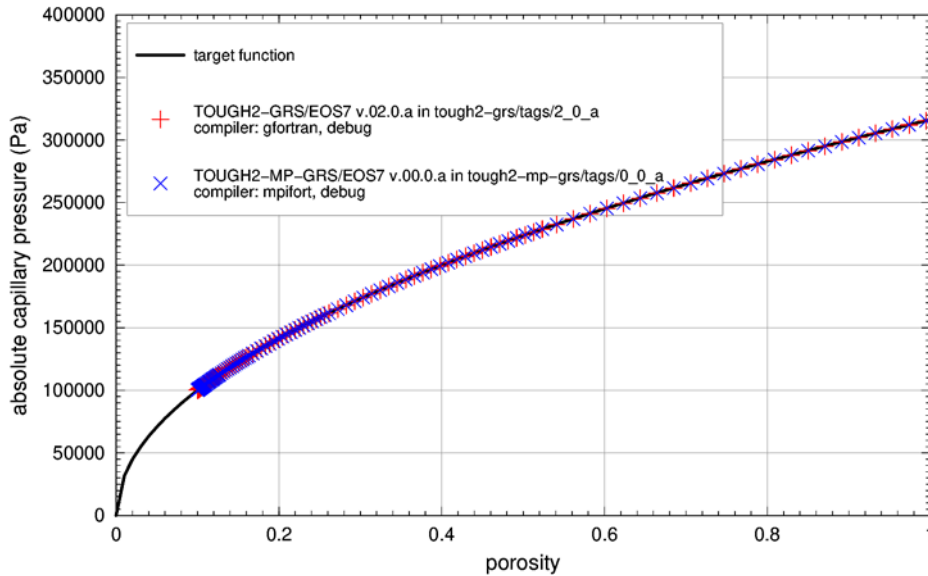


Fig. 10.2 RELA test: Dependency of capillary pressures on porosity

10.3 Temperature-dependent capillary pressure

We consider the saturation process of two elements, one being at a constant temperature of 20 °C the other at a constant temperature of 60 °C. For both elements a capillary pressure function is defined that increases linearly from -100 Pa to 0 Pa as liquid saturation increases from 0 to 1 (TOUGH2 uses negative capillary pressures.) By definition, the capillary pressure function defined in data block ROCKS is the one at reference temperature, which we set to 20 °C using input parameter $PCTTREF$. Input parameter $PCTBETA$ is set to -646.3 °C. This should decrease capillary pressures at 60 °C by a factor of 0.5.

Fig. 10.3 shows the capillary pressure function at 20 °C (reference pressure). Capillary pressures at 60 °C are displayed in Fig. 10.4. Capillary pressures at 60 °C are half of the capillary pressures at 20 °C, which is the intended behavior.

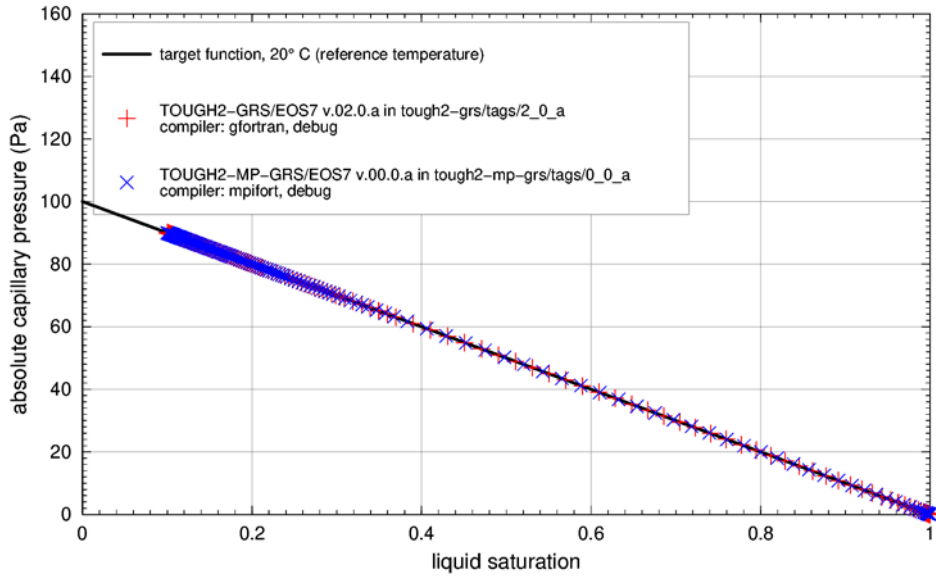


Fig. 10.3 RELA test: Capillary pressures at reference temperature (20 °C)

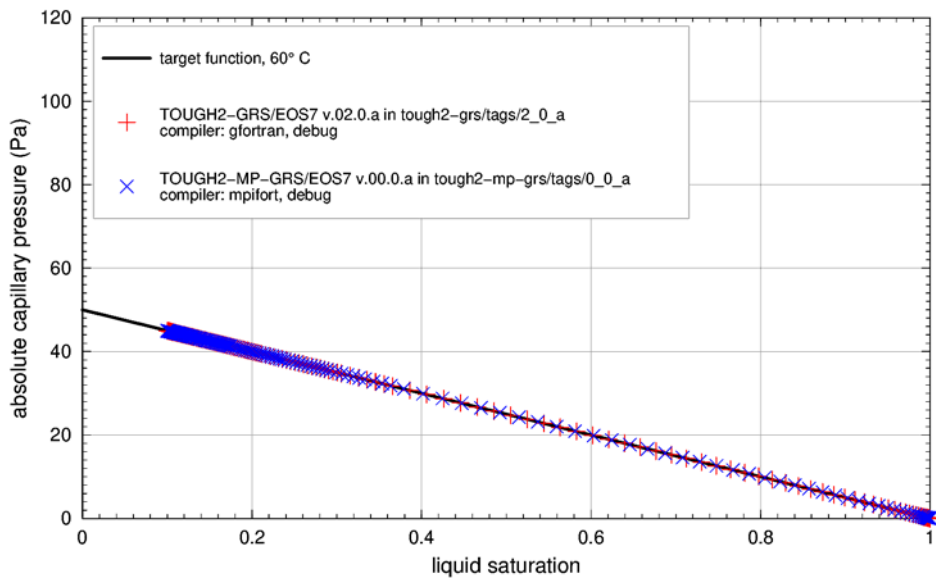


Fig. 10.4 RELA test: Capillary pressures at 60 °C

Capillary pressures should be exactly half of the capillary pressures at 20 °C.

11 RN Module

11.1 Time Stepping Control

The following test case checks the time stepping control of module RN. The time step control of the RN module reduces time steps if they are larger than a user-defined multiple of the minimum half life (input parameter `HALFTIMES`). Half lifes are neglected in this consideration if the mass of the respective radionuclide is smaller than input parameter `MINMASS`.

We consider a horizontal saturated column, which is percolated from the left to the right. Two radionuclides are placed on the upstream side of the column, each with a total mass of 1 g. Radionuclide 2 is mobilized at simulation time 0 and radionuclide 1 at simulation time 50,000 sec.

The first radionuclide has a half-life of $3 \cdot 10^6$ sec, the second one a half-life of 10^6 sec. The half-life of the second radionuclide should therefore provide the first time step limit. Both radionuclides are carried out of the system by the water flow. As soon as the total mass of the second radionuclide falls below `MINMASS` the time limit should switch to the half-life of the first radionuclide.

We set `MINMASS` to 10^{-5} kg and `HALFTIMES` to 10^{-3} . Time step widths should not overstep $3 \cdot 10^6 \text{ sec} \cdot 10^{-3} = 10^3$ sec if the total mass of the second radionuclide is larger than 10^{-5} kg. Time steps widths should also not exceed 10^4 sec if the total mass of the first radionuclide is larger than 10^{-5} kg.

The two graphs of Fig. 11.1 show how radionuclide masses and time step widths evolve. The upper graph shows radionuclide masses, which decrease due to the flushing of the system. The mass of the second radionuclide falls below the mass limit (`MINMASS`) of 10^{-5} kg after about 330.000 sec. According to the lower graph, time step widths stay below 10^3 sec until this time, which is the intended behaviour. After 330.000 sec the time stepper uses the half-life of the first radionuclide ($3 \cdot 10^6$ sec) to define a time limit. Time step widths can increase freely after the total mass of both radionuclides has fallen below the mass limit of 10^{-5} kg. Fig. 11.1 shows, that the implemented time step control works correctly.

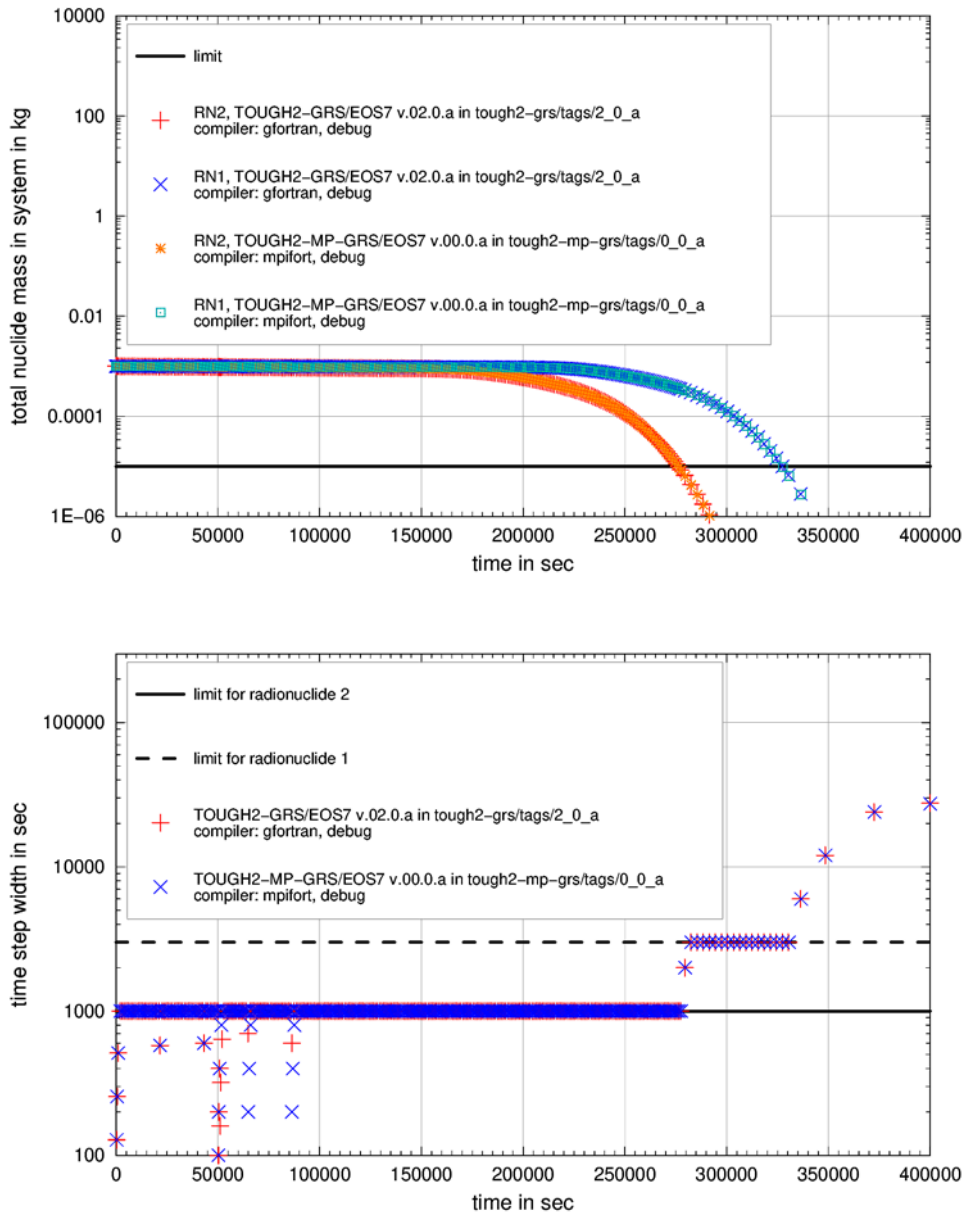


Fig. 11.1 RN test: Total radionuclide mass in the system (above) and time step width (below)

The time step limit of 1000 sec (below) should be discarded as soon as the total mass of radionuclide 2 falls below the limit of $1 \cdot 10^{-5}$ kg (above). The ensuing time step limit of 3000 sec (below) should be discarded as soon as the total mass of radionuclide 1 falls below the same mass limit.

11.2 SAMR1

The test case SAMR1 has been taken from /OLD 95/ and was adopted for the purpose of the RNmod in TOUGH2-GRS. The test case allows for comparing the results of RNmod with EOS7R as well as with the analytic solution /GEN 85/.

11.2.1 Model description

In test case SAMR1, the model domain is a fully saturated horizontal column of 7 m length with inactive elements on both sides. The column is divided in horizontal direction into 200 grid elements of same volume and size. The column material has a porosity of 30 % and a permeability of $1.24 \cdot 10^{-9}$ m². An initial steady state flow field with a pore velocity of 0.1 m/day is imposed on the column by applying a pressure of 100001.75 Pa to the left inactive element and a pressure of 100000 Pa to the right one (center-interface distances of inactive elements are set to $5 \cdot 10^{-6}$ m). Brine properties are set equal to those of pure water. The parent radionuclide RN1 with assumed half-lives of $\lambda=20$ d and $\lambda \rightarrow \infty$ is placed in the left inactive element with a mass fraction of 0.01. Radionuclide diffusion is characterized by a molecular diffusivity of $1.162 \cdot 10^{-7}$ m²/s and a tortuosity of 1. We assume the two cases that radionuclides are not adsorbed (retardation factor $R=1$) and an adsorption of $R=2$. The retardation factor enters in TOUGH via eq. (16) in /OLD 95/.

11.2.2 Analytical solution

The analytical solution of the problem is given in /JAC 09/, /GEN 85/ and details of the underlying equations and the boundary conditions can be found there. Here, we briefly summarize the underlying equations and assumptions.

The model describes transport of four species involved in a consecutive first order decay chain of the form



The one-dimension convective-dispersive transport of the four chain members under transient flow conditions is described by the following set of coupled differential equations

$$\partial_t(\theta c_1 + \rho s_1) = \partial_x(\theta D \partial_x c_1 - q c_1) - \mu_{w,1} \theta c_1 - \mu_{s,1} \rho s_1, \quad (11.2)$$

$$\begin{aligned} \partial_t(\theta c_i + \rho s_i) = \partial_x(\theta D \partial_x c_i - q c_i) + \mu_{w,i-1} \theta c_{i-1} + \mu_{s,i-1} \rho s_{i-1} - \mu_{w,1} \theta c_1 \\ - \mu_{s,1} \rho s_1 \quad (i = 2,3,4), \end{aligned} \quad (11.3)$$

where c is the solution concentration, s the adsorbed concentration, the volumetric water content, q the volumetric flux, D the dispersion coefficient, θ the porous medium bulk density, x the distance. The subscript i depicts the i -th chain member. The coefficients μ

are rate constants of the first-order decay reaction for the liquid and the soil phase, respectively. For radioactive decay it is assumed that

$$\mu_{w,i} = \mu_{s,i}. \quad (11.4)$$

Moreover, two assumptions are introduced. At first, it is assumed that the soil system is homogeneous and is subjected to a steady state flow, i. e. θ and q are constant in time and space. Second, adsorbed concentrations s_i are assumed to be related to the solution concentration c_i by linear isotherms. With these assumptions and the assumptions of steady-state flow and linear equilibrium (11.2) and (11.3) reduce to

$$R_1 \dot{c}_1 = D \partial_x^2 c_1 - v \partial_x c_1 - \mu_1 R_1 c_1 \quad (11.5)$$

$$R_i \dot{c}_i = D \partial_x^2 c_i - v \partial_x c_i - \mu_i R_i c_i + \mu_{i-1} R_{i-1} c_{i-1} \quad (i = 2,3,4), \quad (11.6)$$

where $v = q/\theta$ is the average pore water velocity and the retardation factors are given by

$$R_i = 1 + \frac{\rho k_i}{\theta}. \quad (11.7)$$

The analytic solution in /GEN 85/ is obtained for semi-infinite systems ($0 \leq x < \infty$) with the boundary conditions

$$\partial_x c_i(\infty, t) = 0, \quad t \geq 0 \quad (i = 1,4), \quad (11.8)$$

assuming the system to be initially free of solutes, i. e.

$$c_i(x, 0) = 0, \quad x \geq 0. \quad (11.9)$$

The analytical solution of (11.5) and (11.6) with boundary and initial conditions (11.8) and (11.9) is then derived by standard Laplace transform techniques, see /GEN 85/ and references therein. To evaluate the analytical solution we have re-implemented the program CHAIN introduced in /GEN 85/ and have recalculated the analytical solution.

11.2.3 Main results

The test case SAMR1 serves as a reference test for the RNmod within the quality assurance performed for TOUGH2-GRS, see /HOT 17/ for details. In what follows only a selection of the test results will be presented. Other variations of the parameters mentioned in chapter 11.2.1 have been carried out but are not shown here. All results are calculated with the tag TOUGH2-GRS v.2.0.a and TOUGH2-MP-GRS v.0.0.a. The results for EOS7 correspond to the calculations using the newly developed RNmod /NAV 16/, whereas the results for EOS7R correspond to the original TOUGH2 model to calculate radionuclide transport /OLD 95/. The analytical solution is described in chapter 11.2.2.

11.2.4 No radioactive decay

Fig. 11.2 and Fig. 11.3 show the profile of the mass fraction of RN1 in the flow direction of the solute at time $t = 20 d$ without ($R = 1$) and including ($R = 2$) adsorption, respectively. The results for RNmod and EOS7R coincide very well with the analytic solution.

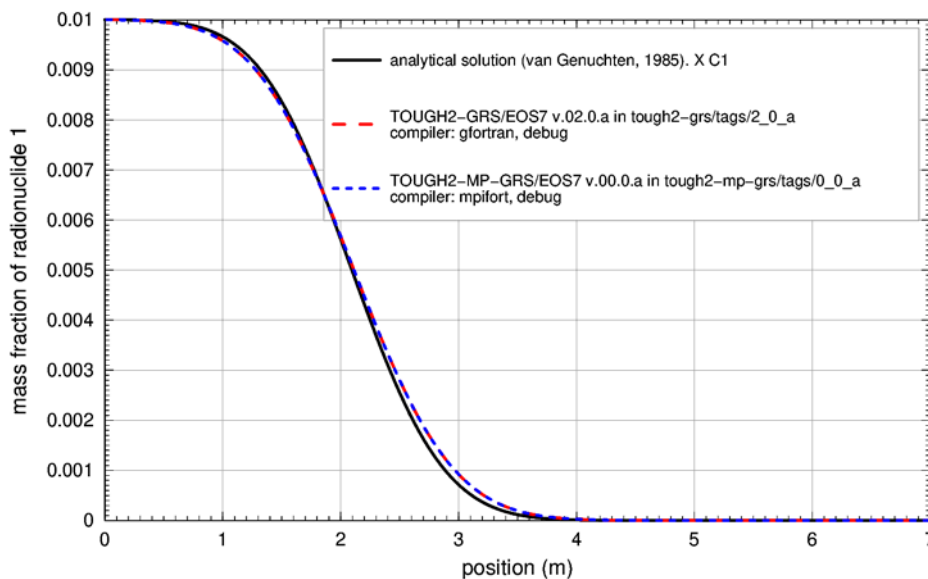


Fig. 11.2 RN test: Profile of the mass fraction of RN1 without adsorption $R = 1$

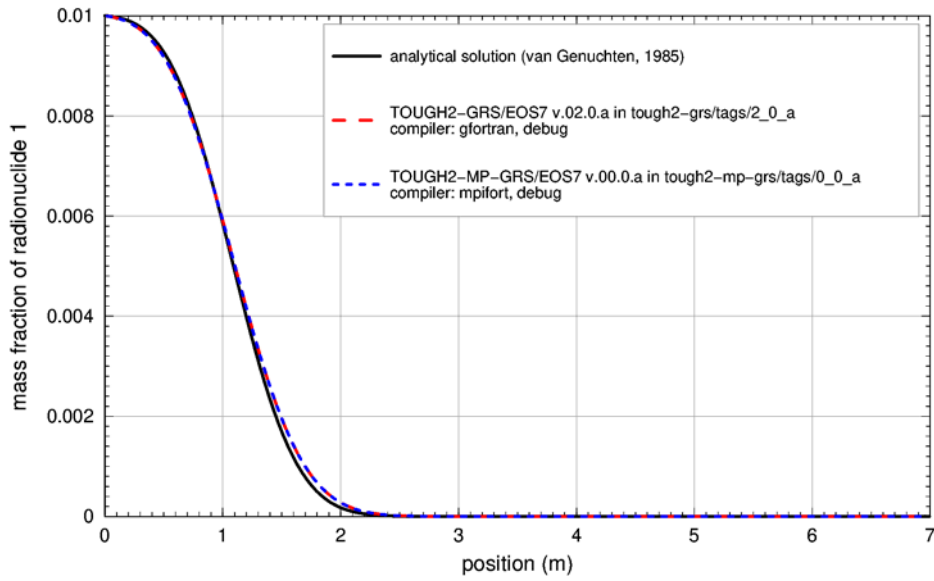


Fig. 11.3 RN test: Profile of the mass fraction of RN1 ($R = 2$)

11.2.5 Radioactive decay

For the case of radioactive decay ($\lambda = 20d$) the mass fraction for both radionuclides is shown for $R = 2$. The results for RNmod in EOS7 and EOS7R show satisfying agreement with the analytical solution. The deviation in the mass fraction for RN2 is within an acceptable range.

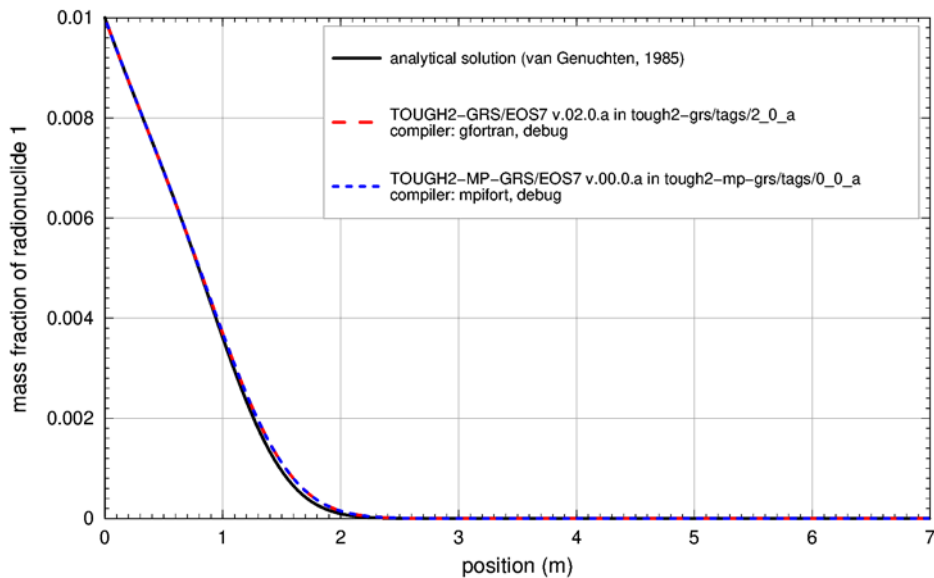


Fig. 11.4 RN test: Profile of mass fraction of RN1 ($R = 2$ and $\lambda = 20d$)

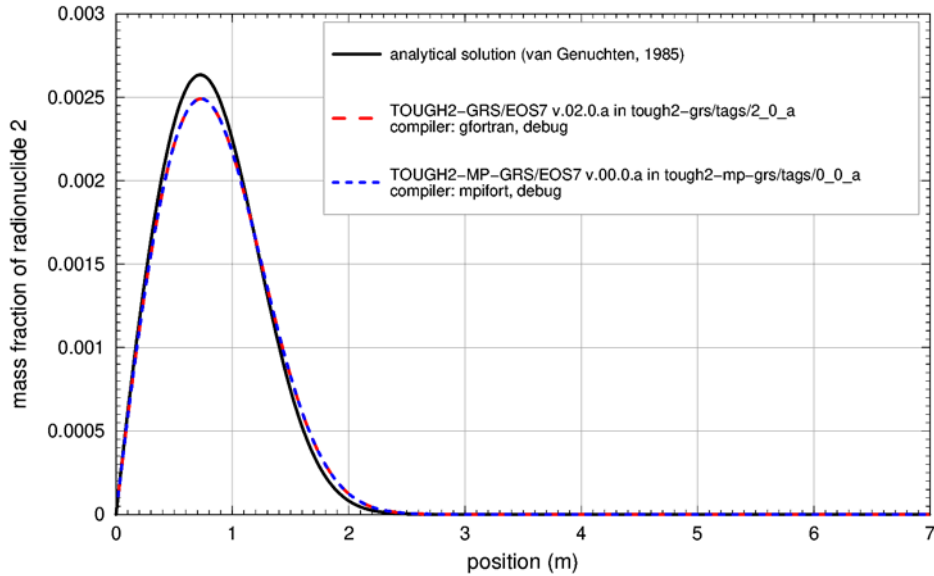


Fig. 11.5 RN test: Profile of mass fraction of RN2 ($R = 2$ and $\lambda = 20d$)

11.2.6 Coarse time discretization

One aspect of the test cases for TOUGH2-GRS is to gain a deeper understanding of the dependency of the simulation results on purely numerical parameters as, for instance, the maximally allowed time step width of the solver for the differential equations.

In both, EOS7R and RNmod, the differential equations for radioactive decay are decoupled from the transport and energy equations. Radionuclide transport during a time step therefore takes place without radioactive decay. This suggests that the simulation results should deviate from the analytical solution if the time step width increases. Also, the error connected to the linear approximation of the decay process during a time step should increase with increasing time step. Possibly for this reason, /OLD 95/ have suggested that the upper time step width limit should be well below the shortest half-life of the modelled radionuclides. As a default, TOUGH sets no upper limit for the time step width ($\Delta t_{max} \rightarrow \infty$) thereby leaving the control of time step widths to the automatic time stepping mechanism. Consequently, time step width is mainly controlled by the differential equation solver but not by radionuclide half-lives. If the user refrains from defining an upper limit for the time step width – maybe because the simulations are time-consuming and require adaptive time stepping – the automatic time stepping mechanism could generate time step widths well above the shortest half-life resulting in significant errors.

In Fig. 11.6 and Fig. 11.7 show the case with radioactive decay ($R = 1$, $\lambda = 20d$) and no adsorption that has been repeated without limiting the time step width ($\Delta t_{max} \rightarrow \infty$). The observed deviations between the analytical solution and the results of EOS7R and RNmod (in connection with TOUGH2-GRS) are striking and underpin the importance of a fine-grained time discretization. However, it has to be noted that the observed deviations depend on the implemented time stepping mechanism.

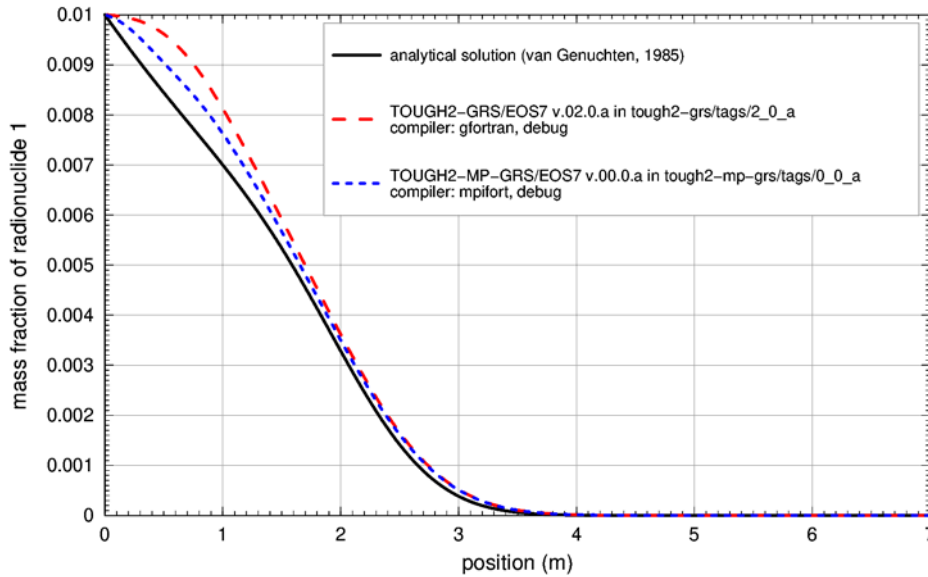


Fig. 11.6 RN test: RN1 mass fraction ($R = 1$, $\lambda = 20d$, $\Delta t_{max} \rightarrow \infty$)

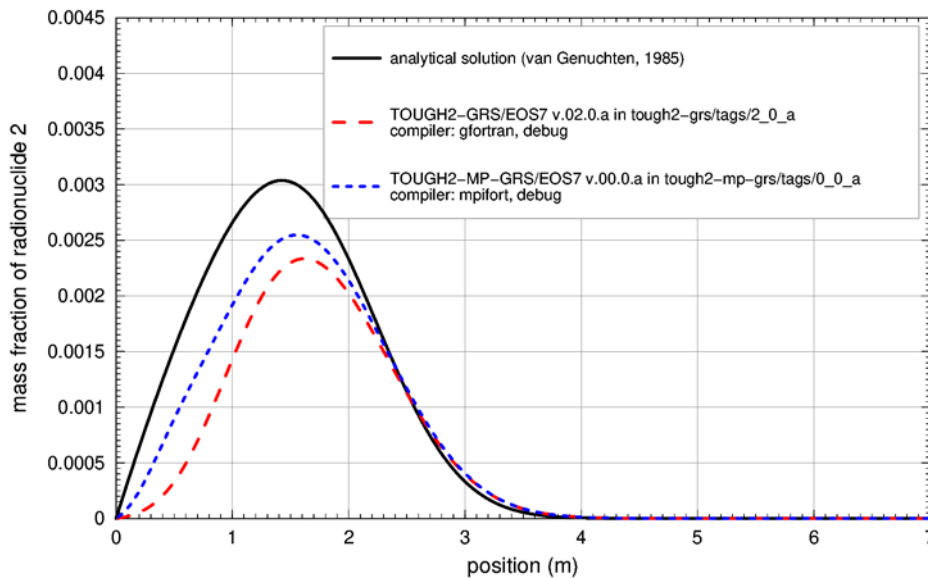


Fig. 11.7 RN test: RN2 mass fraction ($R = 1$, $\lambda = 20d$, $\Delta t_{max} \rightarrow \infty$)

11.3 RN Anion Exclusion

The assumption $R_{\text{flow}} = 0$ (no flow reduction) is used to define two test cases for the anion exclusion feature of the RN module (see the user manual /NAV 18/ for an explanation of parameter R_{flow}).

We consider an upper and a lower horizontal column. Each column has a length of 3 m and is composed of 100 elements per meter. The entire model is saturated. At the left and right ends (position 0 m and 3 m, respectively) there are inactive elements with constant pressure.

The test cases `onlyadvection.json` and `onlydiffusion.json` simulate the advective and diffusive transport of an ideal tracer, respectively. The upper column has a porosity of 0.1, which is entirely accessible to the tracer. The lower column has a total porosity of 0.3 (the porosity variable of TOUGH2) with an accessible porosity of 0.1 (introduced by module RN). The accessible porosity is the same for both columns so that the tracer front should be displaced in both columns with same velocity in both test cases.

11.3.1 Advective Transport

In test case `onlyadvection.json`, the tracer is placed at section 0 m to 1 m (left side of the model) with a concentration of 1 kg/m^3 (mass per accessible pore space).

A concentration of 1 kg/m^3 (mass per accessible pore space) is defined for the inactive elements on the left side of both columns. The same concentration is defined for active elements between position 0 m and 1 m by placing a tracer mass of 0.001 kg.

An effective flow of 1 m/d induced in both columns by applying a pressure difference on both sides of the columns (flow from the left to the right). Fig. 11.8 displays that the concentration front (defined here by the position of concentration 0.5 kg/m^3) move at the same speed in both columns. This shows the correct implementation of anion exclusion for $R_{\text{flow}} = 0$.

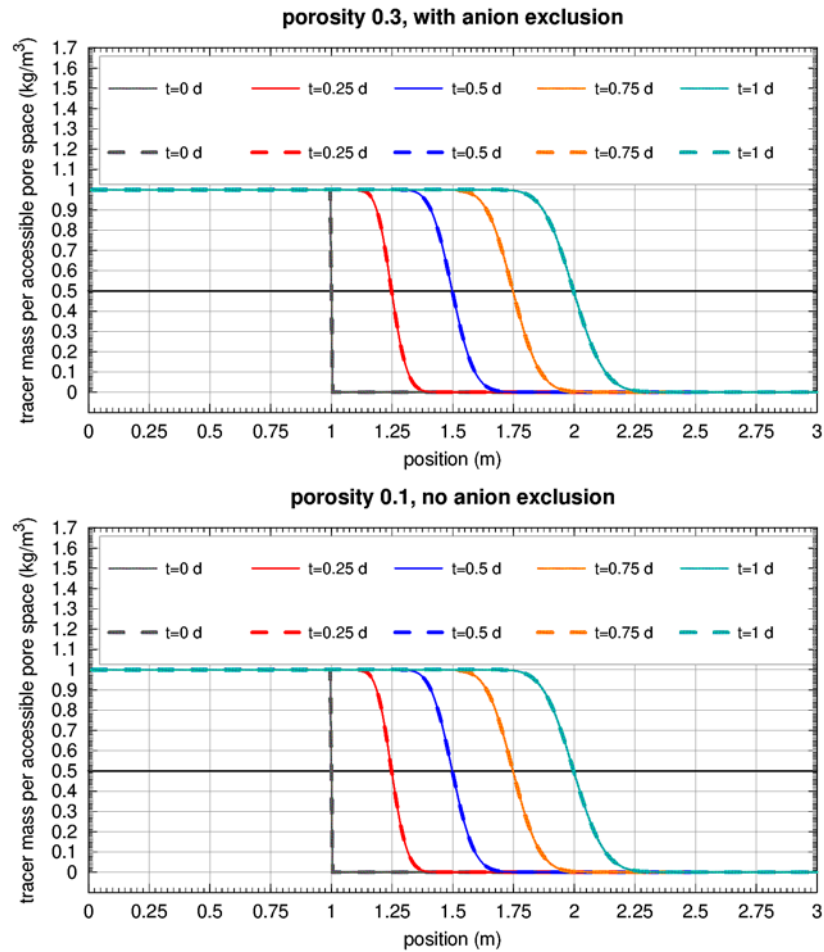


Fig. 11.8 RN test: Position of the concentration front with (above) and without (below) anion exclusion during one day (advective transport)

Solid lines: TOUGH2-GRS v. 2.0.a, dashed lines: TOUGH2-MP-GRS v. 0.0.a.

11.3.2 Diffusive Transport

In test case `onlydiffusion.json`, all inactive elements initially are free of tracer. There is no advective flow (no pressure difference). A high diffusion coefficient of $1 \cdot 10^{-6} \text{ m}^2$ is assigned to the tracers. Fig. 11.9 shows the tracer concentration after one day. The matching curves indicate the correctness of the implemented anion exclusion process for diffusive transport.

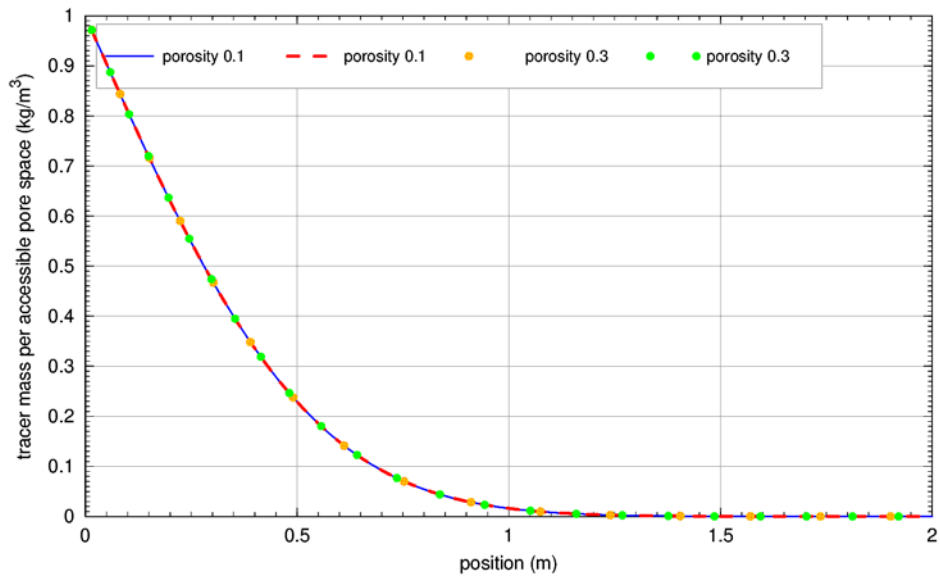


Fig. 11.9 RN test: Tracer concentration with and without anion exclusion after one day (diffusive transport)

Blue line and yellow dot: TOUGH2-GRS v. 2.0.a, dashed red line and green dots: TOUGH2-MP-GRS v. 0.0.a.

References

- /BEC 09/ Becker, D.-A., Buhmann, D., Mönig, J., Noseck, U., Rübel, A., Spiessl, S.: Sicherheitsanalyse für das verfüllte und verschlossene Endlager mit dem Programmpaket EMOS. GRS-A-3454: Braunschweig, 27 March 2009.
- /BFS 09/ Bundesamt für Strahlenschutz (BfS): Sicherheitsanalyse für das verfüllte und verschlossene Endlager mit dem Programmpaket EMOS. P278, BfS-KZL: 9M/23210051/EG/RB/0056/00, 27 March 2009.
- /BRÄ 11/ Bräuer, V., Eickemeyer, R., Eisenburger, D., Grissemann, C., Hesser, J., Heusermann, S., Kaiser, D., Nipp, H.-K., Nowak, T., Plischke, I., Schnier, H., Schulze, O., Sönke, J., Weber, J. R.: Description of the Gorleben site Part 4, Geotechnical exploration of the Gorleben salt dome. ISBN 978-3-9814108-0-8, Bundesanstalt für Geowissenschaften und Rohstoffe (BGR): Hannover, 2011.
- /GEN 85/ Genuchten, M. T. van: Convective-dispersive transport of solutes involved in sequential first-order decay reactions. Computers & Geosciences, Vol. 11, No. 2, pp. 129–147, DOI 10.1016/0098-3004(85)90003-2, 1985.
- /GRS 13/ Software Management Group: Maßnahmen zur Qualitätssicherung bei der Erstellung von Computerprogrammen in der GRS (QM-Richtlinie Programmentwicklung), QM-Handbuch, Teil 3: FA 03 "Fachliche Qualitätssicherung von Arbeitsergebnissen", Anlage IV. Gesellschaft für Anlagen- und Reaktorsicherheit (GRS) mbH, 8 p.: Köln, 21 November 2013.
- /HIR 64/ Hirschfelder, J. O.: Molecular theory of gases and liquids. Structure of matter series, 1249 p., ISBN 0471400653, Wiley: London, 1964, ©1954.
- /HOT 17/ Hotzel, S., Navarro, M., Seher, H.: QS-Handbuch für den Programmcode TOUGH2-GRS. GRS-401, ISBN 978-3-944161-82-2, Gesellschaft für Anlagen- und Reaktorsicherheit (GRS) gGmbH: Köln, 2017.

- /JAC 09/ Jacinto, A. C., Villar, M. V., Gómez-Espina, R., Ledesma, A.: Adaptation of the van Genuchten expression to the effects of temperature and density for compacted bentonites. *Applied Clay Science*, Vol. 42, pp. 575–582, DOI 10.1016/j.clay.2008.04.001, 2009.
- /KOC 13/ Kock, I.: Qualifizierung der in VSG verwendete Rechenprogramme und Codes, Memo zum Arbeitspaket 10, Vorläufige Sicherheitsanalyse für den Standort Gorleben. Gesellschaft für Anlagen- und Reaktorsicherheit (GRS) mbH: Köln, 1 January 2013.
- /KOL 12/ Kolditz, O.: Thermo-hydro-mechanical-chemical processes in fractured porous media, Benchmarks and examples. *Lecture notes in computational science and engineering*, Vol. 86, ISBN 978-3-642-27176-2, Springer: New York, 2012.
- /MAR 02/ Martens, K.-H., Fischer, H., Romstedt, P.: Beschreibung des Rechenprogrammes MARNIE. Gesellschaft für Anlagen- und Reaktorsicherheit (GRS) mbH, GRS-A-3027, 135 p.: Köln, 1 January 2002.
- /NAV 13/ Navarro, M.: Die vereinfachte Berechnung der Konvergenzrate salzgrusverfüllter Hohlräume im Steinsalz. GRS-307, 47 p., ISBN 978-3-939355-86-1, Gesellschaft für Anlagen- und Reaktorsicherheit (GRS) mbH: Köln, 2013.
- /NAV 16/ Navarro, M., Eckel, J.: TOUGH2-GRS, Version 1, User Manual. GRS-403, 87 p., ISBN 978-3-944161-84-6, Gesellschaft für Anlagen- und Reaktorsicherheit (GRS) gGmbH: Köln, July 2016.
- /NAV 18/ Navarro, M.: User Manual, TOUGH2-GRS Version 2, TOUGH2-MP-GRS Version 0. Gesellschaft für Anlagen- und Reaktorsicherheit (GRS) gGmbH, 2018.
- /OLD 95/ Oldenburg, C. M., Pruess, K.: EOS7R, Radionuclide Transport for TOUGH2. Lawrence Berkeley National Laboratory (LBNL), LBL-34868: Berkeley, California, 1 January 1995.

- /PRU 99/ Pruess, K., Oldenburg, C., Moridis, G.: TOUGH2 User's Guide, Version 2.0. Lawrence Berkeley National Laboratory (LBNL), LBNL-43134, 198 p.: Berkeley, California, USA, 1 November 1999, revised September 2012.
- /SEH 16/ Seher, H., Navarro, M.: SITA, Version 0, A simulation and code testing assistant for TOUGH2 and MARNIE. GRS-400, 78 p., ISBN 978-3-944161-81-5, Gesellschaft für Anlagen- und Reaktorsicherheit (GRS) gGmbH: Köln, June 2016.
- /ZHA 08/ Zhang, K., Wu, Y.-S., Pruess, K.: User's Guide for TOUGH2-MP - A Massively Parallel Version of the TOUGH2 Code. Lawrence Berkeley National Laboratory (LBNL), LBNL-315E: Berkeley, California, USA, 1 May 2008.

List of Figures

Fig. 2.1	Isothermal gas flow, steady state pressure profile	5
Fig. 3.1	COMP reference case: Evolution of the convergence rate	13
Fig. 3.2	COMP Reference case: Evolution of porosity	14
Fig. 3.3	COMP test case <i>comp-1</i> : Evolution of the convergence rate.....	15
Fig. 3.4	COMP test case <i>comp-1</i> : Convergence rate versus porosity	15
Fig. 3.5	COMP test case <i>comp-3</i> : Evolution of the convergence rate.....	16
Fig. 3.6	COMP test case <i>comp-3</i> : Evolution of porosity.....	17
Fig. 3.7	COMP test case <i>comp-5</i> : Evolution of temperature	18
Fig. 3.8	COMP test case <i>comp-5</i> : Evolution of porosity.....	18
Fig. 3.9	COMP test case <i>comp-5</i> : Convergence rate versus temperature.....	19
Fig. 3.10	COMP test case <i>comp-5a</i> : Evolution of temperature	20
Fig. 3.11	COMP test case <i>comp-5a</i> : Convergence rate versus temperature.....	20
Fig. 3.12	COMP test case <i>comp-5a</i> : Evolution of porosity.....	21
Fig. 3.13	COMP test case <i>comp-6</i> : Evolution of convergence rate.....	22
Fig. 3.14	COMP test case <i>comp-6</i> : Evolution of porosity.....	22
Fig. 3.15	COMP test case <i>comp-6</i> : Permeability versus porosity	23
Fig. 3.16	COMP test case <i>comp-7</i> : Evolution of convergence rate.....	24
Fig. 3.17	COMP test case <i>comp-7</i> : Evolution of liquid pressure	24
Fig. 3.18	COMP test case <i>comp-7</i> : Convergence rate versus pressure	25
Fig. 3.19	COMP test case <i>comp-7</i> : Evolution of permeability	25
Fig. 3.20	COMP test case <i>comp-7</i> : Permeability versus porosity	26
Fig. 3.21	COMP test case <i>comp-12a</i> : Evolution of convergence rate.....	27
Fig. 3.22	COMP test case <i>comp-12a</i> : Convergence rate versus pressure	27
Fig. 3.23	COMP test case <i>comp-12a</i> : Convergence rate versus temperature.....	28
Fig. 4.1	Compressibility test: porosity evolution	29
Fig. 4.2	Compressibility test: Evolution of the porosity error	30

Fig. 5.1	CORFL test: Evolution of the effective seal permeability	33
Fig. 5.2	CORFL test: Pressure evolution inside the seal.....	33
Fig. 6.1	Evolution of the gas pressure.....	36
Fig. 6.2	Evolution of the degree of corrosion	37
Fig. 6.3	Evolution of the liquid saturation	37
Fig. 6.4	Evolution of the brine mass fraction	38
Fig. 6.5	CORRO test case 2: Degree of corrosion.....	40
Fig. 6.6	CORRO test case 3: Liquid saturation	40
Fig. 6.7	CORRO test case 3: Brine mass fraction.....	41
Fig. 6.8	CORRO test case 5: Liquid saturation	41
Fig. 6.9	CORRO test case 6: Gas pressure.....	42
Fig. 6.10	CORRO test case 6: Mean degree of corrosion for all sources	42
Fig. 6.11	CORRO test case 7: Degree of corrosion.....	43
Fig. 6.12	CORRO test case 8: Degree of corrosion.....	43
Fig. 6.13	CORRO test case 9: Gas pressure.....	44
Fig. 6.14	CORRO test case 9: Liquid saturation	44
Fig. 6.15	CORRO test case 10: Gas generation rate.....	45
Fig. 6.16	CORRO test case 11: Gas generation rate.....	45
Fig. 6.17	CORRO test case 13: Amount of gas produced over time.....	46
Fig. 6.18	CORRO test case 14: Amount of gas produced over time.....	46
Fig. 7.1	DEGRA test: Evolution of the intrinsic permeability	47
Fig. 8.1	FISS test: Relationship between fissure permeability and gas pressure	50
Fig. 8.2	FISS test: Relationship between fissure porosity and gas pressure	51
Fig. 8.3	FISS test: Relationship between fissure permeability and fissure porosity.....	51
Fig. 8.4	FISS test: Evolution of fissure porosity for a constant rate of porosity change	52

Fig. 8.5	FISS test: Evolution of fissure porosity with time for an exponential decrease of the porosity change rate	53
Fig. 8.6	FISS test: Relationship between fissure porosity and excess pressure	54
Fig. 8.7	FISS test: Relationship between the threshold pressure and gas pressure	54
Fig. 8.8	FISS test: Relationship between fissure permeability and excess pressure	55
Fig. 8.9	FISS test: Evolution of the threshold pressure with time.....	56
Fig. 9.1	PRLIM test: Pressure limitation.....	57
Fig. 9.2	PRLIM test: Gas volume removed from the system.....	58
Fig. 10.1	RELA test: Porosity-permeability relation.....	59
Fig. 10.2	RELA test: Dependency of capillary pressures on porosity	60
Fig. 10.3	RELA test: Capillary pressures at reference temperature (20 °C)	61
Fig. 10.4	RELA test: Capillary pressures at 60 °C	61
Fig. 11.1	RN test: Total radionuclide mass in the system (above) and time step width (below)	64
Fig. 11.2	RN test: Profile of the mass fraction of RN1 without adsorption $R = 1$	67
Fig. 11.3	RN test: Profile of the mass fraction of RN1 ($R = 2$)	68
Fig. 11.4	RN test: Profile of mass fraction of RN1 ($R = 2$ and $\lambda = 20d$).....	68
Fig. 11.5	RN test: Profile of mass fraction of RN2 ($R = 2$ and $\lambda = 20d$)	69
Fig. 11.6	RN test: RN1 mass fraction ($R = 1$, $\lambda = 20d$, $\Delta t_{max} \rightarrow \infty$).....	70
Fig. 11.7	RN test: RN2 mass fraction ($R = 1$, $\lambda = 20d$, $\Delta t_{max} \rightarrow \infty$).....	70
Fig. 11.8	RN test: Position of the concentration front with (above) and without (below) anion exclusion during one day (advective transport)	72
Fig. 11.9	RN test: Tracer concentration with and without anion exclusion after on day (diffusive transport).....	73

List of Tables

Tab. 2.1	Some literature/Wikipedia values of gas viscosities.....	9
Tab. 3.1	List of test cases for the COMP module.....	12
Tab. 6.1	Test cases for the CORRO module, which have been derived from test case number 1 (the reference test case).....	38

**Gesellschaft für Anlagen-
und Reaktorsicherheit
(GRS) gGmbH**

Schwertnergasse 1
50667 Köln
Telefon +49 221 2068-0
Telefax +49 221 2068-888

Boltzmannstraße 14
85748 Garching b. München
Telefon +49 89 32004-0
Telefax +49 89 32004-300

Kurfürstendamm 200
10719 Berlin
Telefon +49 30 88589-0
Telefax +49 30 88589-111

Theodor-Heuss-Straße 4
38122 Braunschweig
Telefon +49 531 8012-0
Telefax +49 531 8012-200

www.grs.de